Development of miniaturized dissolution methodologies for rapid screening of amorphous solid dispersions

Proof of concept of an innovative High-throughput screening approach

Joana Branco Amante Macedo Veríssimo

Thesis to obtain the Master of Science Degree in

Pharmaceutical Engineering

Supervisor: Doctor Luís Filipe Ramalho de Almeida e Sousa

Co-Supervisor: Professor Doctor Hermínio Albino Pires Diogo

Examination Committee

Chairperson: Professor José Monteiro Cardoso de Menezes

Supervisor: Doctor Luís Filipe Ramalho de Almeida e Sousa

Members of the Committee: Professor Doctor Paulo José Pinto Salústio

November 2021

“Logic will get you from A to B. Imagination will take you everywhere.“ – Albert Einstein

Declaration

I declare that this document is an original work of my own authorship and that It fulfills all the requirements of the Code of Conduct and Good Practices of the University of Lisbon.

Preface

The work presented in this thesis was performed at Hovione Farmaciencia SA R&D Center, located in Lumiar (Portugal), during the period of November 2020 up to June 2021, under the supervision of Dr. Luís Sousa. The thesis was co-supervised at Instituto Superior Técnico by Prof. Dr. Hermínio A. Pires Diogo, and at Faculty of Pharmacy of The University of Lisbon by Prof. Dr. João Fernandes A. Pinto.

Acknowledgements

In the capacity of author of this master thesis I want to thank all the individuals who either directly or indirectly provided suggestions and scientific input. Your contributions truly enhanced the quality of this work.

First, I would like to address a special thanks to Hovione for this amazing internship opportunity, for supporting high quality research and for creating an atmosphere that was conducive to exploring new ideas and innovation. None of this would be possible without my team of supervisors. To my supervisor Luis Sousa for his guidance and patience, for every lesson, for every extra hours, and above all for mentoring me while still letting my creativity roam. To Prof. João Pinto and Prof. Hermínio Diogo for all the support and valuable scientific inputs, for generously sharing your experience and for being invested since day one.

I want to thank Cíntia Veiga for being my lab companion and closest friend throughout this journey at Hovione, for helping me with everything under every circumstance and for cheering my days up with all our conversations. To Patricia Nunes for your friendship, exquisite sense of humor, valuable inputs and late night Confocal Raman Microscopy tutorial lessons, which certainly elevated my project even further. To Madalena Guedes, a late arrival surprise that inhabited the rheology powder room and who soon became one true friend. To Ana Rita Martins for your companionship throughout this journey, for hearing my concerns and for being there to help whenever needed. To Monica from security, for your friendship and all the check-in conferences in the waiting for safe body temperature levels that daily boosted my motivation for work. To Zaida for all the caring support and for never forgetting to turning off my equipment on Saturdays. And also, to my upper floor neighbours, Susana Farinha and Carolina Lopes for being such great colleagues and friends.

My special thanks to my friends and colleagues, Patricia Morgado and Alexandre Friande, with whom I shared my entire masters journey. Thanks for being one true companions and unique human beings and for all the adventures shared, certainly more are waiting just around the corner.

I would like to acknowledge and express my sincere gratitude to Calouste Gulbenkian Foundation for supporting me throughout my entire academic journey, from the BSc in Biochemistry until the completion of the MSc in Pharmaceutical Engineering.

A special recognition to all my teachers that provided me the tools to grow and pursue my dreams. A special thanks to Edite Jubilot, the best teacher and a friend of every occasion.

A special line dedicated to my sweetest friend Marta Gato for our precious friendship that will certainly last a lifetime, and another to Pedro Cipriano a great person and a friend whom I much treasure.

Most importantly, my heartfelt thanks are owed to my family. My mother and my father for all the love, understanding and sacrifices made. To my grandparents, thank you for encouraging me to be myself and always fight for what I believe in. And last but not least, to my three younger sisters Mariana, Ana and Diana for their love and caring, for their patience during the last five years, for tolerating long hours away from them and still encouraging me to keep moving forward. Without their support, the completion of this thesis and all my academic achievements would not have been possible.

This page was intentionally left in blank.

Abstract

Purpose: Development of a novel miniaturized screening methodologies to study the dissolution behaviour of amorphous solid dispersions (ASDs) prototypes and identify the most promising candidate in terms of maximum drug exposure resulting from dissolution.

Method: The solubility challenges posed by poorly water-soluble compounds can be overcome, during early stages of development of oral dosage forms, by formulating amorphous solid dispersions (ASDs), a drug delivery strategy that allows drug solubility and bioavailability enhancement. Hence, it is of most importance to evaluate the overall performance of ASD formulations, as well as their physical stability since they are thermodynamically metastable. Dissolution testing is a valuable screening tool for selecting the most promising drug-polymer combinations based on their dissolution behaviour. This project consisted in the proof of concept of a novel miniaturized High-throughput screening (HTS) dissolution methodology that can be applied to early screening of ASDs. Two distinct methods were developed for the preparation of ASD films, by solvent evaporation and fusion-based methods, on the surface of a deposition platform fitted to the wells of a 24-well quartz microplate. Dissolution of these films was monitored by UV-Vis absorbance measurements in a microplate reader. To implement the method, Indomethacin (IND) was chosen as model drug and combined at four distinct drug loads (30%, 50%, 60% and 80%) with a pool of eight pharmaceutically relevant polymers (HPMCAS-HF, EUDRAGIT EPO, EUDRAGIT L100-55, PVP K29/32. KOLLIDON K30, COPOVIDONE K28, HPMC E3, HPMC E5) to form ASD films. Thermodynamic and Kinetic solubilities of IND were estimated by the shake-flask method and by a UV extinction method used for liquid-liquid phase separation (LLPS) onset determination, respectively. The dissolution studies of IND ASD prototypes were performed in Phosphate Buffer solutions (PBS) at pH 2.0 and at pH 6.8, via microplate reader, at 37ºC, during 12h, under constant agitation. Biorelevant dissolution studies comprising a media transition from FaSSGF at pH 1.6 to FaSSIF at pH 6.5, were conducted to provide a closer insight on in vivo performances. Additionally, Dynamic Light Scattering (DLS) was used to monitor the molecular species formed in solution during dissolution of IND/HPMCAS-HF and IND/EUDRAGIT EPO amorphous films with 50% drug load in PBS at pH 2.0, whereas Confocal Raman Microscopy (CRM) was applied to evaluate uniformity of deposition and phase separation within the ASD film. The scans of areas representative of the entire film surface were compared to Raman spectra of IND, HPMCAS-HF and EUDRAGIT EPO to produce Colour Bitmaps illustrative of the components' distribution within the film.

Results: The thermodynamic and kinetic solubilities of IND in PBS at pH 2.0 estimated were 3.80 µg/mL and 27.59 µg/mL, respectively, depicting a solubility enhancement (Rs) of 7.3. By using PBS at two different pH values (pH 2.0 and pH 6.8), one above and other below the pKa of Indomethacin ($pKa_{(IND)}$ = 4.5), it was possible to study the dissolution behaviour of ASD prototypes as a function of pH and evaluate the impact of the ionization state and solubility of the drug on the dissolution profiles obtained. The effect of medium pH over polymers was also investigated, with cationic polymers (e.g. EUDRAGIT EPO) yielding a great

performance at pH 2.0 and anionic polymers (e.g. HPMCAS-HF) depicting better performance at more alkaline pH values. The biorelevant testing in FaSSGF at pH 1.6 and FaSSIF at pH 6.5, resulted in two-step curve dissolution profiles with ASD prototypes depicting a strong dissolution rate upon transition to pH 6.5, which reflects the higher solubility of IND, at this pH. The DLS analysis supported the formation of a new drug-rich colloidal phase during dissolution in PBS at pH 2.0, by revealing the presence of molecular species sized within the range of 100-350 nm at maximum drug concentration. At the end of the dissolution run larger particles were detected indicating the formation of small drug crystals aggregates. The CRM analysis depicted a reasonable overall uniformity of deposition, despite the micro-scale discontinuities detected. Molecular homogeneity was further confirmed upon correspondence of the characteristic Raman shifts of API and polymers in the average spectra taken from a pixel point of the area scanned.

Conclusion: The outcome of this project was the development of a fast, cost-effective and reproducible miniaturized dissolution screening approach that can be applied to a wide variety of drug-polymer systems and provide reliable information to support decision making when selecting the best ASD candidates.

Keywords: Miniaturized screening methodologies, Amorphous solid dispersions (ASD), Bioavailability, Performance, Dissolution testing, High-throughput screening (HTS), Indomethacin (IND), Kinetic solubility, Liquid-liquid phase separation (LLPS), Biorelevant dissolution, Dynamic Light Scattering (DLS), Confocal Raman Microscopy (CRM)

Resumo

Objectivo: Desenvolvimento de novas metodologias de triagem miniaturizadas para estudo do processo de dissolução de protótipos de dispersões sólidas amorfas (ASDs) e identificação dos candidatos mais promissores em termos de exposição máxima de fármaco em resultado da sua dissolução.

Método: Os desafios inerentes à fraca solubilidade de alguns compostos em água podem ser superados, durante as primeiras fases de desenvolvimento de formas farmacêuticas para administração por via oral, através de dispersões sólidas amorfas (ASDs), uma estratégia de administração de fármacos que permite melhorar a solubilidade e consequentemente a biodisponibilidade dos fármacos. Assim, é da extrema importância avaliar o desempenho global das formulações de ASD, bem como a sua estabilidade física, uma vez que são termodinamicamente metaestáveis.

Os testes de dissolução são uma valiosa ferramenta de rastreio para seleção das combinações API-polímero mais promissoras com base no seu comportamento de dissolução.

Este projecto consistiu na prova de conceito de uma nova metodologia de dissolução de HTS (*High-throughput screening*) miniaturizada que pode ser aplicada ao rastreio de protótipos de ASD em fases iniciais de investigação e desenvolvimento. Esta metodologia envolve a preparação de filmes ASD, por métodos baseados na evaporação de solvente ou por fusão, na superfície de platformas de deposição idealizadas para caber em poços de uma microplaca de quartzo. A dissolução destes filmes amorfos foi monitorizada por espectroscopia UV-Vis num leitor de placas.

Para testar a implementação do método, a Indometacina (IND) foi escolhida como fármaco modelo tendo sido combinada em quatro proporções distintas (30%, 50%, 60% e 80%) com um conjunto de oito polímeros farmacologicamente relevantes (HPMCAS-HF, EUDRAGIT EPO, EUDRAGIT L100-55, PVP K29/32. KOLLIDON 30, COPOVIDONE K28, HPMC E3, HPMC E5) para formar filmes ASD.

As solubilidades termodinâmica e cinética da IND foram estimadas pelo método de *shaking flask* e pelo método de extinção UV-Vis utilizado para determinação do início da separação de fases líquido-líquido (LLPS), respectivamente. Os estudos de dissolução dos protótipos de ASD contendo IND foram realizados em soluções tampão fosfato (PBS) a pH 2.0 e a pH 6.8, num leitor de microplacas, a 37ºC, sob constante agitação.

Foram realizados estudos de dissolução biorelevantes, compreendendo uma transição dos meios FaSSGF a pH 1.6 para FaSSIF a pH 6.5, a fim de proporcionar uma visão mais próxima do desempenho in vivo.

Além disso, Dispersão de Luz Dinâmica (DLS) foi utilizada para monitorizar as espécies moleculares formadas em solução durante a dissolução em PBS a pH 2.0, enquanto que o Microscopia Confocal de Raman (CRM) foi aplicada para avaliar a uniformidade da deposição do filme e ocorrência de fenómenos separação de fases dos componentes do filme.

Resultados: As solubilidades termodinâmica e cinética da IND em PBS a pH 2.0 foram de 3.8 µg/mL e 27.59 µg/mL, respectivamente, representando um aumento da solubilidade (R_S) de 7.3.

A utilização de PBS a dois valores de pH distintos, um acima e outro abaixo da pKa da Indometacina (PBS a pH 2.0 e pH 6.8), permitiu o estudo do comportamento de dissolução dos protótipos de ASD em função do pH e avaliação do impacto do estado de ionização e solubilidade do API nos perfis de dissolução obtidos. Também foi investigado o efeito exercido pelo pH do meio no comportamento dos polímeros, sendo que os polímeros catiónicos (p.e. EUDRAGIT EPO) registaram um grande desempenho a pH 2.0 enquanto que os polímeros aniónicos (p.e. HPMCAS-HF) apresentaram um melhor desempenho a valores de pH mais alcalinos.

Os testes de dissolução biorelevante em FaSSGF a pH 1.6 e FaSSIF a pH 6.5, resultaram em perfis de dissolução com duas fases, em resultado de uma alta taxa de dissolução aquando da transição de pH 1.6 para pH 6.5, o que reflecte a maior solubilidade da IND nesta gama de pH.

A análise DLS apoiou a formação de uma nova fase coloidal rica em IND, durante a dissolução de filmes amorfos de IND/HPMCAS-HF e IND/EUDRAGIT EPO com 50%(w/w) em PBS a pH 2.0, revelando a presença de espécies moleculares com tamanho entre 100-350 nm em solução. No final da dissolução foram detectadas partículas maiores, indicando a formação de pequenos agregados de IND na forma cristalina.

A análise CRM dos protótipos ASD de IND/HPMCAS-HF e IND/EUDRAGIT EPO preparados pelos métodos de evaporação de solvente e fusão, confirmou uma uniformidade geral de deposição razoável, apesar das descontinuidades detectadas em microescala. Os scans de uma área representativa de toda a superfície do filme foram comparados aos espectros Raman de IND, HPMCAS-HF e EUDRAGIT EPO para produzir mapas coloridos ilustrativos da distribuição dos componentes no filme. A uniformidade de distribuição foi ainda confirmada mediante correspondência entre picos de Raman caracteristicos da IND e dos polímeros nos espectros conjuntos correspondente a um ponto da área digitalizada.

Conclusão: O resultado deste projecto foi o desenvolvimento de uma metodologia de dissolução miniaturizada rápida, rentável e reprodutível que pode ser aplicada a uma grande variedade de APIs e polímeros e fornecer informação fiável para apoiar a tomada de decisões aquando da selecção dos melhores candidatos a ASD.

Keywords: Metodologias de triagem miniaturizadas, Dispersões sólidas amorfas (ASD), Biodisponibilidade, Desempenho, Testes de dissolução, High-throughput screening (HTS), Indometacina (IND), Solubilidade cinética, Separação de fase líquido-líquido (LLPS), Dissolução biorrelevante, Dispersão de Luz Dinâmica (DLS), Microscopia Confocal de Raman (CRM)

Contents

This page was intentionally left in blank.

List of Figures

List of Tables

Acronyms

ACN	Acetonitrile
AFM	Atomic force microscopy
API	Active Pharmaceutical Ingredient
ASD	Amorphous solid dispersion
BCS	Biopharmaceutical Classification System
CRM	Confocal Raman Microscopy
CCD	Charge-coupled device
COPOVIDONE	Polyvinylpyrrolidone vinyl acetate copolymer, PVP/VA
COX	Cyclooxygenase
CRR	Cosmic Ray Removal
DISPO	Digital Smoothing Polynomial
DL	Drug load
DLS	Dynamic light scattering
DSC	Differential Scanning Calorimetry
EUDRAGIT EPO	Dimethylaminoethyl methacrylate, butyl methacrylate, methyl methacrylate copolymer, Amino methacrylate copolymer
EUDRAGIT L100	1:1 Methacrylic acid and methyl methacrylate copolymer, Methacrylic acid copolymer
EVAP	Solvent evaporation method
FaSSGF	Fasted state simulated gastric fluids
FaSSIF	Fasted state simulated intestinal fluids
FTIR	Fourier-transform infrared spectroscopy
FUS	Fusion method
GIT	Gastrointestinal tract
HME	Hot Melt Extrusion
HPLC	High performance liquid chromatography
HPMC	Hydroxypropyl methylcellulose
HPMCAS	Hydroxypropyl methylcellulose acetate succinate
HPMC E3	Hydroxyl propyl methylcellulose 3cP viscosity, METHOCEL E3
HPMC E5	Hydroxyl propyl methylcellulose 5cP viscosity, METHOCEL E5
HTS	High throughput Screening
IND	Indomethacin
IP	Intellectual Property
IVIVC	*In vitro–in vivo* correlation
KOLLIDON 30	Polyvinylpyrrolidone, PVP K30

LLPS	Liquid-liquid phase separation
LOQ	Limit of quantification
NCE	New chemical entity
NSAID	Non-steroidal anti-inflammatory drug
PBS	Phosphate Buffer Solution
PVP	Polyvinylpyrrolidone, Povidone
RH	Relative Humidity
RI	Refractive Index
R&D	Research and Development
RSD	Relative Standard Deviation
SARS-CoV-2	Severe acute respiratory syndrome coronavirus-2
SCF	Supercritical Fluid
SD	Spray Drying
SDDS	Supersaturating Drug Delivery Systems
SDS	Sodium dodecyl sulfate
SG	Savitzky-Golay filter
SIF	Simulated Intestinal Fluid
SPADS	Screening of Polymers for Amorphous Drug Stabilization
STD	Standard Deviation
Sub BG	Subtract Background
UHPLC	Ultra High Performance Liquid Chromatography
UPLC	Ultra Performance Liquid Chromatography
UV-Vis	Ultraviolet-visible
XRPD	X-Ray Powder Diffraction

List of Symbols

Abs	Absorbance
a.u.	Arbitrary units
C	Concentration
ºC	Degree Celsius
C_{max}	Maximum concentration
$CaCO_3$	Calcium carbonate
x g	Gravitational force
ΔG	Gibbs Free Energy
h	Hours
HCl	Hydrochloric Acid
ΔH_{fus}	Enthalpy of fusion
H_2O	Water
H_3PO_4	Phosphoric acid
l	Optical path length
m	Mass
MeOH	Methanol
min	Minutes
M_w	Molecular Weight
NaCl	Sodium chloride
$NaH_2PO_4.H_2O$	Sodium dihydrogen phosphate monohydrated
Na_2HPO_4	Disodium hydrogen phosphate
NaOH	Sodium hydroxide
R	Gas constant
rpm	Rotation per minute
R_s	Apparent solubility ratio
t	Time
T	Temperature
T_g	Glass transition temperature
T_k	Kauzmann temperature
T_m	Melting point, Melting temperature
λ	Wavelength
λ_{max}	Maximum absorbance wavelength
ε	Extinction Coefficient; Molar absorption coefficient

1. Introduction

1.1. Solubility as performance game changer

The up growing investment in R&D in the pursuit of new and innovative medicines has been fueling Pharmaceutical Industry evolution and making it thrive along the years, causing it to reach the forefront of scientific and technological advancements at a worldwide level. [1]

In the demand for innovation, pharmaceutical companies screen thousands of new chemical entities (NCEs) during early stages of development, in the hope of finding novel therapies or even cures for diseases.[2]

According to recent reports, the number of novel chemical entities with low solubility issues, has grown from 40% to around 70%, which lead to the rise of several concerns regarding performance and manufacturability. Poor aqueous solubility has become an enduring problem, owing its increasing prevalence among new drug candidates to the flourishing implementation of High-throughput screening (HTS) approaches, combinatorial chemistry and computational drug design which often prioritize hydrophobicity as driving force for drug-receptor binding.[3–9]

Poor aqueous solubility is indeed one of the major challenges to be overcome by formulation scientists in the early stages of development, since it usually implies slow dissolution rates and lead to low bioavailability, which results in a limited therapeutic efficacy and unsatisfactory clinical outcomes after oral administration.[2, 10, 11]

In 1995, Amidon et al. launched the biopharmaceutical classification system (BCS), a useful decision-making tool, which aided R&D scientists to classify NCEs under four different categories, according to their aqueous solubility and gastrointestinal permeability. Chemical entities categorized under BCS Class II exhibit poor aqueous solubility but a good membrane permeability while drug substances attributed to BCS Class IV lack on both aspects. It is noteworthy that the BCS classification system has been used in pharmaceutical industry to underpin waivers of in vivo bioavailability and bioequivalence studies, which are provided by the regulatory agencies and health organizations for innovative drug products, allowing significant savings in total expenses associated with research and development. [5, 7, 9–14]

Solubility is one of the main factors limiting the dissolution process. Alongside with other parameters such as solid state characteristics, particle size and medium pH, solubility of a drug compound influences the dissolution process, directly impacting the extent to which the drug substance enters solution and progresses under physiological conditions.[11, 16] The entire absorption process may, therefore, be affected mainly in terms of speed and concentration at which the drug attains the target site to initiate a therapeutic response. Thus, in some cases, therapeutic concentrations of the drug in the plasma would not be reached unless an escalation of the dose administered was performed, which could compromise safety, lead to

toxicity issues and negatively affect patient adherence to treatment. As a result, poorly soluble new drug candidates either fail to reach the market or to achieve their maximum potential. [2, 7, 8, 12–17, 22]

On the other hand, the highly lipophilic character of these NCEs offers some great advantages as it tends to promote efficient interaction with target receptors (biological membranes or membrane-associated proteins with lipophilic domains), to convey the ability to pass through biological membranes and to enable reversible binding to lipid carriers circulating in the bloodstream (such as albumin, lipoproteins, blood cells, etc.), which perform transportation/distribution of these compounds throughout the organism. Hence, the major challenging aspect around these compounds is formulation into a delivery platform that allows oral administration, which is by far the most preferred route of administration due to the many advantages conveyed such as convenience, good patient compliance, ease of administration and competitive manufacturing costs, just to mention a few. [7, 8, 13, 15–17,19–21]

Despite all the disadvantages that some of NCEs physicochemical properties may bring, these same properties can also grant these compounds unique features in terms of application and therapeutic potential, making them an object of interest to the pharmaceutical industry. [10,]

Hence, the way of engineering poorly soluble APIs into drug products with ideal performance is through the improvement of both production process and formulation, consisting on the optimization of key parameters that limit bioavailability, such as physicochemical properties of the drug (e.g. solubility), pharmaceutical properties of the formulation and/or the method used to prepare the dosage form, in order to obtain a different form of the same drug ideally owning an improved pharmaceutical performance. [2, 5, 9, 25]

1.1.1. Solubility Enhancing Strategies

Drug solubility is defined as the amount of drug that is present in solution when an equilibrium is established between the drug solute in solution and any excess of undissolved drug to produce a saturated solution at a specified temperature. The equilibrium solubility of a drug compound will depend on its relative affinity towards solvent molecules and other solute molecules. Thus, solubility is affected by the strength of molecular interactions established such as ionic, van der Waals, dispersion and hydrogen bonding interactions. On the other hand, equilibrium solubility is also influenced by the properties and nature of those interactions occurring either in the solid state or in solution state. [3, 12, 25]

Accordingly, with the aim of further exploring the potential of new chemical entities with poor solubility, a wide number of strategies have been investigated in the past few decades consisting on the modification of solution state or solid state properties to overcome solubility challenges, including: solubilisation techniques and supersaturating drug delivery systems (SDDS), see Figure1. [3,7,12,15,26–28]

Modifications in the solution state can be accomplished by solubilisation strategies such as altering solution pH or using additives like co-solvents, surfactants, complexing agents (e.g., Cyclodextrins) and/or lipids in

the formulation to effectively increase the amount of drug dissolved or dispersed in water. Unfortunately, these systems sometimes lead to decreases in drug effective permeability and flux across membranes as a result of lowered concentrations of free drug. [3, 7, 12, 14, 27, 28]

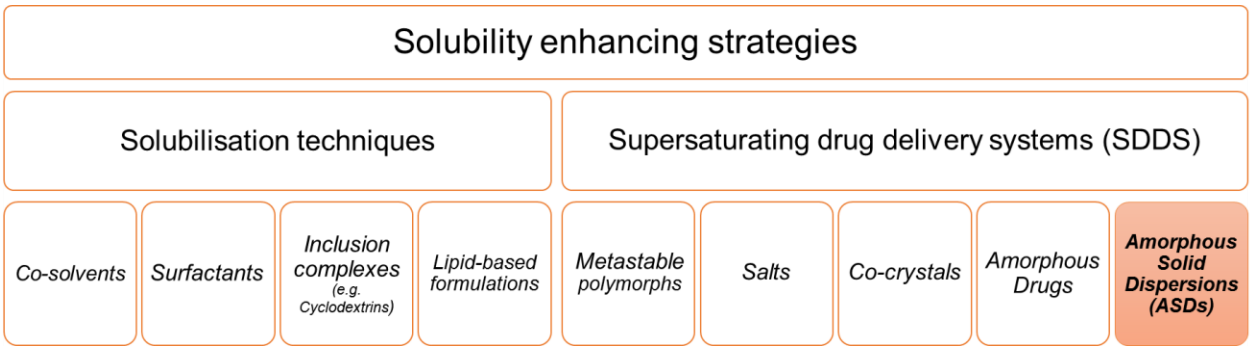

Figure 1. *Solubility enhancing strategies: schematic representation.*

On the other hand, supersaturating delivery systems, able to generate concentrations higher than the thermodynamic solubility of the crystalline drug without compromising effective permeability across membranes, can be accomplished through solid-state modification techniques. The main disadvantage of these systems is that supersaturated solutions are metastable and tend to fall back to equilibrium via crystallization (unless crystallization inhibitors are added to the formulation). [3, 7, 12, 14, 15, 28]

The most relevant SDDS with the potential to generate supersaturated solutions are metastable polymorphs, salts, co-crystals, amorphous drugs, and amorphous solid dispersions (ASDs). [3, 12, 14, 15, 26, 28]

Polymorphism is the ability of a certain compound to exist in different crystalline structures, due to differences in packing arrangement and/or in molecular conformation. Metastable polymorphs have higher crystal lattice energy, lower stability, and higher solubility compared to the thermodynamically stable form. Despite the improved solubility of metastable polymorphs, solubility enhancement ratios are relatively moderate. Similarly to amorphous drugs, the biggest problem associated with the use of the metastable polymorphs is the risk of evolving to the lowest energy state, by conversion into the most stable crystalline form, over time or after exposure to heat or humidity, which leads to a decrease in solubility. [3, 11, 14, 23, 25–27]

Another strategy to enhance solubility is the formation of crystalline salts. When conjugated with a counter ion, acidic or basic drugs, form a solid crystalline structure that dissolves significantly faster than the free drug and that, upon dissociation in an aqueous solution, releases the drug in a highly soluble ionized form. The solubility enhancement of crystal salts strongly depends on dissolution medium pH, since it dictates the degree of ionization of the drug molecules. The difference in pH between the surface of the dissolving salt and the bulk of the solution cause higher concentrations at the unstirred diffusion layer leading to a rapid dissolution rate. [3, 8, 12, 14, 15, 26, 28]

Another type of supersaturating drug delivery systems are co-crystals, crystalline molecular complexes of two or more neutral molecules that combine the stability advantages of crystalline solids with the solubility benefits of high energy solids. The mechanisms by which co-crystals enhance solubility are not completely understood yet. Nonetheless, there is general agreement on the critical role of the co-former physicochemical properties on the overall rate of dissolution. The higher supersaturation state attained upon co-crystal dissolution is due to a quick release of the co-former from the co-crystal lattice and to cluster formation. These clusters consist of supramolecular aggregates of randomly oriented molecules, which behave similarly to amorphous materials, depicting improved dissolution and solubility properties. Even though co-crystals are able to generate high drug concentrations rapidly, they tend to dissociate in solution, converting to a more stable and less soluble crystalline form. Hence, with time it is possible to observe a decay in drug concentration caused by these phase transformations. It is noteworthy, the conversion kinetics may be delayed with the addition of excipients to the co-crystal formulation. Co-crystal formation has several potential advantages over other solid-state modification techniques. [3, 8, 12, 14, 15, 28, 31, 32]

The production of drug compounds in its amorphous form is, sometimes, enough to overcome solubility issues. Structurally, compounds in the solid state can be either in the crystalline or amorphous state. The crystal form is characterized by a three-dimensional long-range order of molecular arrangements in the crystal lattice, whereas the amorphous form lacks on structural order and reveals no translational periodicity in the molecular arrangement. That entails excessive thermodynamic properties, such as enthalpy, entropy and Gibbs free energy, as well as other physical properties like volume and viscosity. As a result, the amorphous state exhibits higher solubility, chemical reactivity and water vapor sorption. However, the amorphous state is a metastable state with inherent thermodynamic instability, hence with high tendency to revert to their most stable crystalline state which often results in precipitation upon dissolution in aqueous media, losing the amorphous solubility advantages. Moreover, the bigger the difference in free energy between the amorphous and crystalline state the higher is the driving force for recrystallization. [3, 8, 12, 14, 15, 28, 33–48]

To overcome this issue, amorphous solid dispersions (ASDs) are often considered during early stage formulation development as a solubility enhancing strategy for poorly water soluble drugs. This formulation strategy consists in the addition of polymeric matrices to the drug in the amorphous form, with the aim of improving amorphous drug physical stability and avoid or delay recrystallization. [3, 8, 12, 14, 15, 21, 28, 49, 50]

1.2. Amorphous solid dispersions

Amorphous solid dispersions (ASDs) are in the forefront of drug delivery, being one of the most widely used solubility enhancing strategies to overcome the limited bioavailability of poorly water soluble APIs. These solid dispersions are composed by an amorphous drug compound and a hydrophilic polymer counterpart that together form an amorphous single phase thus, combining the apparent solubility advantage of the high

energetic amorphous form with the improvements in dissolution rate and stability that result from the incorporation within a polymeric matrix. [9, 50]

The conversion of a crystalline solid drug into an amorphous form is per se an alternative to overcome solubility-rooted issues due to its improved solubility in relation to the crystalline form, as a result of the crystal lattice disruption, which makes it energetically more favourable for the amorphous solid to dissolve. However, the amorphous form is thermodynamically metastable and has a high driving force to revert back to the lowest energy ground state, through crystallization, losing the advantage of greater solubility. [9]

The addition of a polymer counterpart is a stability advantage since it avoids or delays drug crystallization from the high energy solid which could occur during storage or when amorphous drugs are dissolved in aqueous media, with crystallization occurring from supersaturated solutions and/or from the surface of the dissolving amorphous material. The polymers owe their stabilization capacity to their high molecular weight and high entropy. They form a matrix around the drug molecules, reducing the likelihood of molecular motion. Despite different mechanisms have been discussed, the explanation behind solid dispersions stabilization effect over amorphous solids is still not fully understood. [9 ,51–53]

Also chemical stability is equally important to achieve an ideal amorphous solid dispersion. Since the amorphous form exhibits higher chemical reactivity than the crystalline form, it is of most importance to assure that the polymer and any other excipients present in the formulation do not chemically interact with the drug compound. Drug and polymer must exhibit high compatibility, otherwise the stabilization of the drug will not be effective and the probability for recrystallization to occur will increase. [9 ,51–53]

The miscibility of the drug-polymer ASD is a prerequisite for maintaining stable binary ASDs formulations. Miscible drug-polymer combinations are more resistant to drug crystallization than the amorphous drug alone as the chemical potential of the drug is reduced and the kinetic barrier or activation energy to crystallization increases. If miscibility between drugs and polymer happens to be poor, phase separation from the supersaturated solid dispersion may occur, ultimately leading to precipitation of the drug from the initially homogeneous solid solution, during storage. Poor miscibility leads to phase separation, since small drug-rich domains are more likely to precipitate than homogenous drug/polymer solid solution regions. Such occurrence is more prevalent in ASDs with high drug loadings or for those under extreme conditions of heat and moisture. [9 ,51–53]

Strong Intermolecular forces established between drug and polymer, such as hydrogen bonding and ionic interactions, have been considered as critical in ASD stabilization and maintenance of a homogenous phase. [9 ,51–53]

Another advantage of the polymeric drug-carriers is their ability to enhance the dissolution rate and extent of drug release. That is because the expansion of the polymer matrix increases the surface area of amorphous drug which is in contact with the solvent and promotes its impregnability fostering dissolution. [9 ,51–53]

To generate and maintain supersaturation, two conditions must be met: the compounds must be administered as solid-state forms of higher "apparent" or kinetic solubility than the correspondent thermodynamically stable form, and the dissolution rate has to be higher than the rate of precipitation/crystallization. [9 ,51–53]

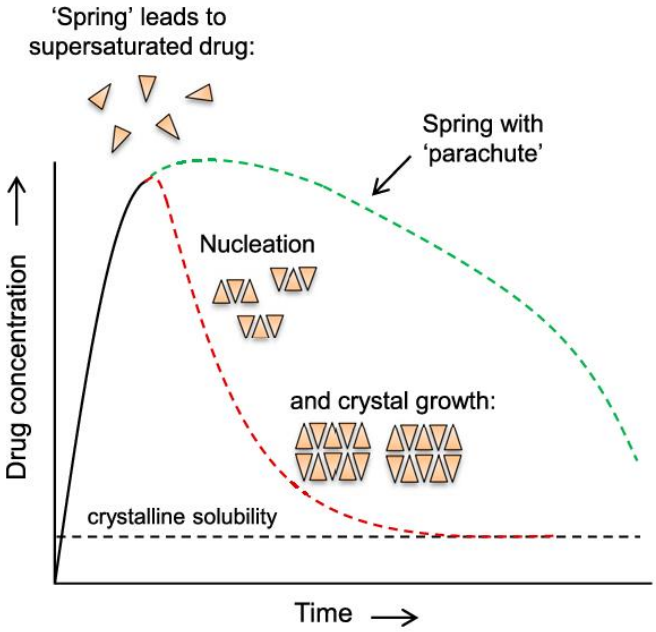

***Figure 2**. Concentration-time profiles obtained upon dissolution of an amorphous drug (red dashed line) and of an amorphous drug comprised in a polymeric matrix (green dashed line). Sourced from the article Williams et al. 2013* [26]

Upon dissolution of the high energy solid (see Figure 2), a steep concentration increase known as the "spring" effect is observed and a supersaturated solution is typically generated. However, drug starts to precipitate soon after due to the high tendency to revert back to a more stable state, which leads to concentrations falling back to equilibrium crystalline solubility. In order to benefit from the supersaturated state generated, the formulation must be able to maintain it during a time period long enough for absorption to occur. Hence, the addition of a polymer is required so that a strong precipitation inhibition can be provided and nucleation and crystal growth can be delayed, resulting in a ''spring-parachute effect'' in the dissolution profile. [9, 26, 51–53]

1.2.1 ASD preparation methods (laboratory and industrial scale)

Nowadays, there are plenty of techniques at our dispose to produce ASDs. At a laboratorial scale the most common are solvent-casting and melt-fusion, followed by solvent-shift, co-precipitation, spin coating, freeze drying (lyophilization), among others. The solvent evaporation processes like solvent casting essentially involves drug and polymer dissolution in organic volatile solvent and a subsequent heating step to promote quick evaporation of the solvent to form a solid dispersion. On the other hand, fusion-based methods consist

on the fast cooling of a liquid melt so that the solid dispersion components manage to acquire an amorphous form and join to form a single-phase solid dispersion. [50]

Concerning large-scale production, both physical and chemical methods can be used. The main difference between those approaches is that in physical methods the composition of substances does not change during the transition, while in chemical methods some changes in chemical potential of the system may occur. Some of the most common processes of amorphization are: Spray drying (SD), Hot melt extrusion (HME), Freeze drying, Supercritical Fluid technique (SCF), Wet polishing, Jet Milling, Co-precipitation, Spray congealing.[27] [5, 34–36]

Among the existing methods to produce ASDs, SD and HME are by far the most widely used. Both techniques are well established in the pharmaceutical industry, compatible with continuous manufacturing processes and effective for improving the bioavailability of poorly soluble drugs. The choice between SD or HME along with the specific polymers to be used in a given ASD formulation depends on the properties of the API and the desired characteristics to be featured on the final drug product.[2, 54–61, 62–67]

SPRAY DRYING

Spray drying is a very powerful technological process with increasing popularity among the scientific community due to its high productivity and wide spectrum of applications. The technique consists on the transformation of a liquid feed solution from a fluid state into a dried particulate form based on the elimination of solvent by spraying the liquid feed into a gaseous hot drying medium. Moreover, spray drying offers the ability to use different feedstock and enables the production of composite materials as well as free-flowing particles with well-defined particle size. It is a process of relative simplicity and ease of operation and offers the possibility for large-scale production even though the optimization of process parameters is often a costly and time-consuming procedure.[56–61,68] The process is developed inside a spray dryer and general working principle is solvent removal by application of heat to the product and controlling the humidity of the drying medium. The overall spray drying process can be summarized in the following steps:

(1) Atomization: A liquid feed solution is pumped to an atomizer, suffering atomization into a spray of small droplets due to a decrease of surface tension, in order to increase surface area. [56–61,68]

(2) Spray – hot air contact: The fine droplets are sprayed into a heated atmosphere chamber to promote solvent evaporation. The direct contact of the spray droplets with a hot drying gas leads to an improved drying rate. [56–61,68]

(3) Solvent Evaporation: As soon as the droplets contact with the drying gas within the chamber, they undergo evaporation and solute condensation, resulting in dried particles due to solvent removal. [56–61,68]

(4) Particle collection: Once the droplet-to-particle conversion is concluded, it is necessary to collect the dried particles. This implies a two-phase separation procedure, in which the dried particles are disassociated

from the drying gas. In a primary separation, the densest particles are recovered at the conical bottom of the drying chamber, as they settle. On a second separation phase, the finest or smallest particles are transferred to external devices, where they are separated from the saturated air. [56–61,68]

HOT MELT EXTRUSION

Hot melt extrusion (HME) is another promising technology for the production of ASDs and other sorts of pharmaceutical drug delivery systems for conveying many advantages in terms of enhancement of solubility and bioavailability of poorly water-soluble compounds, taste masking, and modifying release. It is a continuous solvent-free, cost-effective and very efficient process. HME is easily scalable and offers the possibility to be coupled with other continuous manufacturing platforms and to be monitored inline for product quality purposes. HME has been gathering increasing attention since it enables the production of dosage forms with a specific desired shape and release profile and is extremely useful in cases of high drug loading formulations. In addition, it is also environmentally friendly, having a small ecological footprint at an industrial scale. The principal limitations regarding HME implementation are the large amounts of API required to develop an optimal process and the potentially high processing temperatures and high energy input, which may induce thermal degradation and/or affect the stability of hot melt-extruded products in the short and long term, leading to poor physical stability and precipitation from supersaturated solutions while in the GI tract. Hence, thermolabile compounds or compounds with high melting point are not suitable for HME. Studies on the physicochemical properties, nature of the extrudate products, and use of appropriate additives may overcome these issues to a certain extent. Likewise, effective strategies and experimental designs are also very important to manage product quality matters.[62–67]

The HME process consists on feeding the formulation components into an extruder, which are then transferred into a heated barrel by using a screw system. Subsequently, one of the components, usually the polymer, is submitted to a temperature above its Tg for softening and then, the drug compound is dispersed onto the polymer matrix for melting and/or dissolution. Then, the rotating screws perform the mixing step. If good drug-polymer miscibility is ensured and adequate mixing is provided, the result is a single molten phase, consisting on a homogenous viscous liquid of drug and polymer, which is then extruded through a die, cooled, and when in the form of a solid dispersion phase, subjected to downstream processing. [62–67]

1.3. State-of-the-art on miniaturized High-throughput screening methodologies

Independently of the manufacturing process considered for generation of ASDs, selection of the formulation components and ratios is critical in early-stage development since product performance will be greatly dependent on these. The main goal of an ASD screening program is to find the best drug-polymer combination that yields good in vivo performance and provide benefit to the patient. [69]

This selection is always dependent on the API in a case-by-case decision. Since the type of pharmaceutically relevant polymers available is high and the possibilities for drug-polymer combinations

and drug loads is great, the experimental workload associated with the selection of the best formulation candidate can sometimes be overwhelming and impractical for the typical tight development timelines. [5, 69, 70]

Hence, a successful ASD screening program aims to cover a broad experimental design space using the least API quantity possible and to be able to conduct a large number of experiments simultaneously, preferably using an automated system, in a short period of time. [5, 69, 70]

A complete miniaturized high throughput ASD screening program contemplates two major steps:

- Production of ASD prototypes at miniaturized scale [69]
- Characterization of ASD prototypes under study regarding *in vitro* performance (e.g. supersaturation potential; dissolution behaviour, kinetic solubility) and physical stability (e.g. tendency to crystallize, molecular interactions, phase separation, miscibility). [69]

The output of a miniaturized ASD screening should be a ASD formulation that is able to preserve the amorphous state over the entire product shelf life and capable of assuring generation and maintenance of a supersaturated state during dissolution to enhance API bioavailability and absorption. [5, 69, 70]

For a long time, the quest for the ideal drug-polymer formulation consisted of low-throughput screening approaches, essentially trial and error experiments sustained by current knowledge and empirical experience of researchers. [5, 69, 70]

The ever growing competition in the Pharmaceutical market demanding for fast turnaround times, higher profit margins and lower risks associated with new drug products, led to an increasing interest in deepening the knowledge on ASD formulations, leading to an increasing need for testing as many combinations as possible and, therefore, to invest in the development of novel and faster screening methodologies for shortening the time from lab to large-scale production. [5, 69, 70]

Hence, low-throughput screening methodologies soon proved to be inefficient, costly, time-consuming and API demanding, since normally would require expenditure of huge amounts of API only to test a few drug-polymer combinations, limiting the screening process. [5, 69, 70]

Propelled by scientific and technological advances, several experimentally-based medium to high-throughput ASD screening programs have been implemented to aid narrowing the scope of drug-polymer formulations, selecting the most adequate drug loading and facilitate ASD performance evaluation while coping with workload demands and API quantities required to perform such studies. [5, 69, 70]

Recently, considering all the great advantages conveyed by High-throughput screening (HTS) technologies, some miniaturized ASD screening methodologies have been disclosed in the literature, consisting of improved versions of some existing HTS methodologies or as new approaches capable of bringing API requirements to minimum levels, in the order of milligrams, while still enabling multiple experiments to be

run simultaneously recurring to lab-based equipment. The implementation of miniaturized approaches for ASD screening are highly recommended and can add great value to ASD development, particularly at early stages of formulation development, when availability of API is limited. [5, 69, 70]

They allow fast analysis of ASD formulation using minimal API quantities and allow exploration of a vast pool of polymer candidates at different drug loads and distinct process conditions (e.g. temperature, pH, solvents, addition of extra components to the formulation, etc.) that can be evaluated and serve as guidance to scale up. Miniaturized approaches enable time and resources saving, demanding minimal API quantities and manpower. [5, 69, 70]

1.3.1. Summary of most innovative miniaturized screening programs in the literature

Over the last decade, there have been many technological advances in the scope of miniaturized High-throughput ASD screening, with new preparation techniques, more sophisticated equipment and novel devices being incorporated into screening programs. [69]

The miniaturized screening programs published in the literature encompass different ASD preparation methods and present distinct screening devices and analysis methods depending on the characterization intended to be performed.

The most common experimental preparation methods found in ASD miniaturized screening approaches are solvent casting (film casting) [71–84] and melt-fusion methods [33, 35–39], which are lab-scale approaches for screening of spray-drying and HME ASD candidates. Other preparation techniques with no direct industrial scale process equivalence have been included in miniaturized screening protocols, namely freeze drying (lyophilization) [37, 40–44], solvent-shift and co-solvent quench methods [95–103], co-precipitation[104], spin coating[105–108], among others.[19, 59]

Regarding solvent casting, the drug, polymer and eventually surfactant solutions are prepared using a suitable volatile organic solvent. The solutions are dispensed in various combinations and/or ratios followed by solvent evaporation to form films

The most referenced methods for ASD preparation, regarding miniaturized High-throughput ASD screening programs, are solvent casting methods. The solvent casting protocol initiates with the preparation of stock solutions of drug, polymer and eventually other excipients (e.g. surfactants) in a volatile organic solvent (e.g. acetone, methanol, ethanol), which are then dispensed into an appropriate vessel, being conjugated in countless combinations and/or ratios. Afterwards, the solvent is removed by evaporation to form films at the bottom of the vessel.[21, 22, 27 ,28, 30–32]

For solvent removal through evaporation some miniaturized assays make use of slightly slower approaches like a rotary evaporator [74] or a lab freeze dryer apparatus[83], while others opted for a vacuum dry system [21, 22, 27, 28, 32], a vacuum oven [79], or a stream of inert gas [80] (e.g. Nitrogen) to quickly evaporate the solvent.

For many of these miniaturized screening methodologies, the platform chosen to perform the preparation of ASD films by solvent casting in small scale was a 96-well microplate. [21, 22, 26–28, 30, 32]

Alternatively, Barillaro et al. reported solvent casting ASD preparations carried out inside 10 mL glass vials, using a Tecan robotic workstation to transfer the drug and polymer stock solutions.[81] Moreover, Lauer et al. published a solvent casting preparation based on glass slides [73], whereas Weuts et al. recurred to Teflon plates (15 x 15 cm^2) to perform the film casting process.[79]

The deposition platform chosen for preparation is usually suited to the type of characterization analysis intended to be performed. Hence, according to some articles on miniaturized screening programs, distinct characterization assays often require different ASD preparation methods and/or a distinct device to perform the preparation. [30, 33]

In a 2013 article, Wyttenbach et al. presented a 2-step screening program, named SPADS (Screening of Polymers for Amorphous Drug Stabilization), comprising three different miniaturized assays to study dissolution using UPLC, molecular interactions by FTIR and an Imaging assay to assess miscibility using AFM, each one featuring a different screening platform for ASD film preparation by solvent casting; 96-well microplates, 100 µL DSC aluminum pans and glass slides, respectively[80].

Likewise, Auch et al. presented miniaturized screening approaches using 96-well microplates to produce films by solvent casting method, whereas melt-based ASD films were formed inside DSC pans. Furthermore, this experimental approach also encompassed non-sink dissolution assays performed inside 2 mL round bottom Eppendorf caps to experimentally determine, by HPLC, the dissolution profile of each ASD prototype produced by Spray drying and HME, and establish a comparison with the results obtained from small-scale ASD production methods.[83]

Generally, during screening, polymers are evaluated in terms of physical stability and supersaturation potential, with the best candidates being selected to the next stages of development, whereas the less promising are eliminated along the screening program whenever the requirements are not met.

Often in these articles, miniaturized screening methodologies are conducted as a first screening of most promising ASD combinations. Thereafter, once the best polymer candidates, drug loading and processes are identified, the most suitable drug-polymer combinations advance to ASD lab-scale production or even industrial scale preparation (by Spray drying or HME), so that further in vitro and in vivo assessments on biopharmaceutical performance can be held, such as dissolution testing and biorelevant PK studies. The best prototypes can even be submitted to longer physical stability assays. [19, 26, 30]

For instance, in the previously mentioned SPADS approach by Wyttenbach et al., after submitting ASD prototypes to miniaturized dissolution, interaction and imaging assays, the ASD combinations studied under the scope of this screening program were further subjected to a 2-hour physical stability test involving exposure to stress conditions of temperature and humidity (40 ºC and 75% RH). Afterwards, the selected drug–polymer combinations were also prepared by spray drying and submitted to dissolution testing and to a 6-month physical stability study.[80]

Also, Mansky et al. and Shanghag et al. articles describe a newly developed method for a fast first screening procedure of ternary ASD formulations comprising drug, polymer and surfactant, based on ASD preparation by solvent casting and with high-throughput dissolution testing as characterization method, using 96-well microtiter plates for monitoring dissolution. [27, 28] The method started with the preparation of stock solutions in an organic solvent and their dispense in the wells of a 96-well microtiter plate in various combinations and ratios. After dispensing, the microplates were vortexed to promote a better mixture of the stock solutions and submitted to vacuum centrifugation at a defined set temperature and pressure, during 2.5 h, to evaporate the solvent. As a result of this procedure, ASD films formed at the bottom of each well (total mass ≈ 0.66 mg). The microtiter plates were sealed with adhesive foil and kept at room temperature overnight. The dissolution testing was performed in an aqueous dissolution medium (SIF at pH 6.8) under orbital shaking. After 1h incubation at room temperature, the contents of each microplate well were transferred to a membrane filter plate and vacuum filtered through the bottom filter. The resultant filtrates were then collected in a Varian collection plate. The filtrates were then diluted with an organic solvent (n-propanol) to prevent further precipitation and to eliminate any residual turbidity from fine aggregates or particles, which could have passed through the filter and cause residual light scattering. The diluted filtrates were again transferred to a measurement plate for immediate analysis by UV spectroscopy via microplate reader or by HPLC. [27, 28]

The best ternary ASD formulations from the screening experiments were scaled up to 100 mg using a melt-press method and submitted to dissolution testing in 200 ml of SIF at 37 ºC , using a USP type VII apparatus. At 0, 5, 15, 30 and 60 min, 1mL aliquots were sampled, centrifuged and analyzed by HPLC. [27, 28]

Another example is the systematic step-by-step approach followed by Simões et al., where binary ASD combinations were prepared by film casting inside 48-well microplates and evaluated according to solubilisation capacity and physical stability over 2 months. Hereupon, the best combinations were produced by HME in a mini lab-scale extruder and characterized in terms of dissolution and physical state.[76]

Therefore, whenever the drug compounds under screening show good solubility in volatile solvents, which turns them into suitable spray drying candidates, solvent casting methods are applied for an initial screening.

On the other hand, APIs with low melting point, which are adequate for HME scale-up production, can be screened by melt-fusion methods. Moreover, miniaturized solvent casting methods can also be applied for

HME candidates' preparation as long as they own a high solubility in volatile solvents, which makes this technique a more general high-throughput screening approach. [69]

The melt-fusion methods generate ASD formulations by co-melting of a drug and a polymer or dissolution of a drug in a molten polymer, in a completely solvent-free ASD preparation process. The ASD film takes form when a well-mixed molten solution is solidified upon quench cooling. Intense physical mixing is needed to ensure complete mixing of highly viscous solid dispersions.[69]

The concept of melt-fusion is simple. However, assuring a correct mixing of ASD components in the solid state is one of the main limitations to the development of new miniaturized screening methodologies, considering the rheological properties of the molten solid dispersions. [33, 35–39]

As a result, there is a lack of innovation around new preparation procedures using fusion methods at small-scale and generally, fusion ASD films are produced by HME requiring a small lab-scale extruder as equipment for preparation. Some alternative melt-fusion methodologies have been published in literature using appropriate containers able to withstand high temperatures (e.g. small stainless steel beaker) or DSC pans. Nevertheless, such options are usually girded to a reduced range of applications in terms characterization techniques to which the resultant ASD prototypes can be submitted to. For instance, ASD production by fusion inside DSC pans is usually destined to DSC analysis only.[33, 35, 37,38]

For instance, Foster et al. presented three miniaturized approaches for ASD melt-fusion production: production by HME using a small-scale lab extruder; the production of ASD prototypes by heating drug/polymer blends in a stainless steel beaker on a hot plate followed by submersion in ice-cold water for rapid cooling of the sample; and the preparation of ASD formulations in DSC pans through DSC heating above melting and rapid cooling by placing a stainless steel holder filled with liquid nitrogen over the DSC pan. In this case, the dissolution study in PBS at pH 6.8 or 1 % SDS, with measurements being collected at 10 and 60 min time points, was performed only on ASD formulations which had been produced by beaker melt. [88]

In a 2018 article, a combined approach of solvent casting and fusion-based ASD preparation methods has been presented by Auch et al. for biorelevant dissolution testing inside DSC pans. The innovation consisted on the addition of an extra melting-step to the preparation of solvent-casted ASD films, to closer mimic HME conditions. The process consisted in casting ASD films at the bottom of the aluminum DSC crucibles by mixing drug and polymer stock solutions and performing solvent removal with a freeze dryer apparatus. Thereafter the DSC pans with the solvent casted films were heated and quench cooled for melt-fusion. The dissolution of the ASD films consisted in adding 110 µL of FaSSIF-V1 and one glass ball into each DSC pan, and collecting 55 µL samples after 60 and 120 min to be analyzed by HPLC, upon filtration and dilution in ACN.[83]

Recently, an innovative miniaturized apparatus has been proposed by Guo et al. for the use of acoustic energy in the formation of the amorphous solid dispersions by fusion. The apparatus consisted in a block

with capacity to hold up to 24 glass vials (4 mL) and comprised a metal block assembly so that it could be attached directly to a resonant acoustic benchtop mixer. From the acoustic fusion process, a dense glassy material was formed at the bottom of each vial, corresponding to the drug-polymer solid dispersions that were further processed into a powder through a grinding technique, and submitted to in vitro dissolution studies performed under sink conditions in PBS at pH 6.8, using dissolution testing apparatus set at 37ºC. The resulting supernatant was diluted in ACN and drug concentration was determined by HPLC analysis.[89]

Many innovative microplate-based screening approaches have been arising in the literature, yet encompassing distinct ASD preparation methods and/or other characterization methods rather than dissolution testing. [43, 60–62]

In a 2019 article, Jacobsen et al. reported a novel high-throughput methodology whose innovation relied on the application of a prototype device, a 96-well two-compartment microplate system consisting of a conventional bottom-plate and a top-plate comprising an integrated dialysis membrane, to simultaneously study dissolution and permeation for ASD screening.[93]

The applicability of this screening approach was tested with ASD formulations prepared by freeze drying (lyophilization), which were frozen over night at -80ºC and placed in a desiccator over $CaCO_3$ beads to reach room temperature. The dissolution and permeation screening experiments were used to compare the screening parameters and to establish an in vitro - in vivo correlation. Firstly, the freshly dispersed ASD formulations were added to the bottom-plate (donor compartment) whereas, the acceptor medium (surfactant solution or PBS) was inserted in the top-plate wells (acceptor plate). The top-plate was sealed with pierceable adhesive sealing foil and closed with the corresponding lid. The set was incubated at room temperature under orbital shaking and during that time the drug compound permeated from the bottom to top-wells. Samples collected after 1, 3 or 6 h of incubation were, upon appropriate dilution in ACN and centrifugation (if necessary), submitted to UHPLC-UV analysis for quantification.[93]

1.4. Thesis Proposition: Main Objectives of the project and Experimental Outline

The purpose of this master thesis project was to develop a novel miniaturized screening methodology to evaluate performance of ASD prototypes in terms of supersaturated potential and precipitation inhibition through dissolution study, employing a deposition platform (Figure 3) to be inserted into 24-well quartz microplates, and enable continuous monitoring of ASD dissolution process and collection of dissolution profiles in real-time. The use of quartz microplates is critical since common microplates are made of plastic

and absorb UV light in the region of interest: typical absorbance maxima of pharmaceutical organic compounds overlaps with the absorbance spectrum of plastic microplates.

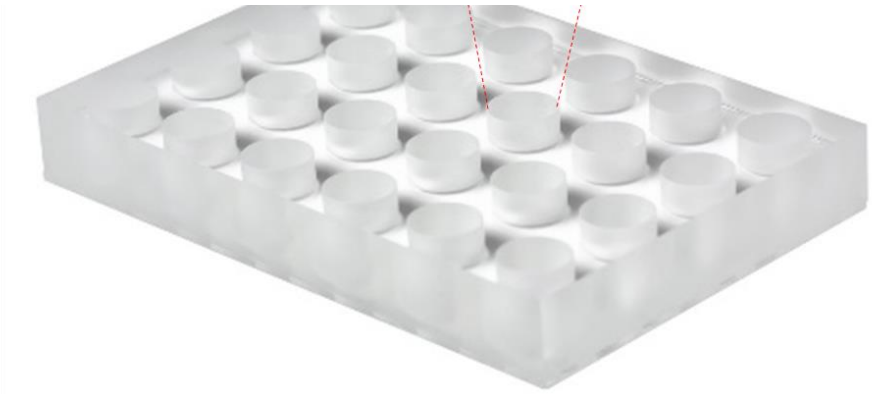

***Figure 3**. Miniaturized screening device: a deposition platform inserted into 24-well quartz microplate.*

Hence, the main propositions regarding the proof of concept and implementation of this miniaturized dissolution methodology consist of:

- Assessing the preparation method – Developing at least one feasible, functional, reliable and reproducible preparation method to produce ASD films on the surface of these deposition platforms;
- Testing the concept – Assessing if the ASD films produced under the scope of this methodology are capable of generating dissolution profiles by monitoring concentrations within the quantification range of the UV spectroscopic technique in use, and representative of ASD prototype performance;
- Improving High-throughput potential of the methodology – optimize the ASD production to cope with fast demand, whilst maintaining quality and assuring reproducibility of the procedure;
- Developing dissolution studies on a wide experimental setup of drug-polymer combinations and several drug loads
- Establishing relations between drug and polymers physicochemical properties and the dissolution behaviour, supersaturation rate and extent and LLPS and/or recrystallization onset;

- Developing biorelevant dissolution testing to study ASD supersaturation potential under conditions mimicking the GI tract environment to enable predictive IVIV correlations with respect to in vivo performance of ASDs.

1.4.1. Experimental Outline

To achieve such goals and implement this HTS methodology, a broad experimental design has been chosen comprising:

1. **Model drug**

The model compound chosen for the study was Indomethacin (IND), a non-steroidal anti-inflammatory drug (NSAID), with antipyretic, anti-inflammatory and analgesic properties, currently used in the treatment of rheumatoid arthritis and other degenerative joint diseases.[113] The pharmacological activity of this API consists of inhibiting cyclooxygenase (COX) enzyme and so the synthesis of prostaglandins and thromboxane from arachidonic acid. Moreover, IND has the therapeutic capacity of inhibiting COX-2, the inflammatory agent at inflamed tissues, and also COX-1 with attendant toxicities, such as gastrointestinal problems. Recently, it has attracted further attention for its anti-tumor activity, with an important role in the inhibition of human-colon adenocarcinoma cell proliferation, but mainly due to its demonstrated antiviral activity in repurposing studies against severe acute respiratory syndrome coronavirus-2 (SARS-CoV-2).[114,115] Given its many application, IND can be delivered to patients by more than one route, being commercially available in the form of capsules, suspensions, suppositories and lyophilized powders to be delivered by intravenous injection.[113]

Due to its chemical structure (Table 1), IND exhibits an entire set of physicochemical properties which are common to many new pharmaceutical drug products. IND is a weakly acidic drug with a pH-dependent solubility, owning a pKa of 4.5, below which it displays an un-ionized form (high lipophilicity, good absorption) and above which it assumes a negatively charged form, and so more hydrophilic. In fact, due to its poor intrinsic solubility, IND has been categorized under BCS Class II, and upon uptake it can cause high local drug accumulations in the tissues which can evolve into GIT irritations and ulcerations, reducing its therapeutic applications for oral use.[116] Balancing all the advantages and drawbacks and also the physicochemical properties of this BCS class II drug, makes of IND a perfect candidate as model drug.[113,117–125]

Table 1. *Physicochemical properties of IND. Summary of information collected from the referenced articles [117–125]*

Indomethacin (PubChem CID: 3715)	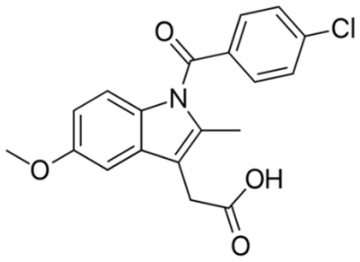
Chemical Name	1-(*p*-chlorobenzoyl)-5-methoxy-2-methylindole-3-acetic acid
M_w	357.9 g/mol
BCS class	II
pKa	4.5 (weak acid)
T_m	162 ºC; 434 K
T_g	41 ºC; 315 K
T	37 ºC; 310 K
ΔH_{fus}	110 (J/g); 39369 (J/mol)
Solubility	5.3 µg/mL (Water) 20.28 mg/mL (Methanol)

2. Drug-carriers

The polymers chosen to be combined with IND into ASD prototypes were: HPMCAS-HF, EUDRAGIT EPO, EUDRAGIT L100-55, PVP K29/32, HPMC E3 Premium LV EP, HPMC E5 Premium LV, KOLLIDON 30 and COPOVIDONE K28. This pool comprises polymers which belong to different classes of polymers (methacrylate, polyvinyl lactam and cellulose derivate) and are present in ASD formulations already available in the market covering a broad set of properties in terms of water solubility, glass transition temperature, molecular weight, charge and hydrophilicity, among many others. In table A1, that can be found in APPENDIX section, are summarized some of the most relevant properties of these polymers. It is noteworthy that KOLLIDON 30 and PVP K29/32 are two versions of the same polymer (Polyvinylpyrrolidone) provided by distinct suppliers.

3. Organic solvent

There was a need to select an organic solvent to be used in the preparation of ASD films by the solvent evaporation method. Methanol was chosen as organic solvent to perform such preparations since it is a very volatile solvent and in which IND is highly soluble (with a solubility almost 4 thousand times higher than in water).

4. Dissolution media

The selection of a dissolution medium fell upon two types of Phosphate Buffer Solution (PBS) as dissolution media to evaluate the performance of ASD combinations: PBS pH 2.0 and PBS pH 6.8 (see Figure 4).

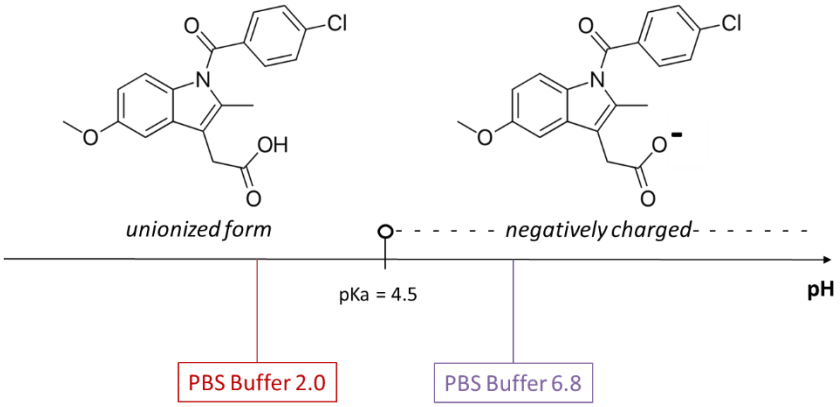

Figure 4. *Schematic representation of Indomethacin's ionization state within the selected pH range.*

The extent of ionization of a weak acid or weak base drug can significantly affect solubility and, therefore, the rate and extent of dissolution. Hence, these medium pH values were selected in order to account with the interference of different ionization states of IND and of some of the polymers in the dissolution process comprehension.

In Figure 5 it is provided a schematic representation of the experimental outline of this project. Since the purpose of this study was to develop a miniaturized HTS methodologies that allowed to study dissolution and evaluation of in vitro performance of ASD prototypes, a model drug along with 8 polymers candidates, combined at different drug loads within a range of 30-80% (w/w), were selected to test proof and validate this technique. The preparation of the amorphous films was done using two different techniques: a solvent evaporation method and a fusion method, both encompassing a quench cooling step to promote ASD formation and avoid crystallization right after preparation. The dissolution profiling of all ASD prototypes was carried out inside the wells of a 24-well quartz microplate and quantification was performed in real time by UV-Vis Spectroscopy. Solubility studies to determine both thermodynamic and kinetic solubilities were conducted prior to dissolution testing in order to understand the concentration boundaries and allow interpretation of the results. In some cases, the phase behaviour and molecular species formed in solution during dissolution were monitored through Dynamic Light scattering (DLS). Uniformity of deposition along

with drug-polymer miscibility within the amorphous films produced were evaluated through Confocal Raman Microscopy (CRM), involving Raman spectra and imaging acquisition.

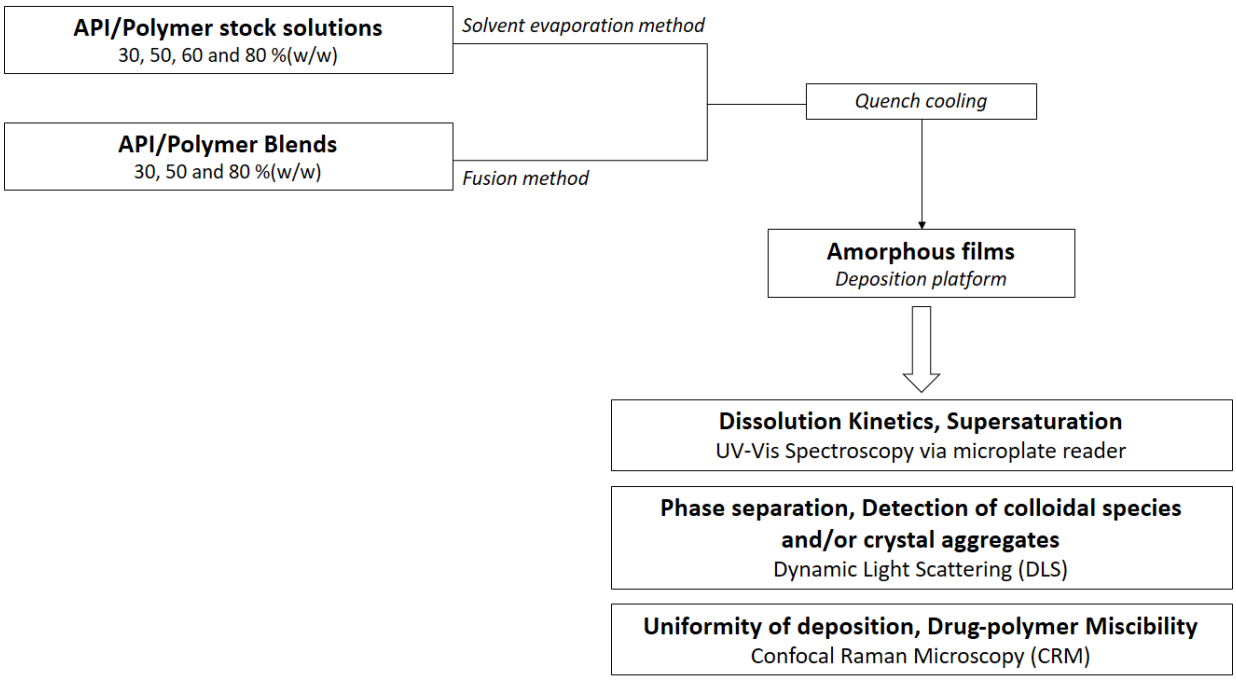

Figure 5. *Experimental Outline*

2. Materials and Methods

2.1. Materials

Indomethacin, the model API used in the studies herein described, was purchased from Sigma-Aldrich (St. Louis, MO, USA). To produce the ASDs prototypes a total of eight polymers were acquired: HPMCAS-HF supplied by Shin-Etsu Chemical Co., Ltd. (Tokyo, Japan); Eudragit E PO and Eudragit L100 were obtained from Evonik Industries AG. (Essen, Germany); PVP K29/32 was purchased from Ashland (Covington, KY, USA); HPMC E3 (METHOCEL E3 Premium LV EP) and HPMC E5 (METHOCEL E5 Premium LV) provided by The Dow Chemical Company Europe (Horgen, Switzerland); KOLLIDON 30 and COPOVIDONE K28 bought from BASF Pharma SE (Ludwigshafen, Germany).

Regarding the aqueous media under study, to produce both types of PBS buffer solutions the following reagents were obtained: Sodium dihydrogen phosphate monohydrated ($NaH_2PO_4.H_2O$), Disodium hydrogen phosphate (Na_2HPO_4), Phosphoric acid (H_3PO_4) from Sigma-Aldrich (St. Louis, MO, USA), Sodium Chloride (NaCl) from Merck KGaA (Darmstadt, Germany).

Additionally, FFF01 from Biorelevant.com Company was purchased for the preparation of FaSSGF medium and the respective Transition medium.

2.2. Methods

2.2.1. Solubility studies

2.2.2.1. Determination of crystalline drug solubility

The equilibrium solubility of IND was experimentally assessed employing the analytical shake-flask method, which consisted in adding an excess amount of drug to a Falcon tube containing 30 ml of a dissolution medium (50 mM PBS pH 2.0 + 2% (v/v) MeOH), in order to saturate the solution. The small volume of organic solvent added to the PBS pH 2.0 intended to mimic the solvent system under which the amorphous solubility was determined by the UV-Vis extinction method (see section 2.2.2.3). The goal was to compare the crystalline and amorphous solubility of IND in the same solvent system.

After mixing and assuring the falcon tube was tightly capped, it was roughly stirred to promote dissolution, and then left to rest inside a drying oven kept at 37ºC, during 24h. After the 24-hour period, the excess non-dissolved material was discarded and, carefully aided by a micropipette, a small aliquot (1 ml) of homogenous saturated solution was collected.

Regarding UV-Vis spectral scan analysis, two different approaches were followed:

1. Direct analysis in the UV-Vis spectrophotometer
2. Ultracentrifuge prior to UV-Vis analysis

The ultracentrifugation was performed in Optima™ Max-XP Tabletop Ultracentrifuge (Beckman Coulter, Inc.), for a period of 20 min, at a speed of 300000 x *g* and at a constant temperature of 37ºC.

Each condition was studied in duplicate (n=2) and spectral scans were acquired between 200nm and 600nm in a SPECORD200 PLUS UV-Vis spectrophotometer (Analytik Jena GmbH).

In order to estimate equilibrium solubility concentration, the 320nm wavelength was selected as maximum absorbance wavelength (λ_{max}= 320nm), and the respective measurements converted into concentration units through the application of Lambert-Beer Law.[126,127]

$$A = \varepsilon\, l\, C \qquad (1)$$

The optical path length (l) of the cuvette used in this UV-Vis analysis corresponds to 1 cm and the molar absorption coefficient (ε) was determined through the construction of a calibration curve with standard solutions of well-known concentration prepared by dissolving IND in the same solvent used (in this case, PBS pH 2.0 + 2% MeOH). The molar absorption coefficient (ε) corresponded to the slope of the linear relationship between plotted Absorbance versus concentration.

2.2.2.2. Estimation of theoretical amorphous solubility

The theoretical amorphous solubility, also known as apparent solubility of an amorphous drug, ($C_{amorphous}$) was estimated using the the equilibrium solubility of the crystal form ($C_{crystal}$), the free energy difference

between the crystal and amorphous forms ($\Delta G_{c\rightarrow a}$) and the activity of the amorphous drug saturated with water ($e^{-I(a_2)}$), as described in equation (2). [3, 9, 117]

$$C_{amorphous} = C_{crystal} \cdot e^{-I(a_2)} \cdot e^{\frac{\Delta G_{c\rightarrow a}}{RT}} \quad (2)$$

The term referent to the free energy of conversion of the crystal form into the amorphous form can be calculated using the Hoffman equation (3): [3, 9, 117]

$$\Delta G_{c\rightarrow a} = \frac{\Delta H_{fus}(T_m - T)T}{{T_m}^2} \quad (3)$$

Where T corresponds to the temperature of conversion, T_m to the melting temperature and ΔH_{fus} corresponds to the melting enthalpy of the compound. [3, 9, 117]

The term $e^{-I(a_2)}$ is a correction factor introduced by Murdande et al. to account for a reduction in thermodynamic activity due to the presence of water in the amorphous phase. [3, 9, 117]

Another approach was presented in a different article by the same author, where the apparent solubility enhancement ratio (R_s) of IND in water, a ratio between the maximum concentration of amorphous IND and the equilibrium solubility of crystal IND (equation 4), was found to be equal to 4.9. [3, 9, 117]

$$R_{s\ (Indomethacin)} = \frac{C_{amorphous}}{C_{crystal}} = 4.9 \quad (4)$$

This relation was used to determine the amorphous solubility of IND in PBS pH 2.0 and is valid in cases where the pH in solution is lower than pKa (pH < 4.5) since IND is mainly in the un-ionized form. However, since IND is an acidic drug compound with a pKa of 4.5, when pH is higher than pKa (pH > 4.5) the following relation must be applied so that the ionized fraction of drug can be taken into account: [3, 9, 117]

$$C_{amorphous} = (ionized\ fraction).C_{crystal} + (unionized\ fraction).C_{crystal} \cdot R_s \quad (5)$$

For an acidic compound, the un-ionized and ionized fractions can be estimated by application of equations (6) and (7) derived from Henderson–Hasselbalch equation:[130]

$$ionized\ fraction = \frac{1}{1 + 10^{(pKa-pH)}} \quad (6)$$

$$ionized\ fraction + unionized\ fraction = 1 \quad (7)$$

2.2.2.3. Experimental determination of apparent amorphous solubility (UV-Vis Extinction Method)

Quantifying the amorphous solubility allows for an understanding of the solubility enhancement provided by an amorphous solid dispersion formulation.

The UV-Vis Extinction Method is a spectrophotometric method which through the study and characterization of phase separation phenomena enables the determination of the maximum supersaturation that can be attained in a homogeneous solution.

The principle governing Liquid-liquid phase separation (LLPS) is simple. When the maximum concentration of amorphous free drug in solution is attained, occurs the formation of a new drug-rich phase in solution (colloidal aggregates or crystalline precipitates). Hence, UV-VIS spectroscopy can be used to monitor this phenomenon, since the formation of this new phase results in an increase in the light scattering which can be detected by an increase in the baseline of the UV-Vis absorption spectra at wavelengths where de drug compound exhibits no absorption (extinction region). This is the reason why changes in baseline at non-absorbing wavelengths can be used to monitor phase separation phenomena. At a macro level, solutions undergoing LLPS show turbidity, exhibiting a milky appearance and/or a bluish tinge under unaided eye observation.

The experimental strategy set to better study the phase separation phenomena consisted in preparing a set of supersaturated solutions of different concentrations, comprising the theoretical amorphous solubility. Hence, holding as theoretical reference the value of amorphous solubility previously estimated (25.97 µg/mL), a total of 12 supersaturated solutions were chosen to perform this study, six of them below and other six above the amorphous solubility.

The solvent shift method, also known as co-solvent quenching method, was carried out as a way to generate those supersaturated solutions in situ. To perform this method adequately and avoid interference of other factors in this determination, two conditions must be met:

1. The drug must first be solubilized in an appropriate organic solvent at a concentration 50 times higher than the theoretical amorphous solubility (Note that the drug must be highly soluble in the organic solvent)
2. The volume spiked into the solution must not exceed 2% v/v in a way of assuring that the organic solvent present in solution does not exert any influence in the solubilisation capacity of the medium nor impact the LLPS concentration achieved.

The supersaturated solutions were generated by spiking a small aliquot of a stock solution of IND in Methanol (1.25 mg/mL) into a glass vial containing 10 mL of PBS pH 2.0 maintained at 37ºC under a constant orbital shaking in a bench magnetic stirrer. This determination was performed at a pH value where the drug is completely un-ionized ($pKa_{(IND)}$ = 4.5) and each solution was prepared and analyzed individually. Information on all supersaturated solutions regarding volumes spiked along with the respective concentrations generated can be found in table 2.

Table 2. *Supersaturated solutions of IND in PBS at pH 2.0 prepared by the solvent-shift method.*

Supersaturated solutions IND/ PBS pH 2.0 (+ 2% MeOH)												
Concentration	µg/mL	3.75	7.5	11.25	15	18.75	22.5	26.25	30	33.75	37.5	41.25	45
$V_{(spike)}$	µL	30	60	90	120	150	180	210	240	270	300	330	360

The next step after the spike was to transfer an aliquot of the supersaturated solution into a quartz cuvette to acquire the spectral scan between 200 nm and 600 nm in a SPECORD200 PLUS UV-Vis spectrophotometer (Analytik Jena GmbH), at 37 °C. Light scattering was detected by monitoring the extinction at three different non-absorbing wavelengths: 450 nm, 500 nm and 550 nm. Finally, using the ORIGINS PRO software, the intensity of light scattered was plotted against the respective concentrations to determine LLPS transition concentration, which corresponds to the point at which a significant increase in the intensity of light scattered was observed.

2.2.2. Preparation of API/Polymer mixtures

2.2.2.1. API/Polymer solutions

A total of 32 different API/polymer standard solutions were prepared by combining IND with each one of the 8 polymers under study at 4 different drug loads (30%, 50%, 60% and 80%). All the components were weighted in a METLER TOLEDO scale, transferred to the respective volumetric flasks (of 50ml or 100ml) completed to the final volume with Methanol, labeled and taken to the Ultrasound bath to dissolve.

2.2.2.2. API/Polymer blends

A total of 24 different API/polymer blends were prepared by combining IND with each one of the 8 polymers under study at 3 different drug loads (30%, 50% and 80%). All the components where weighed in a METLER TOLEDO scale and transferred to a spherical grinding bowl.

The blending process was performed in a FRITSCH Mini-Mill PULVERISETTE 23 Ball mixer. The ball mixer was set to perform vertically oscillating movements with 9 mm of amplitude at 25 oscillations per second, during 1 minute. The blend was formed upon grinding, mixing and homogenization of the API/Polymer mixture promoted by the impact and friction between solid particles with the two grinding balls rolling against the inside wall of the spherical grinding bowl. Afterwards, the blend was removed from the grinding bowl and transferred to a small glass flask aided by a stainless steel spatula.

2.2.3. ASD film preparation

2.2.3.1. Fusion method

The fusion method used the deposition platform (Hovione IP) for deposition of the films. This preparation procedure is new and may be applied for the preparation of ASD films during early stages of formulation development. Figure 6 depicts a schematic representation of the process steps involved in the preparation of an ASD film of approximately 1 mg.

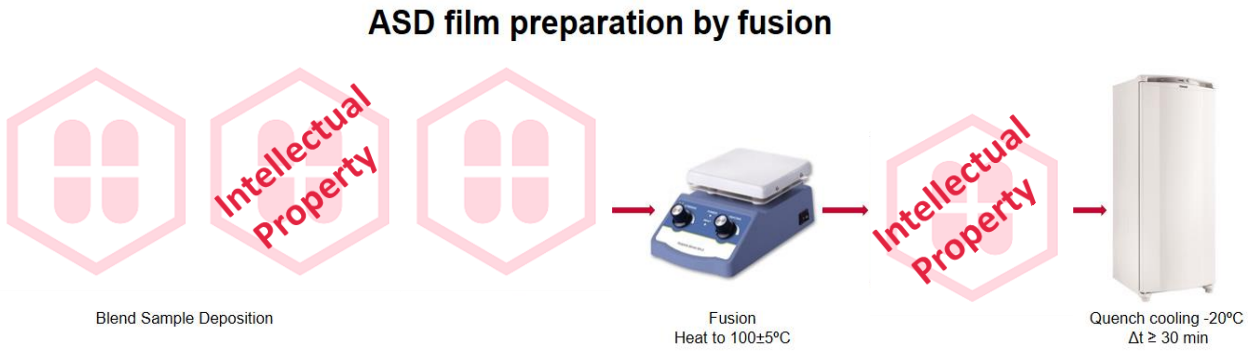

Figure 6. *Schematic representation of the preparation method developed to produce an ASD film on the deposition platform by fusion.*

Firstly, the initial mass of all the deposition platforms to be used in a single experiment (one for each well of a 24-well quartz microplate) was recorded. The step that follows is to deposit in each deposition platform 1 mg of the respective API/Polymer blend (this quantity is a result of optimization studies). This procedure needs to be performed close to a bench scale so that the deposited mass can be controlled.

After that, the melting set up that consists of a heating plate connected to a temperature control sensor embedded in SYLTHERM™ Heat Transfer Fluid solution was assembled inside a fumes hood. The system was preheated to 100±5ºC (this temperature slightly varies depending on the Tg of the API/Polymer combination), and one must assure it is kept constant throughout the entire procedure. Afterwards, the deposition platforms containing 1 mg of blend must be carefully placed in an aluminum foil sheet on top of the heating plate. Along the process, the handling of the deposition platforms is done with the aid of a bent sharp point tipped tweezers. Upon complete melting, the deposition platforms are stored in a freezer set at -20ºC for at least 30 min, so that the ASD films can be formed. After that 30-minute period, the deposition platforms can be taken off, to rest at room temperature for around 15 minutes. Finally, it is mandatory to register the final mass of all the deposition platforms so that they can proceed to the characterization screening assays.

2.2.3.2. Solvent evaporation method

A solvent evaporation method was also developed to prepare ASD films in deposition platforms. The ASD preparation process (Figure 7) starts with the registration of the initial mass of all the deposition platforms

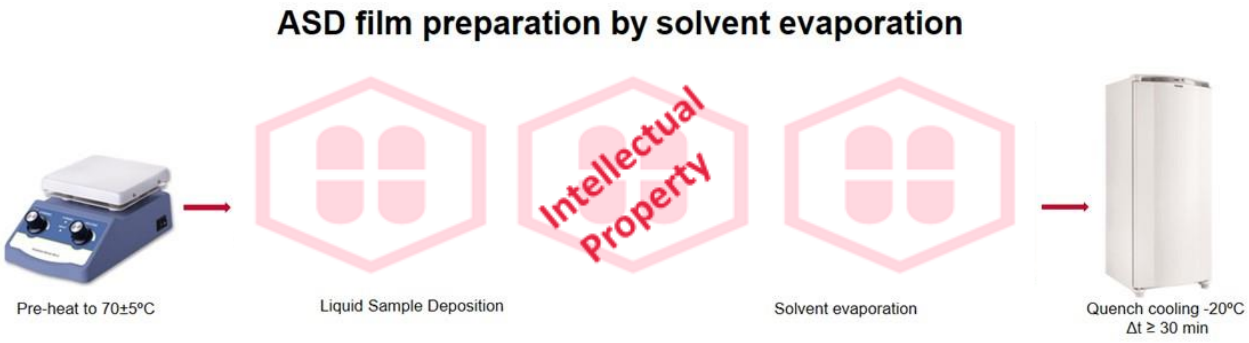

Figure 7. *Schematic representation of the preparation method developed to produce an ASD film on the deposition platform by solvent evaporation.*

that will be used in a single dissolution experiment (one for each well of the 24-well microplate). The next step occurs inside a fume hood and consists in covering the top of a bench heating plate with a thin aluminum foil and preheating the system to a temperature of 70±5ºC, assuring it is kept constant throughout the entire procedure. The temperature is controlled with a thermostat sensor embedded in a SYLTHERM™ Heat Transfer Fluid solution. The deposition platforms are placed in the heating plate and left to equilibrate to temperature for 2 to 3 minutes. Then, aided by a P200 micropipette, 150 µl (this volume is a result of optimization studies) of the respective API/Polymer stock solution are pipetted onto each deposition platform covering its entire top surface. This is a high precision step only possible due to the surface tension of the liquids, and so should be done carefully.

After solvent evaporation, the deposition platforms shall be stored in a freezer set at -20ºC for at least 30 minutes so that the ASD films can be formed. After that 30-minute period, the deposition platforms can be taken off the freezer, to rest at room temperature for around 15 minutes. The handling of the deposition platforms is done with the aid of a bent sharp point tipped tweezers. The following step is to register the final mass of all the deposition platforms and then they are ready to proceed to the characterization screening assays.

2.2.4. Dissolution studies

2.2.4.1. Calibration curves

Calibration curves are essential to determine the linear range of measurements for UV-Vis quantification studies performed in a microplate reader since the Lambert-Beer Law is not applicable once optical path length is not a computable constant under such experimental conditions.

Calibration curves of Indomethacin in Methanol

A total of 7 standard solutions were prepared in 250 mL volumetric flasks by dilution of a 5mg/mL stock solution of IND in Methanol, so that the target concentrations (1, 2, 5, 10, 30, 40 and 50 µg/mL) could be attained. In the UV-Vis spectroscopic analysis, absorbance values at 320nm and 600nm were acquired by a SYNERGY HTX multi-mode microplate reader (BIOTEK). The first step was to scan the empty quartz microplate at 320nm and 600nm so that it could serve as a blank measurement of the microplate material absorbance. The standard solutions were studied in triplicate (n=3) and so, the following step consisted in transferring 1.5 mL of each standard solution into 3 wells of the microplate. Then again, the microplate was scanned to collect the Absorbance at λmax (320nm) and at the baseline (600nm). Upon data pre-treatment, which consisted in subtracting the blank measurements and the baseline to all absorbance values, the calibration curve was obtained by plotting the final Absorbance at 320nm against the respective standard solutions concentrations.

Calibration Curves of Indomethacin in PBS pH 2.0 and pH 6.8

Another calibration curve was performed to better account with dissolution media conditions used in ASD dissolution studies in an attempt to more reliably quantify the amount of drug released into solution by each ASD formulation under evaluation. The first step was to scan the empty quartz microplate at 320nm and 600nm to obtain a blank measurement of the microplate material absorbance. The following step, was to pipette into each plate well 1.5 mL of PBS pH 2.0 and right after, spike a volume of standard solution correspondent to 2% of that volume (30 µL). The concentration of each standard solution of IND in Methanol was calculated so that the 2% fraction of total plate well volume could be able to generate the desired concentration inside the well. The study of each concentration was performed in triplicate (n=3). Similarly to the previously described calibration curve, the absorbance at λmax (320nm) and at the baseline (600nm) was registered by a SYNERGY HTX multi-mode microplate reader (BIOTEK). Upon baseline correction, the calibration curve was obtained by plotting the final Absorbance at 320nm against the concentrations generated by each standard solution. For both calibration curves, the final averaged values obtained for Absorbance at 320nm were evaluated in terms of precision and reproducibility through relative standard deviation (RSD) determination**,** a useful measure of dispersion which conveys information on how precise an average value is in relation to the mean value of the correspondent set of data. The Lower the RSD the more precise is the measurement and so, an RSD value inferior to 30% was taken as a validity criterion for all the results obtained.

2.2.4.2. Dissolution profile acquisition in PBS medium

All dissolution studies were performed using a 24-well quartz microplate in a SYNERGY HTX multi-mode microplate reader (BIOTEK).

The first step of the protocol used to analyze all the deposition platform sets comprised in this study consisted of adding 1.5 ml of dissolution medium into each plate well and then insert the plate in the

microplate reader to collect the blank readings. These values were subtracted to the dissolution data to eliminate dissolution medium and deposition platform interference/absorbance. The experiments held under the scope of this protocol comprised two dissolution media, PBS at pH 2.0 and PBS at pH 6.8, and the same procedure was applied for both conditions.

In the step that followed, deposition platforms carrying the ASD films were inserted into the respective microplate wells with the help of a bent sharp point tipped tweezers. The amorphous films of every drug-polymer combination under test were prepared in duplicate (n=2).

After all the deposition platforms were inserted into the microplate wells, the microplate was reinserted in the microplate reader to initiate the second part of the protocol. The second protocol step consists in a 12-hour dissolution run with readings being taken every 30 seconds at both 320nm and 600 nm wavelengths. The temperature was set constant at 37ºC and a continuous orbital motion was applied to the microplate during the entire assay. After the 12-hour period, the microplate along with the deposition platforms were removed and cleaned and the readings exported from the Gen 5 3.02 software for further data treatment and analysis.

2.2.4.3. Biorelevant Dissolution profile acquisition

All biorelevant dissolution studies were performed using a 24-well quartz microplate in a SYNERGY HTX multi-mode microplate reader (BIOTEK). The inclusion of a pH shift step renders a more complex dissolution protocol which can be divided into two parts:

(1) Dissolution in FaSSGF (pH 1.6) during 30 minutes;

(2) Dissolution in FaSSIF (pH 6.5) during 2 hours.

In the first part, 750 µl of FaSSGF (pH 1.6) were pipetted into each plate well and then the plate was placed in the microplate reader to collect the media blank readings. Then, the microplate was ejected and the deposition platforms carrying ASD films were inserted in the respective plate wells for a first run that lasted 30 minutes.

Afterwards the microplate was ejected and 750 µl of Transition medium (pH 7.5) were added to trigger a pH shift from pH 1.6 to 6.5 and simulate biorelevant conditions of stomach-intestine passage through the conversion of biorelevant medium FaSSGF into FaSSIF. The microplate was inserted back in the microplate reader immediately after adding the transition medium to all wells to initiate the second part of the protocol, which lasted for 2 hours. Also, for these protocols, the readings were taken every 30 seconds at both 320 nm and 600 nm wavelengths, at a constant temperature of 37ºC and under continuous orbital agitation. After the two and a half hour assay, the microplate along with the deposition platforms were cleaned and the readings exported from Gen 5 3.02 software for further data treatment and analysis.

2.2.5. Dynamic Light Scattering (DLS): Particle size analysis

DLS was used to measure the size of the particles present in the dissolution medium at two specific time points during dissolution process profiling: at C_{max} and at the end of the dissolution run (after 12h) for IND/HPMCAS-HF and IND/ EUDRAGIT EPO ASD films. Upon interruption of the dissolution process at these specific time points, 250 µl aliquots were sampled directly from the microplate well and transferred to a disposable micro UV-cuvette (10 mm path length, 2 mm slit) (BRAND GmBH, Germany) to be analyzed in a Nano-Zetasizer (Nano-ZS) (Malvern Instruments). The instrument was set to backscatter mode at an angle of 173° and samples were equilibrated to 37°C during 10 seconds prior to analysis. The material parameters regarding refractive index (RI) and absorption were defined as 1.440 and 0.001, respectively. Whereas, dispersant parameters regarding refractive index (RI) and viscosity were defined as 1.330 and 0.6864 cP, respectively. Each sample analysis consisted of 3 measurements comprising 11 runs of 10 seconds each.

2.2.6. Confocal Raman Microscopy (CRM)

Raman spectroscopy coupled with Confocal Microscopy (CRM) were used as a characterization methodology for screening of ASD prototypes in terms of both characterization of film uniformity and homogeneity of distribution of components. This analysis was applied to IND/ HPMCAS-HF and IND/EUDRAGIT EPO ASD films with 50% drug load, produce by solvent evaporation and by the fusion method. Raman Spectra acquisition experiments were performed using a Confocal Raman Microscope Alpha 300 RA, from WITec GmbH, equipped with an excitation laser operating at 532 nm wavelength, coupled with a UHTS 300 WITec spectrometer and connected to an Andor DU401 BV CCD detector. For all experiments the laser power was set at 10mW. The WITec Control Five 5.0 acquisition software was used for the Raman imaging set up.

2.2.6.1 Image Stitching

To record an Image Scan of a deposition platform carrying an ASD film it was necessary to place the film deposition platform in the Confocal Raman Microscope in a central position and those coordinates were set as central position coordinates. Image acquisition was carried out using a ZEISS EC EPIPLAN x10 / 0.25 objective lens and an integration time of 0.1 seconds. The Geometry of the image was defined 16000 µm width and 16000 µm height and the size parameters X and Y were both set as 500 pixels.

2.2.6.2. Large Area Scans

Large area scans of a region on the surface of the deposition platforms containing a certain ASD prototype were performed with the ZEISS EC EPIPLAN x10 / 0.25 objective lens and with integration times of 0.5 seconds. Each scan encompassed 150 points per line and 150 lines per image, resulting in a total scanned area of 1500 µm x 1500 µm and a spatial resolution of 10 µm per point. Upon pre-treatment these large area scans resulted in Combined Bitmaps, colour-coded according the respective components detected in the Raman spectrum of each scanned point within the image.

2.2.6.3. Single Spectrum

Single Raman Spectra of IND, HPMCAS-HF and EUDRAGIT EPO were acquired by displacing a small quantity (approximately 1 mg) of each compound in a glass slide for analysis of the Raman spectrum of the pure compounds. These Single Spectra acquisition were carried out using the ZEISS EC EPIPLAN x20 / 0.4 objective lens, with an integration time of 0.5 seconds and 10 accumulations.

2.2.6.4. Pre-processing of Raman Spectra

To enable generation of images and RAMAN spectra conveying useful information on the systems under study, a set of pre-processing treatment steps was performed, using the WITec Project 5.0 software. Analysis of Raman data required some aspects to be corrected: baseline, noise, differences in scale, spikes and dead pixels. Therefore, filters or mathematical algorithms were applied to single spectra as well as to spectral data sets generated upon large area scans in a way to correct such aspects. The following data treatment were applied: Subtract Background (Sub BG), Cosmic Ray Removal (CRR), Savitzky Golay Smoothing (SG) and True Component Analysis.

3. Results and Discussion

3.1. Solubility studies

3.1.1. Experimental determination of crystalline solubility

The solubility of a crystalline drug corresponds to its concentration in solution following attainment of equilibrium between the crystalline solid and the solution phase.

The equilibrium solubility of IND was determined by adding an excess amount of the compound of interest into a dissolution medium comprising sodium phosphate buffer solution (PBS) at pH 2.0 plus a 2% (v/v) of Methanol, at 37 ºC for 24 hours. Two different sample preparation procedures were followed: one using an ultracentrifugation step to separate the supernatant from the excess solid, and the other without any separation step.

The collected samples were analyzed in duplicate through UV-Vis Spectroscopy in a wavelength range between 200nm and 600nm, using PBS at pH 2.0 as blank. The spectral scans of the solutions prepared with and without ultracentrifugation are depicted in Figure 8.

The absorption profiles of all spectral scans acquired showed reproducibility between replicates and a good concordance between experimental assays.

Two maximum UV-Vis absorption peaks were detected at 245 nm and 320 nm wavelengths. Hence, the Absorbance peak selected to monitor IND's concentration under such experimental conditions was the 320

nm wavelength since it shows minimal interference of the solvent or other medium components absorbance and is in agreement with other studies on IND's crystalline solubility previously reported in literature. [131,132]

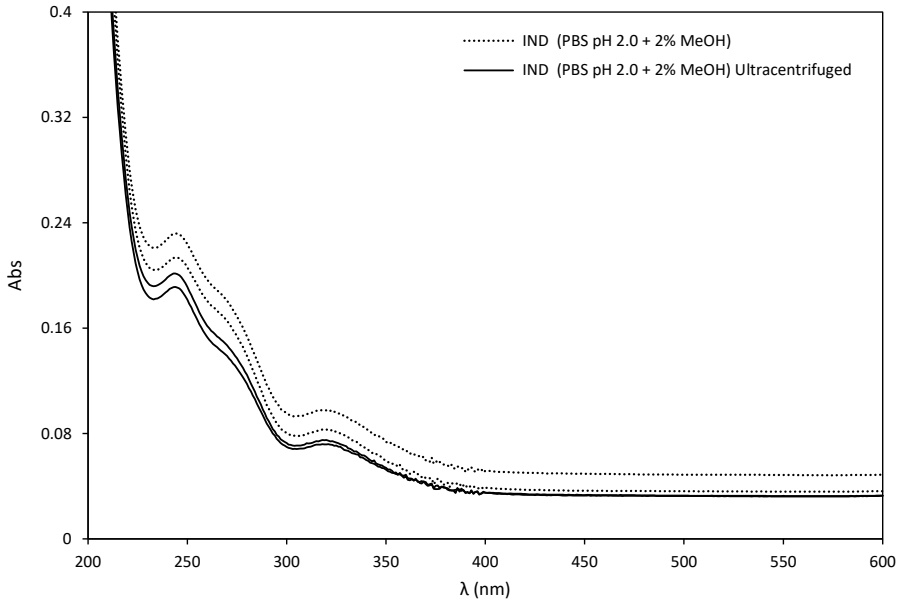

Figure 8. *UV-Vis spectral scans within the range of 200-600 nm of samples produced by the shake-flask method to study crystal solubility of IND in PBS with 2% (w/w) Methanol at pH 2.0.*

In the spectral scans of the samples none submitted to ultracentrifugation there were registered differences in the baseline denoting light scattering phenomena occurring due to interaction of light with particles in suspension. The pre-treatment with ultracentrifugation allows a reduction of the interference of such phenomena occurring in solution with the measurements being collected.

Table 3 depicts the absorbance measurements correspondent to each replicate sample at the maximum absorption wavelength of IND (λ_{max}= 320nm) corrected by subtraction of the baseline absorbance at 600nm along with the respective concentrations calculated with the respective extinction coefficient of the calibration curve prior constructed for the same medium conditions.

The crystalline solubility of IND in a dissolution medium composed by PBS at pH 2.0 with 2% (v/v) methanol was determined before and after sample ultracentrifugation corresponding to 4.67 µg/mL and in 3.80 µg/mL, respectively. After being corrected, the absorbance values showed great similarity resulting, upon conversion, in also similar concentrations. In terms of precision, a good data reproducibility was observed with a relative standard deviation (% RSD) inferior to 30%.

Table 3. *Determination of IND crystalline solubility in Phosphate Buffer (PBS) with 2% MeOH at pH 2.0, by the shake-flask method.*

Sample	Abs $_{320\ nm}$ (*)	C (µg/mL)	$C_{crystal}$ (µg/mL)	STD	RSD (<30%)	R_S
IND (PBS pH 2.0 + 2% MeOH) (replicate 1)	0.0488	4.79	4.67	0.17	3.69	5.9
IND (PBS pH 2.0 + 2% MeOH) (replicate 2)	0.0468	4.55				
IND (PBS pH 2.0 + 2% MeOH) Ultracentrifuged (replicate 1)	0.0425	4.02	3.80	0.32	8.40	**7.3**
IND (PBS pH 2.0 + 2% MeOH) Ultracentrifuged (replicate 2)	0.0388	3.57				

$\varepsilon_{(IND)}$ = 0.0082

$C_{amorphous}$ = 27.59 µg/mL **(*)** corrected

The averaged values obtained for IND's crystalline solubility upon dissolution in PBS at pH 2.0 with 2% (v/v) methanol present similarity with the one previously determined by *Murdande et al*. for crystalline solubility of IND in water (5.3 µg/mL), a good indicative since both determinations are performed in an aqueous chemical environment.[117,133] Accordingly, the concentration of 3.8 µg/mL was taken as the equilibrium solubility of IND throughout the entire analysis that follows.

The same procedure was followed to determine the equilibrium solubility of IND in PBS at pH 6.8, but since at this pH the negatively charged form of IND conveys enhanced hydrophilicity and solubility to the drug compound, it wasn't possible to attain reliable results within the quantification limits of the techniques at our disposal, since it was expected to completely dissolve.

3.1.2. Theoretical and Experimental determination of Amorphous Solubility

The conversion of a crystalline drug compound into an amorphous form of higher entropy, enthalpy and free energy results in an enhanced solubility and dissolution rates.

For this reason, an accurate estimation of the apparent amorphous solubility in the experimental conditions tested is crucial during ASD formulation development to evaluate the in vitro performance in terms of supersaturation rate and extent and also to enable comparison between distinct ASD prototypes under screening.

The apparent solubility of an amorphous compound is the upper limit of supersaturation way above crystal solubility, in which a liquid-liquid equilibrium is established between a drug-rich phase and a solvent-rich phase. This Liquid-liquid phase separation (LLPS) phenomena usually occurs in a metastable region of the API's phase diagram and so it is usually associated to a high driving force for crystallization which can occur from either the water-saturated amorphous drug or the bulk solution phase since the system is supersaturated. As a consequence, the experimental determination of the solubility advantage of the amorphous form can be difficult and may lack reproducibility, when a dissolution approach is used to determine amorphous solubility.

Likewise, in order to avert crystallization, the solvent shift method was conducted as a quick way of generating supersaturated solutions stemming from the spiking of a small volume of a 1.25 mg/mL stock solution of IND in Methanol into a vial with 10 mL of PBS at pH 2.0. This stock solution, which was used to obtain 12 supersaturated solutions within a range of concentrations between 3.75 – 45 µg/mL, was prepared in a concentration approximately 50 times higher than the theoretical amorphous solubility of 25.97 µg/mL (calculated through the equations presented in section 2.2.2.2.) so that the volume of organic stock solution added at LLPS concentration is minimal (below 2% v/v of organic solvent).

The UV-Vis extinction method was carried out to estimate the transition point at which this pseudo-equilibrium is attained. This method is based on the detection of changes in the light scattering properties of the medium, above the amorphous solubility, where the drug-rich colloids are generated. These changes in light scattering are monitored at wavelengths where the drug does not absorb (extinction).

The UV-Vis spectral scans acquired for all supersaturated solutions between 200nm and 600 nm are represented in Figure 9.

By examining the absorption profile of each supersaturated system generated is possible to detect maximum absorbance peaks at 265nm and 320 nm, which is in agreement with the previous UV-Vis spectroscopic analysis performed to estimate IND's crystal solubility. By monitoring the extinction region located between 450 nm and 550nm, it is possible to denote a gradual increase in the baseline absorbance values with concentration, due to changes in light scattering.

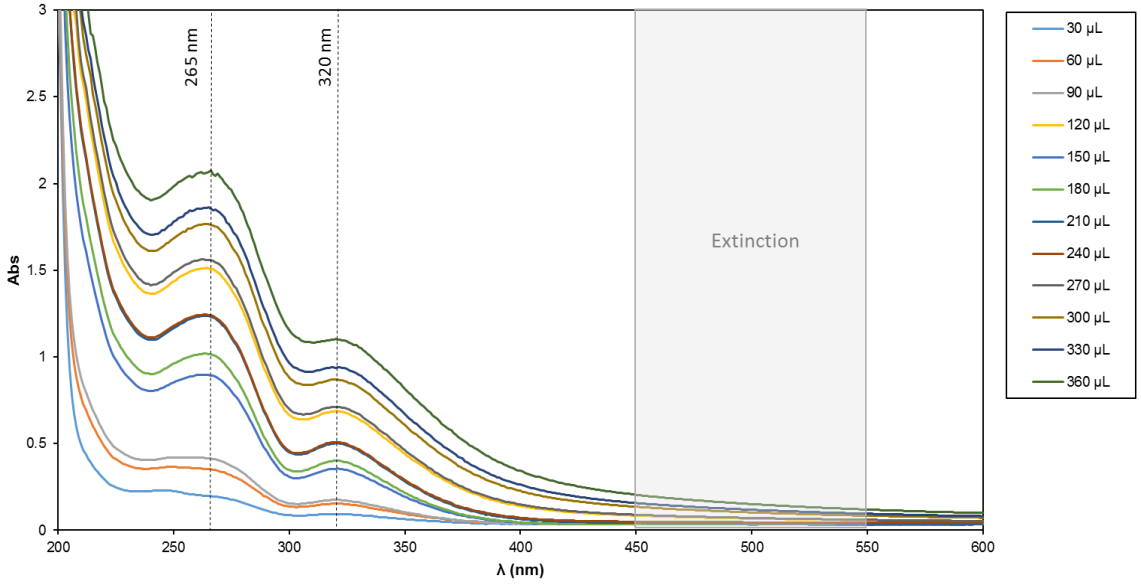

Figure 9. *UV-Vis spectral scans within wavelength region of 200-600 nm regarding 12 supersaturated solutions of IND in Methanol into 10 mL of PBS at pH 2.0 resultant from the solvent-shift method. Vertical dashed lines depicting the correspondence of maximum absorption peaks at 245 nm and 320 nm. Extinction region (grey zone).*

The absorbance values registered for all generated supersaturated solutions at 450 nm, 500nm and 550 nm extinction wavelengths were plotted against the respective concentrations as depicted in Figure 10.

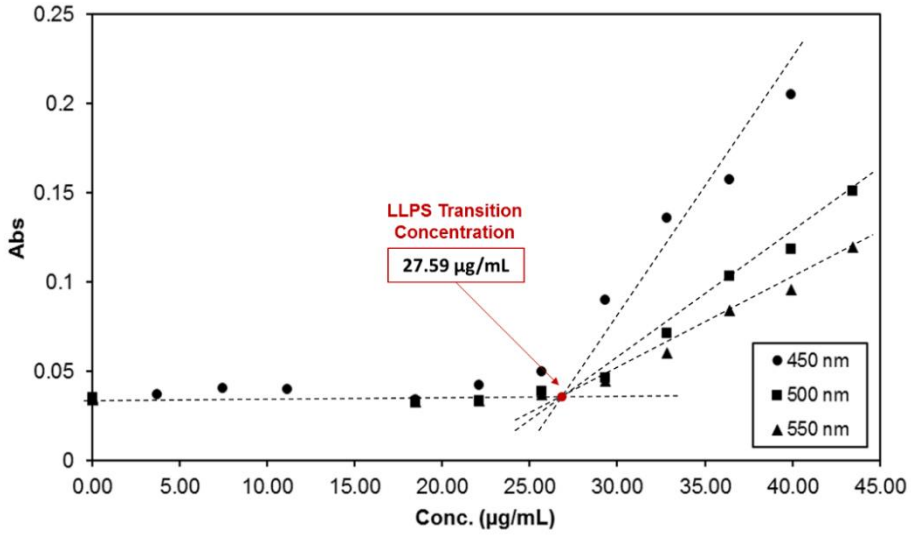

Figure 10. *Determination of LLPS onset transition concentration by monitoring UV extinction at 450nm, 500nm and 550nm. LLPS transition concentration (red point).*

The Extinction values plotted in Figure 10 were fitted to trend lines depicted in a dashed pattern. The interception point between dashed lines corresponds to the LLPS onset concentration, also known as LLPS transition point, after which the solution changes from a single phase homogeneous solution to a two phase system, as indicated by a rapid increase in the extinction.

Therefore, amorphous IND at 37°C undergoes LLPS in PBS at pH 2.0 when the concentration exceeds approximately 27.59 µg/mL, yielding a hazy solution.

The increase in extinction readings upon generation of a new phase can be due to either crystallization or liquid-liquid phase separation phenomena. At a macro level observation, it was possible to assess that the resultant highly supersaturated solutions revealed a hazy appearance and a slight bluish color. Although such observations can be indicative of the occurrence of liquid-liquid phase separation (LLPS), they are not enough by itself to assure that no crystallization has taken place during the evaluation process. Also the solvent shift method was conveniently fast in the generation of each supersaturated system so that the time span between preparation and readings could be short.

The estimated LLPS onset concentration was considered as apparent amorphous solubility of IND and related to the previously estimated crystal solubility to assess the solubility enhancement ratio (R_s), as depicted in the Table 3 from the previous section.

3.1.3. Calibration curves

The evaluation on ASD formulation prototypes performance will be made through dissolution testing held inside microplate wells, with quantification being carried out in real time in a UV-Vis microplate reader, a technique based on the determination of absorbance at the API's maximum absorbance wavelength.

Calibration curves obtained from data collected in the microplate reader are essential for conversion of UV-Vis absorbance data to concentration since the absorbance readings collected must be corrected to account with differences with respect to light path length.

Whenever UV-Vis spectroscopic assays are carried out in a cuvette, the samples inside it are horizontally radiated with a light beam, with the light traveling a fixed path length characteristic of the type of cuvette used to perform the study. Moreover, since the optical path length traversed is well known, concentration measurements can be acquire by converting absorbance readings using the Lambert-Beer law.

On the other hand, when UV-Vis spectroscopy is held in a microplate well, the light beam travels across the sample vertically and so, the optical path length depends mainly on the thickness of the liquid layer, sample volume, microplate well dimensions and the meniscus effect of the liquid surface.

Because of these differences in optical path length resulting from different sample volumes used, there was the need to define a different strategy to convert the absorbance values collected during dissolution testing into concentration of IND in solution.

Calibration curves of IND standard solutions prepared in Methanol, in PBS at pH 2.0 and in PBS at pH 6.8 were obtained through UV-Vis spectroscopy analysis via microplate reader (Figure 11).

The concentrations of IND standard solutions prepared in Methanol fall within the range of 1 µg/mL up to 50 µg/mL whereas the standard solutions of IND in PBS at pH 2.0 and in PBS at pH 6.8 were prepared with concentrations from 1 µg/mL up to 300 µg/mL.

The Absorbance readings were registered at IND's maximum absorption wavelength (320nm), corrected to baseline and plotted against standard solution concentrations. The linearity of measurements was evaluated for the ability of relating absorbance signals with the concentrations of reference standard solutions, by linear regression analysis. The respective slopes correspond to extinction coefficient (ε).

The coefficients of determination (r^2) obtained for linear statistic verification of IND calibration curves were comprised within the interval of 0.995 and 0.999, showing satisfactory linearity and consistent proportionality between the studied concentration ranges.

The UV absorbance measurements of IND standard solutions prepared in an organic solvent (Methanol) and in PBS at pH 2.0 were monitored at IND's maximum wavelength of absorption, λmax = 320nm. By a direct comparison of both curves it is possible to acknowledge a distinct linearity evolution, translated by different extinction coefficients of IND present in the generated standard solutions. For concentrations higher

than 120 µg/mL is was registered a loss of this linearity since the system was no longer abiding by the Beer-Lambert Law.

In fact, the molar absorptivity of IND in methanol proved to be higher than the one determined in Phosphate Buffer Solution (PBS) at pH 2.0. These differences are explained by the fact that, at pH 2.0, colloidal species are formed above ~28 µg/mL (amorphous solubility) and these species absorb radiation differently. On the other hand, no colloidal species are formed in methanol since crystalline IND is highly soluble in methanol. It can be concluded that the colloidal species absorb less light energy compared to the free drug molecules.

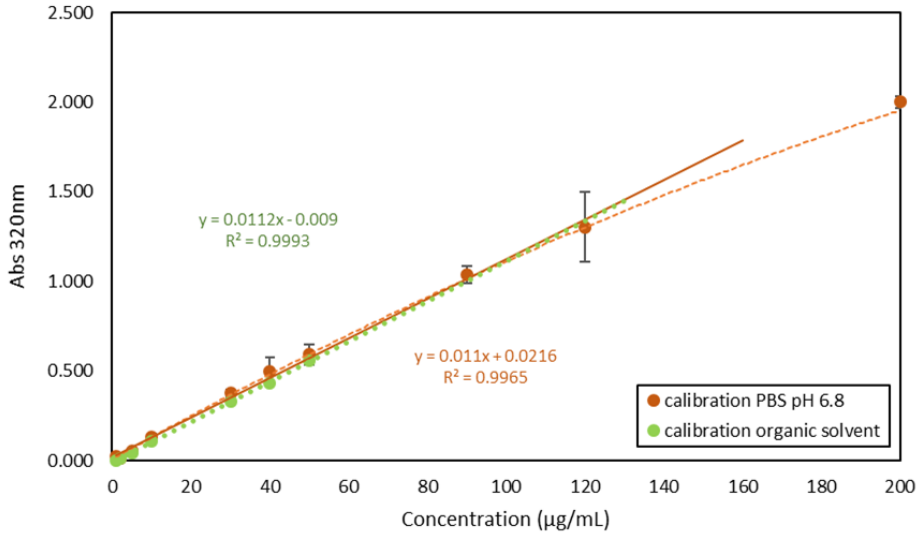

Figure 11. *Calibration curve of IND in Methanol constructed using standard solutions whose concentrations are comprised with a range of 1 – 50 µg/mL (green). Calibration curve of IND in PBS at pH 6.8 constructed using standard solutions whose concentrations are comprised with a range of 1 – 300 µg/mL (dark orange). The linear standard curve depicted by a solid line was obtained by linear regression analysis on measurements of the standard solution concentrations from 1 – 120 µg/mL. Means (n=2) along with respective standard deviation error bars.*

Unlike prior results, the calibration curves obtained for IND in Methanol and in PBS at pH 6.8 (Figure 12) are very similar up to 120 µg/mL, which means that the extinction coefficients are similar. These results are aligned with the fact that IND is highly soluble at pH 6.8 and, therefore, no colloidal species are formed in the range of concentrations tested. Therefore, the extinction coefficients are similar because all IND molecules are dissolved in both cases.

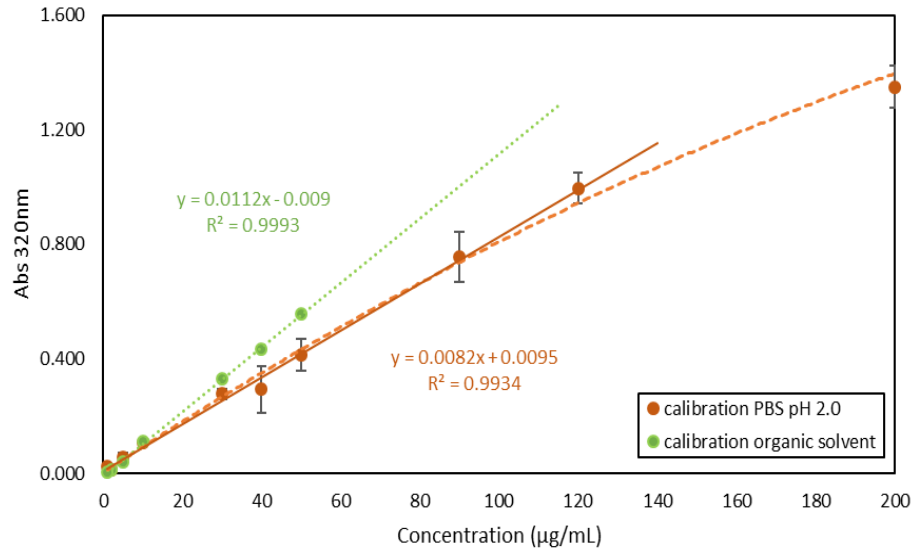

Figure 12. *Calibration curve of IND in Methanol constructed using standard solutions whose concentrations are comprised with a range of 1 – 50 µg/mL (green). Calibration curve of IND in PBS at pH 2.0 constructed using standard solutions whose concentrations are comprised in the range of 1 – 300 µg/mL (dark orange). The linear standard curve depicted by a solid line was obtained by linear regression analysis on measurements of the standard solution concentrations from 1 – 120 µg/mL. Means (n=2) along with respective standard deviation error bars.*

3.2. Development of a solvent evaporation-based method to produce ASD films

Several approaches for generating ASD films by solvent evaporation were followed in an attempt to develop a method that can be applied to a broad variety of ASD prototypes combining different drug compounds and polymer candidates.

The main aspects that were considered for optimization were: liquid sample deposition method, suitable volume, temperature and time expenditure, compound degradation, sample wastage, material handling, uniformity of the film, method reproducibility and preparation speed.

The proof of concept of the solvent based method consisted in varying one or more of the previously stated aspects simultaneously until reaching a methodology able to deliver consistent and uniform amorphous films in a reproducible and fast way.

The handling of the deposition platforms was an aspect to be sorted out given the dimensions and fragility of samples in order to ensure sample integrity and operator safety in every experimental step and also to avoid contaminations. Therefore, a special type of tweezers, with bent sharp point tips, was selected to perform such task.

Table 4. *Different procedures that have been tested during the development of a solvent evaporation method to ASD preparation using deposition platforms (Hovione IP). Brief description of the respective procedure along with main advantages and disadvantages associated.*

Solvent casting preparation procedures	
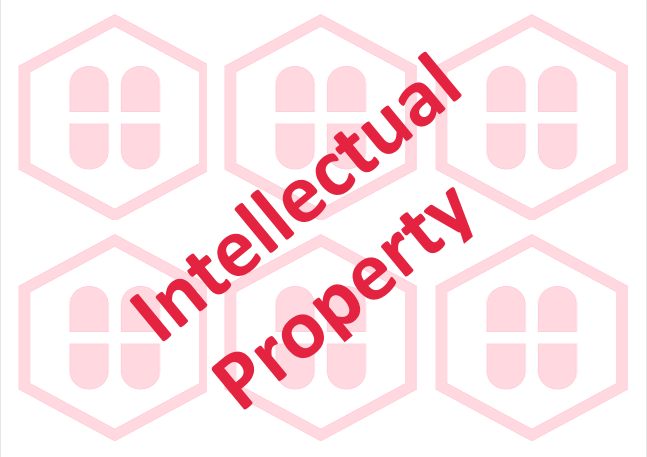	**Petri Dish** Consisted in submersing the deposition platforms in a certain volume of liquid sample inside a petri dish and then heating to promote solvent evaporation **Advantages** - Preparation of several ASD films at a time **Drawbacks** - Sample waste - Material accumulation in sections of the deposition platform and in the petri dish surface - Lack of reproducibility in terms of controlling the mass of the films formed
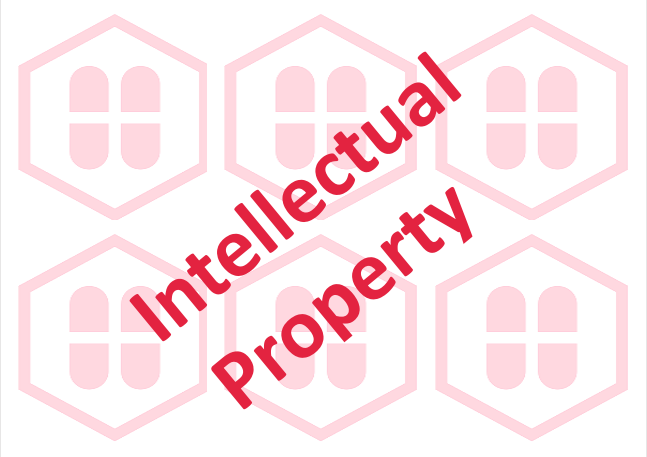	**Heating block assembly** Consisted in submersing the deposition platform placed in the central support and inside the cup with around 1 mL of liquid sample and then, heating to promote solvent evaporation. **Advantages** - Allows controlling the volume of liquid sample **Drawbacks** - Sample waste - Material accumulation in sections of the deposition platform, in the container and in the spaces between them - Low-throughput method (one-at-a-time preparation) - Slow process (volume needed to submerse vs. evaporation time)
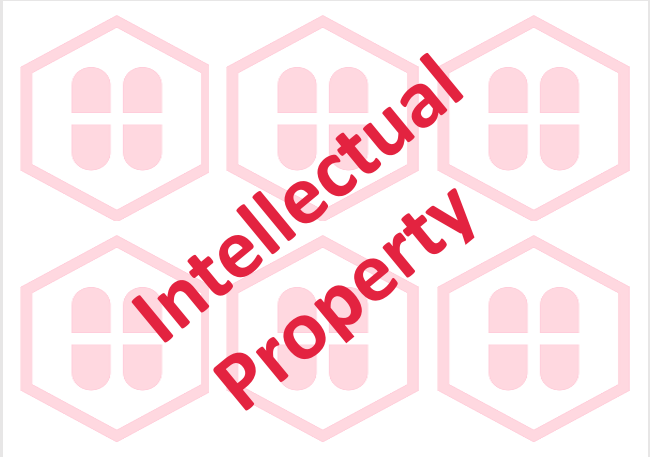	**Disposable Microplate** Consisted in submersing the deposition platform placed inside a microplate well with around 1 mL of liquid sample and then, heating to promote solvent evaporation. **Advantages** - Enables to control de volume of liquid sample - Preparation of several ASD films at a time **Drawbacks** - Sample waste - Material accumulation in other sections of the deposition platform, in the well and in the spaces between - Slow process (volume needed to submerse vs. evaporation time)

Aluminum Tin

Consisted in submersing the deposition platform placed in a aluminum tin with around 1 mL of liquid sample and then, heating to promote solvent evaporation.

Advantages

- Enables to control the volume of liquid sample
- Preparation of several ASD films at a time

Drawbacks

- Sample waste
- Material accumulation in sections of the deposition platform, in the tin and in the spaces between
- Low-throughput method
- Slow process (time to prepare one aluminum tin per deposition platform

Micropipette deposition

Consisted in pre-heating the deposition platform in a heating plate covered with aluminum foil and afterwards, with the aid of a micropipette (P200), carefully add the liquid sample volume so that it can cover the entire deposition platform quickly before solvent evaporation.

Advantages

- Enables to control de volume of liquid sample
- Preparation of several ASD films at a time
- High-throughput method
- Low waste of material
- Quick evaporation
- Thin films with high consistency and uniformity

Drawbacks

- Operator skills on micropipetting
- Requires a micropipette P200 and no other type.

The liquid deposition method in the deposition platform was prioritized during development of the methodology. Different assemblies were tested as liquid holders to maintain the liquid sample in contact with the deposition platform during organic solvent evaporation. Table 4 summarizes of all the approaches tested and the main conclusions taken regarding each method.

The method that was implemented was the micropipette deposition (Figure 13) method, since it allows reproducibility and speed whilst ensuring film consistency and uniformity, Furthermore, it requires almost no additional equipment apart from the micropipette P200 and the aluminum foil to perform the liquid sample deposition, conveying low sample waste.

This method relies mainly on the surface tension properties of liquids to form a uniforms layer of liquid on the deposition platform without spilling or leaving any uncovered areas. Therefore, not all volumes of liquid sample are suitable to cast the films in the deposition platform. A study on the range of volumes that can be

pipetted onto the deposition platform and produce the desired effect by covering the entire surface area was performed.

Figure 13. *Schematic illustration of the liquid sample deposition process on the deposition platform with the aid of a micropipette P200.*

Volumes within a range between 65 µL and 200 µL were tested. For volumes inferior to 145 µL the liquid didn't cover the entire surface of the film deposition platform leading to the formation of inconsistent ASD films. On the other hand, concentrations in a range between 145 µL up and 175 µL created the desired layer of liquid, whereas for volumes above 175 µL the surface tension forces were not strong enough to keep the liquid shape and so, the liquid was spilled out.

Within the range of volumes to consider, the volume of liquid selected as appropriate to be used in all the experiments was 150 µL. All the drug/polymer solutions were adjusted so that 150 µL of liquid sample could produce an ASD film, which upon dissolution would be capable to generate the desired target concentration.

The only process steps common to both solvent evaporation and fusion-based methods are the heating and the cooling step, since the remaining steps were optimized according to the needs and specifications of each method.

3.3. Development of a fusion-based method to produce ASD films

Several approaches were tested in an attempt to develop the most adequate method to produce ASD films by fusion, for application to a wide variety of prototypes using different drug compounds and polymer candidates.

The main aspects that were considered to be optimized were: blend deposition method, amount of material deposited, temperature and time expenditure, compound degradation tendency, sample waste, material handling, uniformity of the film, method reproducibility and preparation speed.

The proof of concept of a fusion based preparation method consisted in inserting some variations on one or more of these aspects simultaneously until reaching the best approach in terms of achieving a method able to produce consistent and uniform amorphous films in a reproducible and fast way.

The heating block assembly portrayed in Figure 14 was developed to aid the preparation of the ASD films by two methods.

Figure 14. *Preparation set (Hovione IP).*

In a first approach, the preparation set used the three pieces and the process consisted in assembling the components according to image (c) Figure 14, adding an excess quantity of blend high enough to cover the entire surface area of the deposition platform. Then, the entire preparation set was heated and, after melting, immediately cooled in order to promote the formation of an amorphous film.

Variations of this experiment were performed with new adjustments made at every trial regarding quantity of material added, the temperature used, the deposition of material and even the order by which each component of the preparation set was being added to the heating plate.

The major problem with this procedure was the waste of material and also sample degradation, since it required a lot of energy to heat the entire preparation set and maintain temperature in the assembly. The heating problems and the fact that a lot of material was used lead to issues such as uneven fusion, material accumulation and encrustation that ultimately precluded the formation of a consistent film layer and hindered the process of removing the central support and making it impossible to isolate the deposition platform without compromising the integrity of the film.

Furthermore, the use of the preparation cup hindered process speed, since it required a tedious and time consuming cleaning procedure between each preparation to avoid sample contaminations, which would turn out to be impracticable.

The alternative found to solve the problem was to cover the top surface of the heating plate with an aluminum foil and add the deposition platforms directly to promote the fusion of the blend material. This implied the development of a new deposition strategy separated from the heating step.

To do so, the process of material deposition in the deposition platform was optimized. The central piece of the preparatory device was used to hold the deposition platform (Figure 15 (a)), the addition of material was performed with the aid of a small spatula (Figure 15 (b)) and an additional deposition platform was added on top to compress the material and promote its even distribution over the entire surface of the deposition platform (Figure 15 (c)). The process of deposition was optimized several times in order to perfect the addition method and the creation of such thin layers of material.

Figure 15. *Step-by-step illustration of the Blend deposition process. (a) Central support and deposition platform. (b) Addition of powder blend material. (c) Addition of a second deposition platform to perform the compression step. (d) Formation of a thin layer of blend material and (e) Removal of the top deposition platform at the end of the procedure.*

Hence, the blend deposition process was no longer a rate limiting step and was applied to the preparation of all sets of different ASD prototypes to be screened, at a fast and reproducible way. This process step was always performed near by a bench scale so that the deposited mass could be controlled.

After optimizing the preparation method, two IND/Polymer blends were tested and a total of six different quantities were used to assess the most suitable quantity to use in ASD film production. The respective ASD films were subjected to dissolution testing in PBS at pH 2.0, at 37ºC, and the resultant dissolution profiles are depicted in Figure 16.

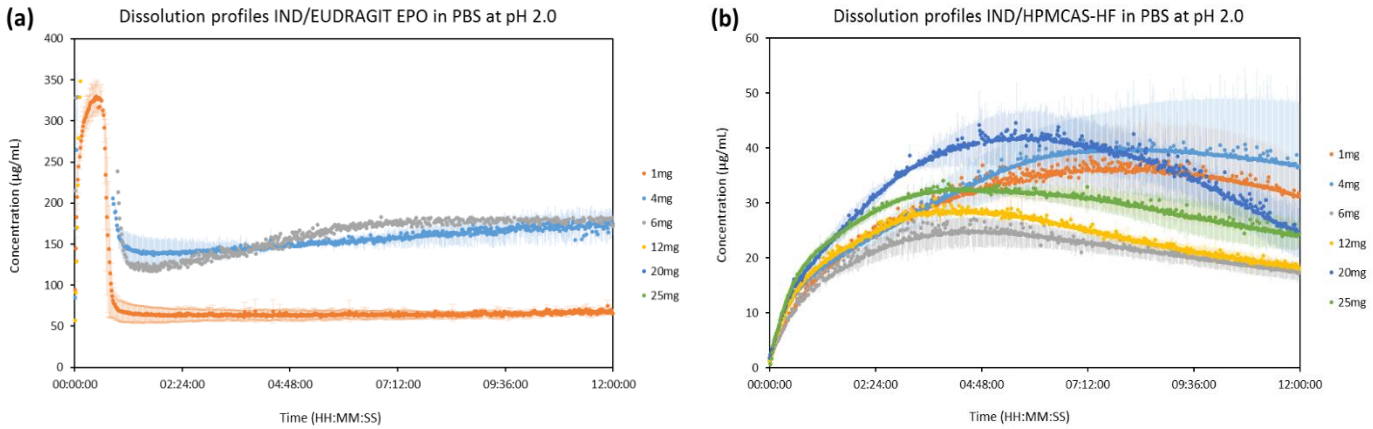

Figure 16. *Dissolution profiles of IND ASD films produced by the fusion method with total mass of 1, 4, 6, 12, 20, 25 mg, in PBS at pH 2.0, during a 12h period, at 37ºC, under constant orbital shaking: (a) IND/ EUDRAGIT EPO ASD films with 50% drug load; (b) IND/ HPMCAS-HF ASD films with 50% drug load. Values represent mean IND concentration (n = 2) and Y-error bars indicate the standard deviation.*

As shown in Figure 16 (a), the dissolution profiles acquired upon dissolution of the IND/EUDRAGIT EPO ASD films with 1 mg, 4 mg and 6 mg depict very similar performances, differing only in the supersaturation levels attained after the concentration decay. On the other hand, for the ASD films with 12 mg, 20 mg and 25 mg, data was only collected in the initial minutes of the 12-hour dissolution run, since absorbance values increased beyond the range of the UV-Vis microplate reader. It must be referred that even though maximum concentration values, around 350 µg/mL, were determined with the help of the calibration curve, linearity was only demonstrated up to 120 µg/mL. Therefore, all values above this concentration should not be considered accurate. Hence, if the amorphous films were to be prepared in very high quantities, the probability that absorbance values would fall outside the range of the equipment is very high. Mostly, this applies to drugs that dissolve in a medium where solubility is high or ASDs that contain polymers that are highly soluble and thus promote fast release of the drug, such as EUDRAGIT EPO in pH 2.0.

On the other hand, the profiles obtained upon dissolution of IND/HPMCAS-HF ASD prototypes (image (b), Figure 16) were similar in terms of dissolution behaviour and degree of supersaturation generated. Thereby, increasing film mass did not lead to impact the extent of release nor altered drastically the dissolution profiles, only causing differences in the initial dissolution rates. Since higher quantities did not impact he dissolution profiles collected, no other motifs may justify their application and so they were disregarded given the scarce quantities of API available during early stages of formulation development.

To sum up, despite high quantities resulted in thicker films with greater consistency and more uniformly spread onto the deposition platform, the majority of the API used in the production of these films either wasn't released or, having been released, surpassed the quantification limits of the technique thus precluding an adequate evaluation of the results. Among the smaller quantities, the choice fell upon 1 mg,

since it enabled the production of consistent and uniform films and the acquisition of representative results whilst requiring small amounts of API.

3.4. Dissolution studies

Dissolution studies are essential to assess the rate and extent at which a certain drug compound is delivered into solution, being a great tool to evaluate the performance of the formulation or dosage form. This type of testing allows understanding the behaviour of a formulation by correlating the concentration-time profile with the underlying physical processes taking place, assuming an even greater importance for drug delivery systems in which drug release is a rate-limiting step for absorption and therapeutic efficacy.

Dissolution testing is therefore important to evaluate critical physicochemical attributes of compounds present in a certain formulation and a great way of evaluating the impact of the manufacturing process, helping to build quality into the final drug product. As far as ASDs are concerned, dissolution studies are very important to assess drug-carrier properties in terms of its ability to promote dissolution, to maintain a supersaturated state and to delay crystallization either in solution or by influencing solid-state stability of the amorphous drug substance. Dissolution testing is widely used in the pharmaceutical industry for formulation optimization and quality control but in this project it is particularly important as a screening methodology for the selection of ASD prototypes.

The dissolution profiles of 56 different types of amorphous drug-polymer films, prepared either by solvent evaporation or by fusion method, and resulting from the combination of drug and polymer in different drug loads, were acquired using PBS as dissolution medium at physiologically relevant pH 2.0 and pH 6.8.

The analysis and discussion of results will be focused on the dissolution profiles of IND/HPMCAS-HF and IND/EUDRAGIT EPO case studies, since these two polymers are extreme examples of the influence of polymeric drug-carrier on the dissolution and crystallization kinetics of drugs and, consequently in the supersaturation potential and performance of an ASD formulation.

Despite having similar molecular weights and of having both pH-dependent solubilities, these polymers are soluble in different intervals of the pH scale, hold very despair glass transition temperatures and while HPMCAS-HF is anionic EUDRAGIT EPO is cationic Moreover, they have very different glass transition temperatures (Tg): $T_{g\,(HPMCAS\text{-}HF)}$ is much greater than $T_{g(EUDRAGIT\ EPO)}$. Hence, all these aspects render these polymers interesting case studies in terms of drug-polymer interactions, supersaturation potential and stabilization capacity.

The very same approach was pursued for the remaining polymer candidates and all the dissolution profiles acquired can be found in the APPENDIX section.

The analysis of dissolution profiles was performed assuming that experimental conditions such as temperature, pressure, motion, ionic strength and total volume of dissolution medium were kept constant throughout readings and that, for both ASD preparation methods employed, a homogeneous molecular dispersion of the drug in the hydrophilic carrier was achieved.

3.4.1. Dissolution in PBS pH 2.0

Regarding dissolution of ASD films prepared by the solvent evaporation method in PBS at pH 2.0, two sample amounts were tested to yield two different target concentrations after dissolution inside the microplate wells:

I. 20 µg/mL, within the range of concentrations between IND's equilibrium solubility and apparent amorphous solubility
II. 120 µg/mL, a concentration way above apparent amorphous solubility threshold.

These target concentrations were defined prior to film preparation in order to evaluate the impact of polymers in the generation and maintenance of supersaturation below and above IND's apparent amorphous solubility, which had been estimated as 27.59 µg/ml.

Regarding the preparation of ASD films through the fusion based method, instead of defining a specific target concentration, this method fixed the mass to be deposited in the deposition platform to produce amorphous films of 1 mg.

3.4.1.1. Dissolution of amorphous IND films in PBS pH 2.0

Both solvent evaporation and fusion methods developed were applied to produce amorphous films of pure IND using the same target concentration (120 µg/mL) and mass (1 mg). The concentration-time profiles resultant from dissolution in PBS at pH 2.0 can be found in APPENDIX section (Figure A8). In both cases, the amorphous form by itself was able to generate an initial concentration peak of around 40 µg/mL, surpassing the intrinsic crystal solubility limit. However, due to the absence of polymeric stabilization and to the inherent tendency for crystallization, concentrations started to decrease right after peaking. Another important aspect to mention is that amorphous films with distinct API masses delivered similar amounts of API into solution.

3.4.1.2. Dissolution of IND/ HPMCAS-HF ASDs in PBS pH 2.0

The binary ASD formulations of IND/HPMCAS-HF combined at 30%, 50%, 60% and 80% drug loads were investigated for their dissolution behavior in PBS medium at pH 2.0 monitored at IND maximum wavelength of absorbance (λ_{max}= 320nm).

Figure 17, shows the concentration-time profiles of IND/ HPMCAS-HF ASD formulations prepared to meet the 20 µg/mL target concentration when dissolved in PBS medium at pH 2.0, with drug loads ranging from 30% up to 80%.

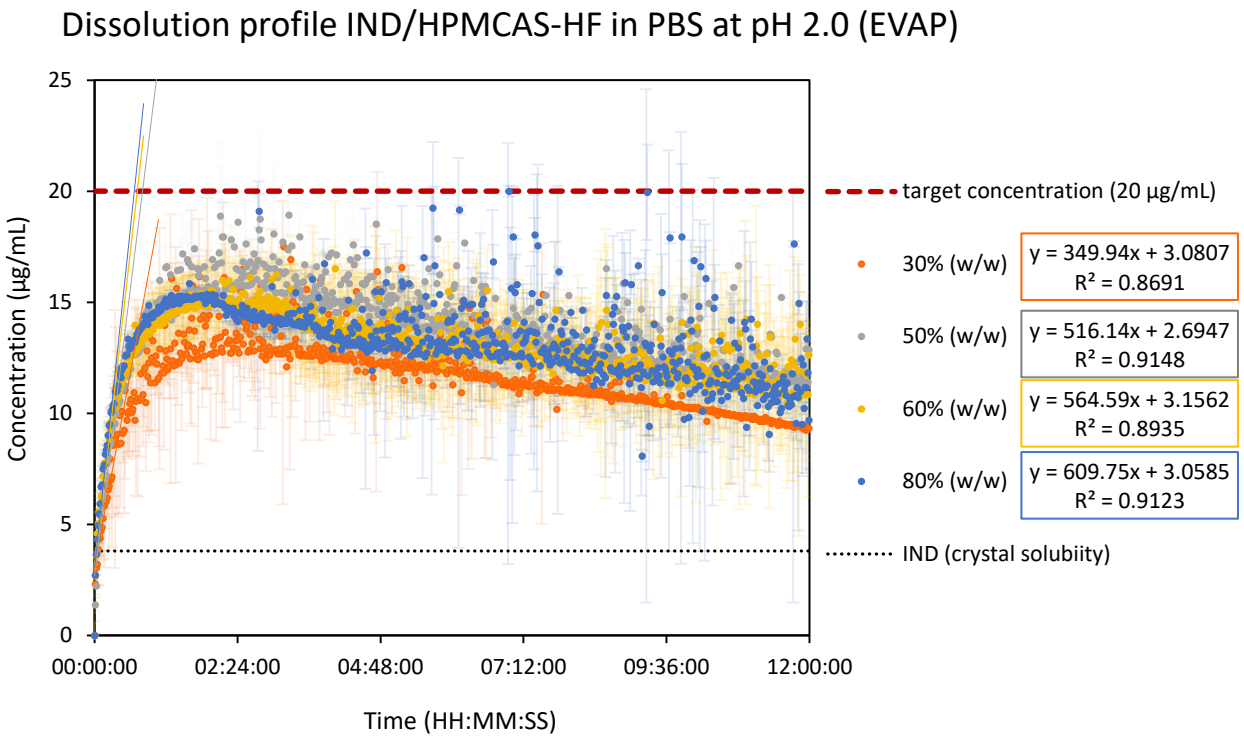

Figure 17. *Dissolution profiles of IND/ HPMCAS-HF ASD films produced by solvent evaporation with 30% drug load (orange), 50% drug load (grey), 60% drug load (yellow) and 80% drug load (blue), in PBS at pH 2.0, during a 12h period, at 37ºC, under constant orbital shaking. Target concentration 20 µg/mL (Red dashed line). IND's crystal solubility (black dashed line). Values represent mean IND concentration (n = 2) and Y-error bars indicate the standard deviation.*

All IND/HPMCAS-HF amorphous films exhibited very similar release profiles and supersaturation behaviour. Every IND/HPMCAS-HF formulation here depicted yielded IND concentrations above crystalline solubility (3.8 µg/mL), and produced solutions that persisted in a supersaturated state within the entire experimental time frame without falling below crystalline solubility. This trending behaviour identifies HPMCAS-HF as a drug-carrier with some stabilization capacity over IND in solution leading to a crystallization delay.

Despite all formulations failing to reach the target concentration, the fraction of total API released managed to generate concentrations between 13 and 15 µg/mL, corresponding to 65-75% of the maximum concentration they were intended to generate.

The maximum concentrations were registered approximately 2 hours after the beginning of the dissolution run and, even though all IND/HPMCAS-HF formulations display similar dissolution kinetics, the fastest and

the slowest dissolution rates were achieved with the 30% and the 80% drug loaded formulations, respectively. This may lead to the conclusion that IND/HPMCAS-HF ASD formulations with high drug loads perform better than those where the polymeric counterpart is greater. These results may be explained by the poor solubility of HPMCAS-HF at pH 2.0, which impacts negatively the release of drug from the ASD.

After reaching maximum concentration, the drive for crystallization is greater than the dissolution kinetics and concentrations start decaying from then on. In addition, it was verified that the average values presented great variability after the onset of crystallization, which suggests the occurrence of drug precipitation from solution and a possible interference of small drug aggregates that were taking form in solution, causing scattering of the incident UV light. This variability in the data collected after crystallization is also reflected by the magnitude of the error bars associated.

Such outcome was mostly observed in the dissolution profiles of IND/HPMCAS-HF ASD formulations with drug loads superior to 50%, for which the polymer ratio revealed ineffective to inhibit precipitation.

Also important to bear in mind that the amorphous films from which these dissolution profiles result, were produced by the solvent evaporation method with minimal quantities of API and polymer, exhibiting minimal thickness and a high surface area-to-volume ratio, being more in contact with the dissolution medium.

The same experimental protocol was executed to obtain dissolution profiles (Figure 18) for IND/HPMCAS-HF ASD formulations ranging from 30% to 80% drug loads, prepared by the solvent evaporation method targeting 120 µg/mL after dissolution in PBS at pH 2.0.

All the IND/HPMCAS-HF amorphous films screened were able to generate concentrations above IND's crystalline solubility, having achieved a level of supersaturation above the apparent amorphous solubility limit estimated as 27.59 µg/mL for IND in PBS at pH 2.0.

The depicted dissolution profiles can be explained by the influence of the acidic pH medium over HPMCAS-HF and IND solubilities and also on the rate and extent of dissolution of the ASD formulations.

Hence, despite having been designed to achieve a target concentration above the apparent amorphous solubility, about six times higher than the concentration targeted for previous evaluated amorphous films, these IND/HPMCAS-HF amorphous films only reached 20 – 30% of the target concentration they were intended to generate.

In terms of dissolution rate, the IND/ HPMCAS-HF ASD formulations with higher drug loads show faster initial release rates, as depicted by the corresponding slopes of the trend lines fitted to the initial section of each dissolution profile. However, the differences in dissolution rate are not pronounced. To better explain the results, a deeper understanding of what is happening on a molecular level, regarding dissolution kinetics, must be gathered.

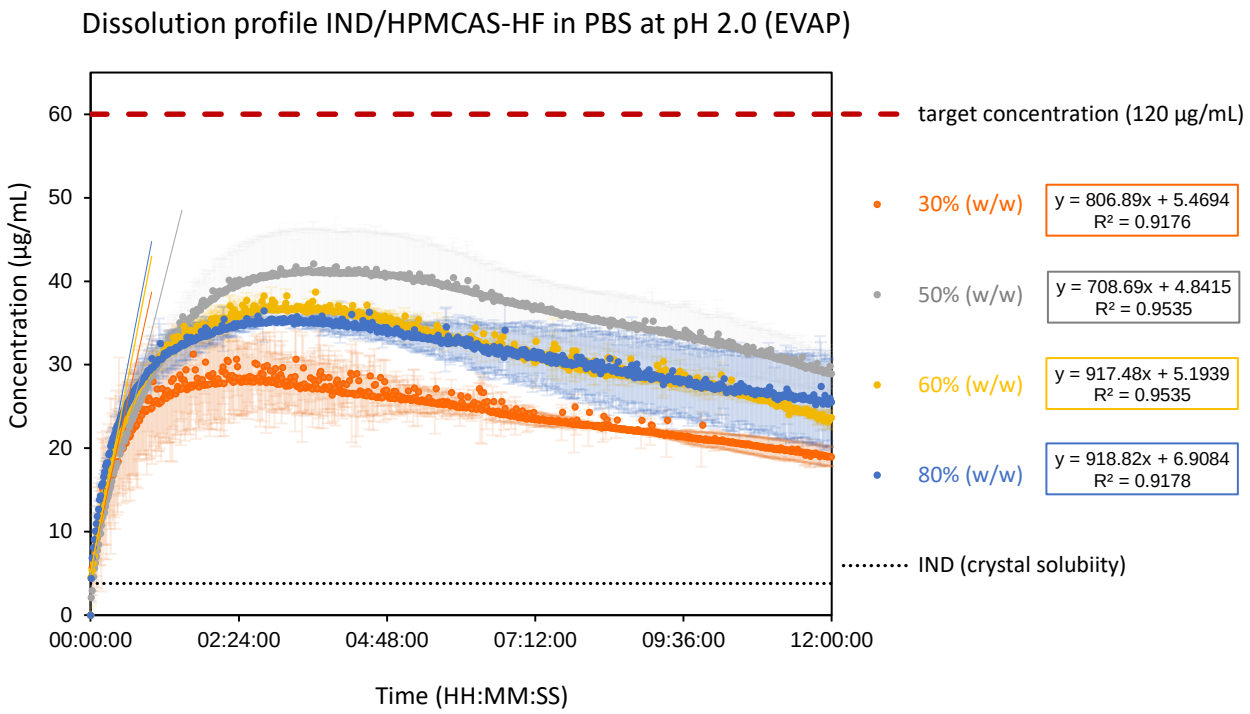

Figure 18. *Dissolution profiles of IND/ HPMCAS-HF ASD films produced by solvent evaporation with 30% drug load (orange), 50% drug load (grey), 60% drug load (yellow) and 80% drug load (blue), in PBS at pH 2.0, during a 12h period, at 37ºC, under constant orbital shaking. Target concentration 120 µg/mL (Red dashed line). IND's crystal solubility (black dashed line). Values represent mean IND concentration (n = 2) and Y-error bars indicate the standard deviation.*

Due to its intrinsic poor aqueous solubility at lower pH, HPMCAS-HF dissolves at a slower rate compared to IND. This lack of solubility of HPMCAS-HF translates into a gradual enrichment of the amorphous film surface layer in HPMCAS-HF and gradual decrease in IND content at the surface, which results in slower drug dissolution rate. Hence, despite IND's higher tendency to dissolve, the accumulation of non-dissolved HPMCAS-HF at film surface starts to act as a barrier, leading to an entrapment of the API molecules located at deeper film layers and preventing higher supersaturation levels to be attained.

The poor solubility of HPMCAS-HF at pH 2.0 also impacted the extent of supersaturation produced by these ASD formulations. The high polymeric content present in IND/HPMCAS-HF ASD films with a lower drug load hampered IND's release process and, therefore, the overall quantity released. As a result, the performance of IND/HPMCAS-HF formulation with a drug load of 30% was highly impacted by the HPMCAS-HF effects, having attained a maximum concentration of around 28 µg/mL.

On the other hand, IND/HPMCAS-HF ASD formulations with higher drug loads (60% and 80%) were capable of attaining higher supersaturation states around 37 µg/mL and 35 µg/mL, respectively, because of the lower polymeric content. For the IND/HPMCAS-HF amorphous films with higher drug load, the thickness

of the film was smaller since the amount of API deposited was constant for all formulations. Therefore, the barrier effect exerted by HPMCAS-HF is less influent, managing to release a higher quantity of IND into solution and attain a higher level of supersaturation.

The exception appears to be the IND/HPMCAS-HF ASD formulation with 50% drug load, which has shown the best performance by delivering a maximum concentration higher than 40 µg/mL. In this particular case, the API and polymer were combined in equal quantities and so, by direct comparison with the other drug loads under test, this condition comprises the best balance between the polymer effect as crystallization inhibitor and the barrier effect for IND release.

Regarding supersaturation maintenance, the dissolution profile of all IND/HPMCAS-HF ASD formulations manifested similar downward trends, registering concentration reductions of 30±5%, as a consequence of crystallization kinetics predominance over dissolution kinetics.

Considering the poor solubility of HPMCAS-HF at pH 2.0, the diffusion of the polymer from the ASD films matrix into the solution phase is considered minimal and insufficient to provide great stabilization of free IND molecules present in the supersaturated solution and hence to delay its crystallization.

Moreover, since the apparent amorphous solubility limit was surpassed by all the IND/HPMCAS-HF ASD films when dissolved in PBS at pH 2.0, the driving force for both crystallization and LLPS phenomena is increased, and the occurrence of such phenomena is highly probable. The variations in concentration measured during and after maximum concentration was reached, and when the concentration starts decreasing, support the coexistence of both phenomena, with LLPS replenishing the supersaturation level during the early stages until crystallization kinetics overcome the dissolution kinetics. More information on the occurrence of this kind of phenomena was gathered with DLS analysis and the results will be presented in subchapter 3.6.

To conclude, since the medium conditions were not favorable to HPMCAS-HF dissolution, as far as solubility is concerned, ASD formulations with higher drug loads manage to deliver a better performance since the dissolution process in such cases is majorly dependent on the dissolution of amorphous drug, despite the negative pH effect on IND solubility. Still, HPMCAS-HF stabilization effect can be denoted by a delay in crystallization depicted by the slow downward trend common to all dissolution profiles.

To standardize the amount of ASD film deposited (different film masses were deposited using the solvent evaporation method), the experimental screening protocol for dissolution in PBS at pH 2.0 was extended to IND/HPMCAS-HF ASD formulations ranging from 30% to 80% drug loads, prepared by the fusion method, and the respective dissolution profiles depicted in Figure 19.

The evaluation of IND/HPMCAS-HF ASD prototypes, with drug loads ranging from 30% to 80%, manufactured by the fusion method, regarding dissolution behaviour in PBS at pH 2.0, rendered dissolution

profiles with very low variability associated to the concentration measurements, as can be acknowledged from the standard deviation magnitude.

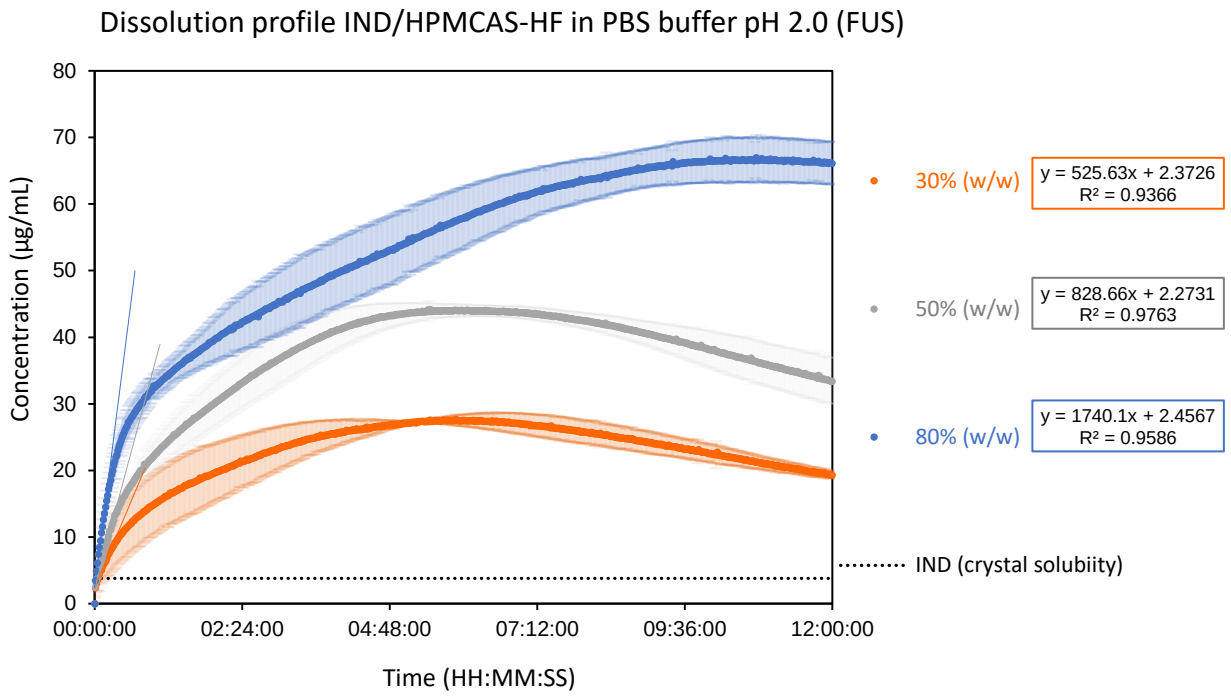

Figure 19. *Dissolution profiles of IND/ HPMCAS-HF ASD films produced by fusion with 30% drug load (orange), 50% drug load (grey) and 80% drug load (blue), in PBS at pH 2.0, during a 12h period, at 37ºC, under constant orbital shaking. IND's crystal solubility (black dashed line). Values represent mean IND concentration (n = 2) and Y-error bars indicate the standard deviation.*

All IND/HPMCAS-HF ASD formulations here presented were able to generate supersaturated solutions above equilibrium solubility of IND. In fact, these IND/HPMCAS-HF amorphous films managed to equal or surpass the apparent amorphous solubility estimated for IND in PBS at pH 2.0 (27.59 µg/mL), achieving high degrees of supersaturation. In the case of IND/HPMCAS-HF ASD formulation with 80% drug load, maximum concentrations were approximately 12 times higher than crystal solubility (66,6 µg/mL). Also IND/HPMCAS-HF ASD formulations with 30% and 50% drug loads managed to reach maximum plateau concentrations of 27.5 µg/mL and 44 µg/mL, respectively, 5h 30min into the dissolution experiment, which they managed to maintain for at least 1h before crystallization kinetics started to take over the dissolution kinetics.

Despite the high supersaturation levels attained by these ASD formulations, the drug concentrations generated by these IND/HPMCAS-HF prototypes in solution never matched the maximum concentrations expected upon complete release (around 200 µg/mL, 333 µg/mL and 533 µg/mL for ASD films with 30%, 50% and 80% drug loads, respectively).

The influence of HPMCAS-HF poor solubility at pH 2.0 on ASDs performance can still be noted in these results. ASD formulations with low drug load, due to their high polymer content, are more predisposed to the polymeric barrier effect that occurs due to the surface enrichment in HPMCAS-HF, hindering the release of total API content comprised in the film by entrapping the API molecules located at lower layers. On the other hand, IND/HPMCAS-HF prototypes with higher drug loads showed greater performance.

Moreover, the fusion method results in amorphous films of higher thickness, since the amount deposited was greater, hampering access of the dissolution medium to all drug content in the film. In fact, in comparison with amorphous films produced by the solvent evaporation method, the films prepared by the fusion method contain more API quantities but the fraction released is much inferior.

Furthermore, the dissolution profiles obtained show a prolonged release and delayed onset of crystallization. The prolonged release may be explained by the higher film mass and, consequently, drug available to dissolve, which results in faster dissolution kinetics. As a result, the kinetics of crystallization will only overcome the kinetics of dissolution later in the experiment. The delayed onset of crystallization can also be explained by the crystallization inhibition effect of the polymer, which is also present in solution at higher concentrations, a consequence of the higher film mass, despite its low solubility.

The stabilization effect exerted by HPMCAS-HF on the amorphous IND compensates issues inherent to thickness of amorphous films produced through the fusion method, by inhibiting IND precipitation whilst the drug is undergoing a slow dissolution/release process fostering supersaturation state maintenance.

3.4.1.3. Dissolution of IND/EUDRAGIT EPO ASDs in PBS pH 2.0

The binary ASD formulations of IND/EUDRAGIT EPO combined at 30%, 50%, 60% and 80% drug loads were investigated for their dissolution behavior in PBS medium at pH 2.0 monitored at IND maximum wavelength of absorbance (λ_{max}= 320nm). Figure 20, shows the concentration-time profiles of IND/EUDRAGIT EPO amorphous solid dispersions prepared by solvent evaporation to meet the 20 µg/mL target concentration when dissolved in PBS medium at pH 2.0.

The IND/EUDRAGIT EPO amorphous films exhibited very similar release profiles and supersaturation behaviour upon dissolution in PBS at pH 2.0.

For every IND/EUDRAGIT EPO ASD prototype here tested, the amount of IND released into solution allowed the generation of supersaturation systems, surpassing by far IND's crystalline solubility (3.8 µg/mL).

All ASD formulations managed to reach maximum concentrations, close to the target concentration of 20 µg/mL, very early in the dissolution run, approximately after 5 min after the start.

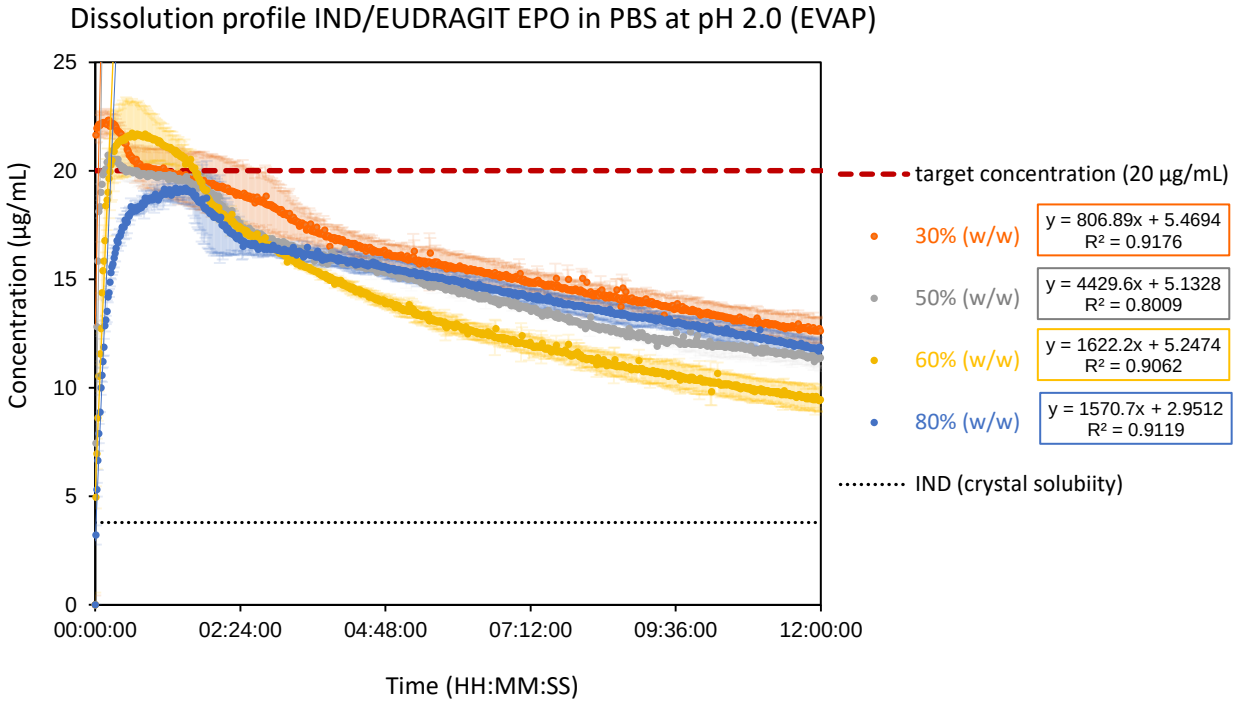

Figure 20. *Dissolution profiles of IND/ EUDRAGIT EPO ASD films produced by solvent evaporation with 30% drug load (orange), 50% drug load (grey), 60% drug load (yellow) and 80% drug load (blue), in PBS at pH 2.0, during a 12h period, at 37ºC, under constant orbital shaking. Target concentration 20 µg/mL (Red dashed line). IND's crystal solubility (black dashed line). Values represent mean IND concentration (n = 2) and Y-error bars indicate the standard deviation.*

The IND/EUDRAGIT EPO ASD formulations with 30%, 50% and 60% drug loads attained maximum concentrations quicker than the one with a drug load of 80%. The reason behind such occurrence can be the higher content in EUDRAGIT EPO, which is a polymer highly water soluble at pH values below 5.0. Hence, the higher polymer content (lower drug load), results in faster dissolution rate at which IND enters solution, since the high polymer tendency to dissolve fosters the release of API, leading to an almost instant dissolution and generation of high supersaturation degrees.

As depicted in the dissolution profiles of IND/EUDRAGIT EPO ASD formulations, after reaching maximum concentration, a plateau was maintained during a short time span, as a consequence of polymer's capacity to inhibit IND crystallization. However, as a consequence of having attained such high levels of supersaturation the driving force for crystallization increased drastically, demanding from the polymeric counterpart a good stabilization effect.

The presence of EUDRAGIT EPO wasn't enough to avoid crystallization and so a drop in INDconcentrations was observed, indicative of the predominance of crystallization kinetics over dissolution kinetics. Therefore, crystallization inhibition was not enough, causing the dissolution profiles to follow a slow decay in concentration to equilibrium levels, but never reaching them within the experimental time frame.

Despite following a downward trend, the IND concentrations persist at supersaturated levels, as a sign of the capacity of EUDRAGIT EPO to stabilize the IND in solution and delay its crystallization, regardless of the ratio at which it was combined with IND to form the ASD prototypes.

The dissolution profiles presented in Figure 21, resulted from the application of the same experimental protocol to four different IND/EUDRAGIT EPO ASD formulations ranging from 30% to 80% drug loads, prepared by the solvent evaporation method to reach 120 µg/mL target concentration when dissolved in PBS medium at pH 2.0. Important to bear in mind that higher quantities of EUDRAGIT EPO and of IND were comprised in the amorphous films responsible for such profiles, since they were targeted to achieve an upper supersaturation state.

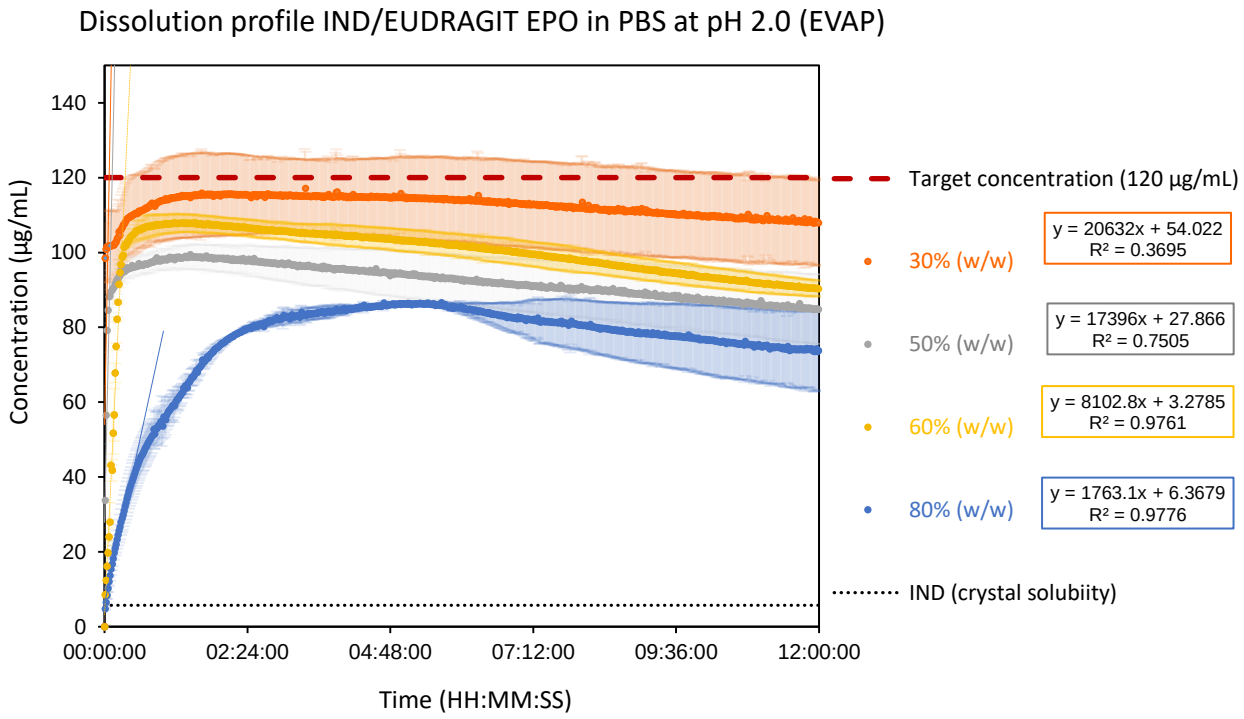

Figure 28. *Dissolution profiles of IND/ EUDRAGIT EPO ASD films produced by solvent evaporation with 30% drug load (orange), 50% drug load (grey), 60% drug load (yellow) and 80% drug load (blue), in PBS at pH 2.0, during a 12h period, at 37ºC, under constant orbital shaking. Target concentration 120 µg/mL (Red dashed line). IND's crystal solubility (black dashed line). Values represent mean IND concentration (n = 2) and Y-error bars indicate the standard deviation.*

Upon dissolution profile analysis, it is possible to acknowledge that the four different IND/EUDRAGIT EPO amorphous films screened were able to generate supersaturated systems when in solution, reaching concentrations way above the kinetic solubility limit estimated as 27.59 µg/mL for IND in PBS at pH 2.0.

The IND/EUDRAGIT EPO formulations with lower drug loads (higher polymer contents) exhibited fast dissolution rates suggesting that higher quantities of EUDRAGIT EPO fostered the fast release of IND into solution. The high solubility of EUDRAGIT EPO at pH 2.0 can be the explanation behind such occurrence, since its driving force to dissolve might have exposed IND at the same rate, mediating its diffusion from the solid dispersion to the solution phase, leading to a quick attainment of a supersaturation state.

In contrast, formulations with higher drug load, as is the case of IND/EUDRAGIT EPO ASD formulation with 80% drug load, take longer to achieve maximum supersaturation potential since the content of highly soluble polymer is lower. This formulation yielded the lowest level of supersaturation (87 µg/mL), taking 4h45 min to peak maximum concentration, about four times longer than the other ASD formulations under test.

In terms of supersaturation extent, IND/EUDRAGIT EPO amorphous films with 30% and 60% drug loads delivered the best performance by achieving the maximum concentrations of IND into solution, 115 µg/mL and 108 µg/mL, respectively.

The IND/EUDRAGIT EPO ASD at 30% drug load managed to deliver the best performance because of the higher content in EUDRAGIT EPO, which created a predominant kinetic driving force for polymer dissolution leading to higher drug release rates into solution through polymer-mediated diffusion. On the other hand, the ASD formulation of IND/EUDRAGIT EPO at 80% drug load performed the worst for the exact opposite reasons. A low EUDRAGIT EPO content, caused diffusion/dissolution and maximum supersaturation state to rely predominantly on IND's inherent physicochemical properties. Notwithstanding, polymer stabilization and crystallization inhibition effects can still be observed by the plateau that persisted for several hours.

On the other hand, the fact that IND/EUDRAGIT EPO amorphous formulation at 60% drug load delivered a better performance than the 50% drug load formulation, despite the dissolution profile being similar. That can be explained by the small differences in terms of polymer content between formulations and the inherent variability associated with the determinations. At 60% drug load the dissolution rate is slower due to a low polymer content but not so slow that it compromises the concentration attained.

The dissolution profiles of all IND/ EUDRAGIT EPO ASD formulations under test portray high stabilization of IND in the presence of EUDRAGIT EPO during the entire time span of the experiment. This effect is reflected in the slow decay of maximum concentrations yielded by each ASD over time, enabling the maintenance of high levels of supersaturation. At the end of the dissolution run, the IND/EUDRAGIT EPO amorphous films with drug loads of 30%, 50%, 60% and 80% had registered maximum concentration drops of 6%, 3%, 17% and 15%, respectively, which are great performance indicatives.

The experimental screening protocol for dissolution in PBS at pH 2.0 was also followed to evaluate IND/EUDRAGIT EPO ASD formulations, ranging from 30% to 80% drug loads, prepared by the fusion method, and the respective dissolution profiles are depicted in Figure 22.

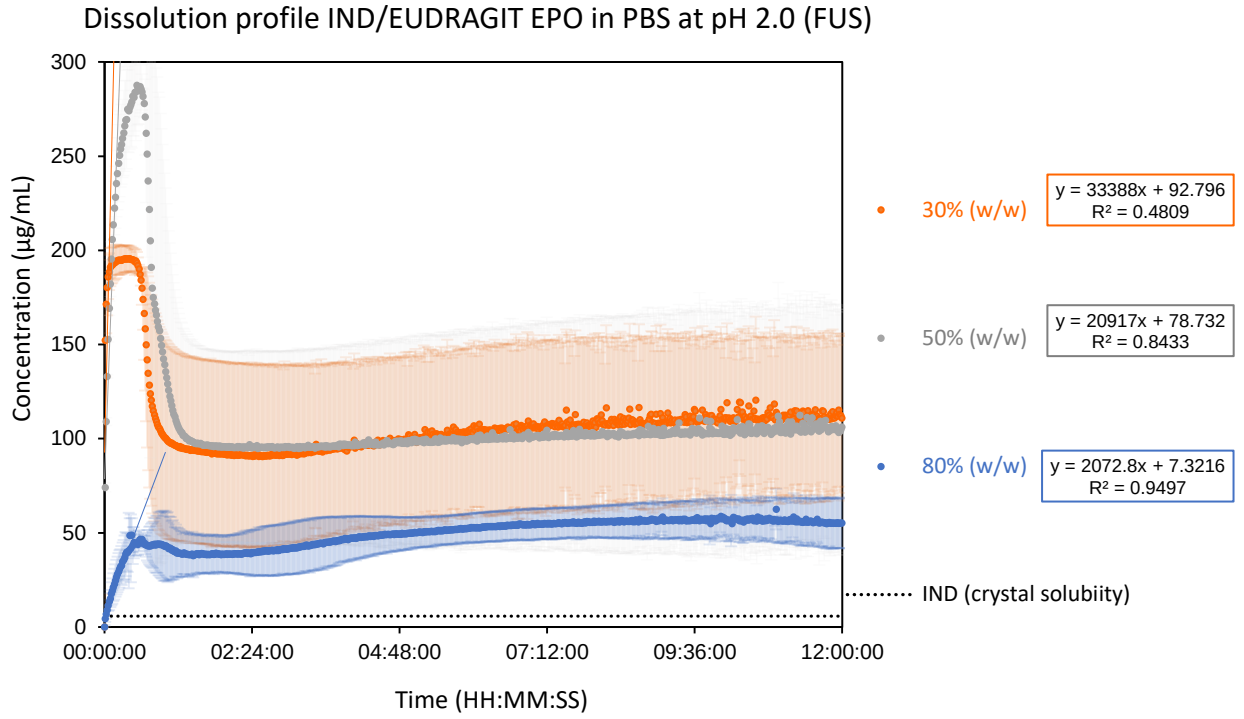

Figure 22. *Dissolution profiles of IND/ EUDRAGIT EPO ASD films produced by fusion with 30% drug load (orange), 50% drug load (grey) and 80% drug load (blue), in PBS at pH 2.0, during a 12h period, at 37ºC, under constant orbital shaking. IND's crystal solubility (black dashed line). Values represent mean IND concentration (n = 2) and Y-error bars indicate the standard deviation.*

Through the normalization of thickness and blend quantities deposited in the deposition platform to produce the amorphous films (1 mg films), we aimed to minimize the film surface differences impacting on diffusion, dissolution rate and extent. The resultant amorphous films own different API contents having the potential to generate different maximum concentrations.

When dissolved in PBS at pH 2.0, IND/EUDRAGIT EPO amorphous films screened were able to generate supersaturated systems, reaching concentrations way above the kinetic solubility limit estimated as 27.59 µg/mL. In terms of dissolution rate, it was verified that for lower drug loads, dissolution is faster, which is in agreement with previously discussed results regarding IND/EUDRAGIT EPO amorphous films prepared by the solvent method.

The dissolution profiles resultant from dissolution testing of IND/EUDRAGIT EPO solid dispersions with 30% and 50% drug loads showed the highest supersaturation degrees, having attained maximum concentration

peaks of 195.5 µg/mL and 285.7 µg/mL, respectively, early on the dissolution run. For both samples, after a drastic rise in concentration, a sudden downward trend succeeded as a result of the inherent tendency of supersaturated systems to evolve to a more stable state through crystallization phenomena.

It should be noted that these concentration values are not accurate since linearity was only demonstrated, using the calibration curves, up to 120 µg/mL. Nevertheless the lowest ASD drug loads yielded very high drug concentrations compared to the 80% drug load ASD.

On the contrary, the dissolution of IND/EUDRAGIT EPO ASD formulation with higher drug load (80%) produced a lower peak concentration when in solution reaching approximately 45 µg/mL, since there was less EUDRAGIT EPO quantity in the film available to promote API dissolution or even stabilize the API in the solution phase. Nonetheless, since the driving force for crystallization is proportional to the supersaturation level attained, the polymer content succeeded in maintaining the attained level of concentration leading to a slightly pronounced rise of IND's concentration delivered into solution phase by means of prolonged release.

The dissolution behaviour of IND/EUDRAGIT EPO amorphous films appears to consist of fast generation of a supersaturated solution upon polymer mediated-diffusion into solution, followed by crystallization from solution until reaching equilibrium solubility.

3.4.1.4. General Overview on IND/Polymer ASDs dissolution in PBS pH 2.0

Figure 23, shows the dissolution profiles of every ASD prototype under the scope of this project which were produced by the solvent evaporation method upon combination of one polymer candidate from a pool of 8 pharmaceutically interesting polymers with IND at 50% drug load, with a target concentration of 120 µg/mL.

Upon dissolution in PBS at pH 2.0, all IND/Polymer amorphous films with 50% drug load managed to produce supersaturated solutions surpassing crystalline solubility limit, reaching concentrations way above apparent amorphous solubility estimated as 27.59 µg/mL, except IND/EUDRAGIT L100-55 formulation which attained its maximum concentration at 26 µg/mL.

The highest maximum concentrations were attained by ASD formulations comprising the polymers EUDRAGIT EPO, HPMC E5 and HPMC E3 at 98.8 µg/mL, 94 µg/mL and 87.7 µg/mL, respectively.

EUDRAGIT EPO is a cationic polymer, highly soluble at pH values below pH 5.0 and so, when comprised in a binary ASD and tested in PBS at pH 2.0 managed to deliver a great performance in terms of dissolution rate and extent of supersaturation, having attained the highest concentration (98.8 µg/mL) 1h and 15 min after the beginning of the dissolution run. Besides, EUDRAGIT EPO is the only polymer of the pool capable of establishing strong counter-ionic interactions with IND, forming ion pair complexes with the drug, able to stabilize the drug in solution.[66,134–141] As a result, upon dissolution, the IND/EUDRAGIT EPO ASD

formulation only started to crystallize after 2h 30 min and, at the end of the dissolution run, concentrations only dropped by 14% below maximum concentration.

The second-best dissolution profiles were obtained for ASD films with HPMC E3 and HPMC E5 as drug-carrier, which are nonionic cellulose-based polymers with high molecular weight and Tg, renowned for their crystallization inhibition potential and inability to get absorbed from the gastrointestinal tract, being commonly used in the stabilization of amorphous solid dispersions. [142, 143]

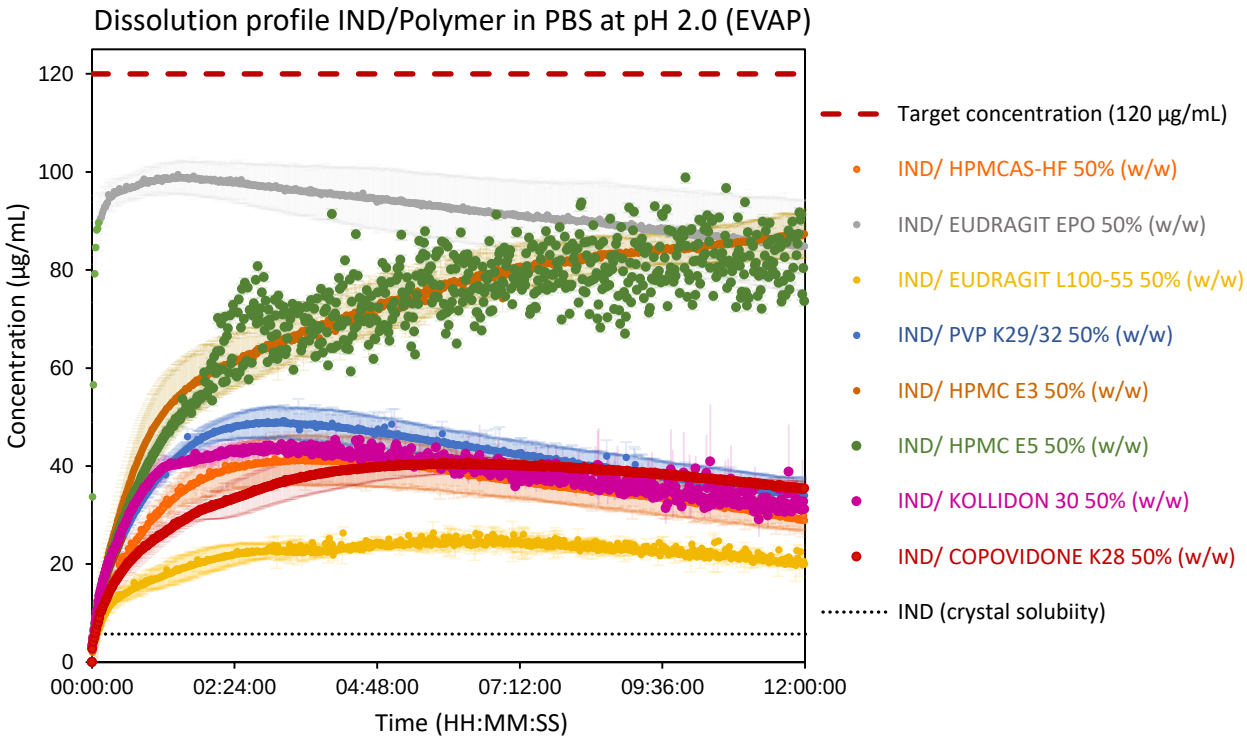

Figure 23. *Dissolution profiles of all different ASD films produced by solvent evaporation combining IND with one of the polymers under study at 50% drug load in PBS at pH 2.0, during a 12h period, at 37ºC, under constant orbital shaking. IND's crystal solubility (black dashed line). Target concentration of 120 µg/mL (red dashed line). Values represent mean IND concentration (n = 2) and Y-error bars indicate the standard deviation.*

The binary ASD films combining IND with both of these cellulosic polymers at 50% drug load dissolved in PBS at pH 2.0 at a fast rate until reaching a point, around 55 µg/mL, after which concentrations kept rising but at a slower pace, registering a maximum value at the end of the 12-hour dissolution run. In both cases, dissolution kinetics prevailed over crystallization due to high polymer viscosity and effective inhibition of crystallization from solution. The results confirm the excellent crystallization inhibition effect of these cellulosic polymers. [142, 143]

Another explanation for the change in kinetics of dissolution above 55 µg/mL is the formation of colloidal species that have a lower extinction coefficient compared to free drug, as previously discussed. Considering this difference in extinction coefficient, it is possible that the kinetics of dissolution remain unaltered above 55 µg/mL and the change in the slope is explained by this extinction coefficient effect. It is also possible to see that, in the case of HPMC E5, data scattering is significant above 55 µg/mL, and may be explained by the generation of colloidal species in solution, above amorphous solubility, that impact the medium light scattering properties.

Another factor that may have affected the dissolution profiles collected is the gelling properties displayed by these class of polymers upon hydration, which has been reported to cause delays in the dissolution process due to hampering of the diffusion of drug molecules out of the ASD matrix.[144]

Located at an intermediate level of the plot, are the dissolution profiles of both IND/PVP K29/32 and IND/ KOLLIDON 30 ASD films with 50% drug load, resultant upon dissolution in PBS at pH 2.0. The resultant dissolution profiles shared similar initial dissolution rates to those exhibited by the ASD binary films using HPMC E3 and HPMC E5, for the first 30 minutes of the dissolution run. From that point on, the dissolution rate of the IND/PVP K29/32 and IND/ KOLLIDON 30 ASD films started to slow down resulting in a belated attainment of maximum concentrations around 49 µg/mL and 44 µg/mL, respectively, obtained 3h after the beginning of the dissolution run.

Unlike cellulosic polymers which revealed to be more effective in maintaining supersaturation, being great precipitation inhibitors, the ASD films using PVP K29/32 and KOLLIDON 30 started to crystallize early after reaching maximum concentration, showing a concentration drop of 30±1% with respect to the maximum supersaturation level achieved.

Similar polymer properties have been identified in articles that described supersaturation systems generated by ASD combining the weakly basic drugs Felodipine, Itraconazole, and Celecoxib with a cellulosic polymer and a polyvinyl lactam polymer.[107,119,142,145]

Another polyvinyl lactam (co) polymer, COPOVIDONE K28, was combined with IND to originate an ASD formulation, which upon dissolution in PBS at pH 2.0, depicted a prolonged release having attained a maximum concentration of around 41 µg/mL in twice the time expended by PVP K29/32 and KOLLIDON 30 based ASDs. The different dissolution performance of IND/COPOVIDONE K28 ASD prototype may be explained by the vinyl acetate (VA) content of COPOVIDONE K28, which causes lower propensity to hydrogen bond with the API and is associated to attainment of lower degrees of supersaturation.[146] Nonetheless, COPOVIDONE K28 conveyed a better stabilization effect enabling longer supersaturation maintenance with a short concentration drop of around 10%. This stabilization effect may also be explained by the lower supersaturation level attained and, thus, the lower driving force for crystallization.

By opposite, the bottom maximum concentration was achieved by ASDs encompassing EUDRAGIT L100-55 as polymeric counterpart and corresponded to 26 µg/mL. This polymer is both anionic and poorly soluble

at pH values below 6.8, which make of PBS at pH 2.0 an unfavorable environment for dissolution. Despite sharing similar properties, HPMCAS-HF managed to attain a higher level of supersaturation above the estimated apparent amorphous solubility of IND, whereas the IND/EUDRAGIT L100-55 ASD followed a prolonged release profile trend at a lower level of supersaturation.

The same approach was followed to analyze dissolution of amorphous films prepared by the fusion method. The dissolution profiles of every ASD prototype combining the model drug with all the 8 polymer candidates at 50% drug load is depicted in Figure 24.

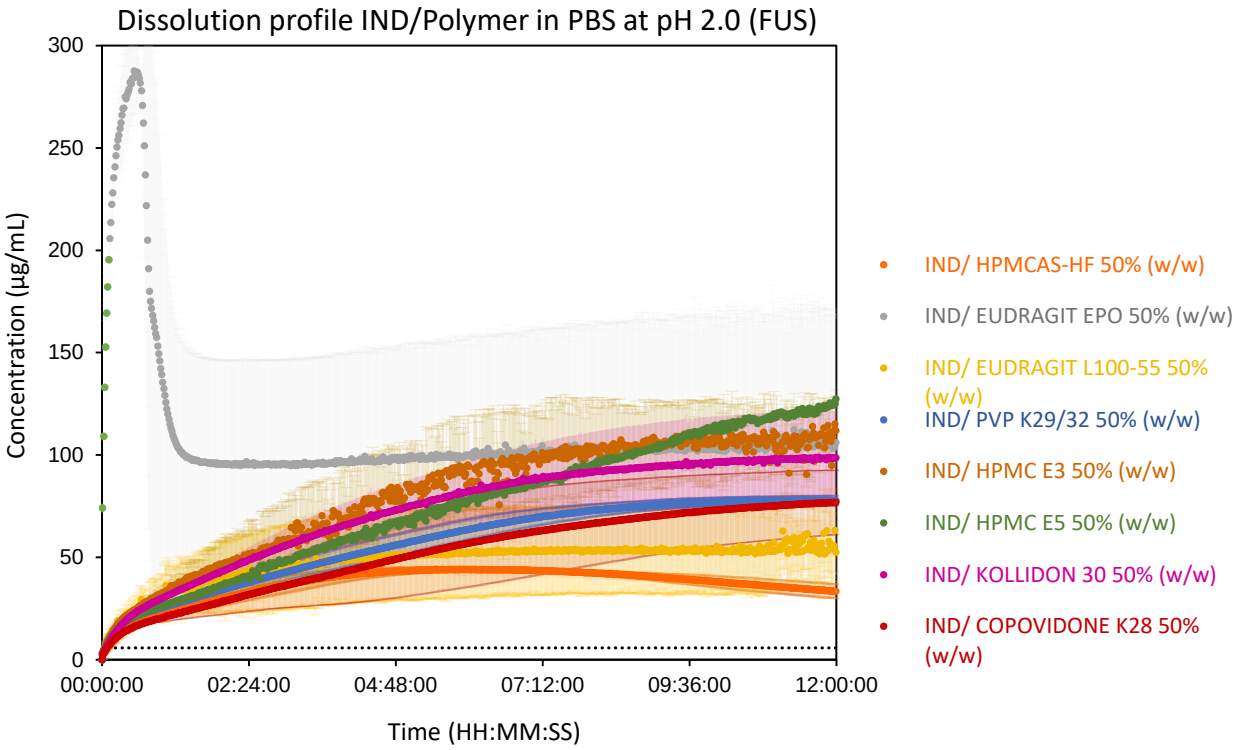

Figure 24. *Dissolution profiles of all different ASD films produced by fusion, combining IND with one of the polymers under study at 50% drug load in PBS at pH 2.0, during a 12h period, at 37ºC, under constant orbital shaking. IND's crystal solubility (black dashed line). Values represent mean IND concentration (n = 2) and Y-error bars indicate the standard deviation.*

Since the same amount of material was deposited in each deposition platform, the fusion method allowed normalizing the thickness and blend quantities deposited to produce the amorphous films, minimizing the influence of surface area on diffusion and, ultimately on dissolution rate and extent. All IND ASD films managed to produce supersaturated systems surpassing IND's intrinsic crystalline solubility limit.

The higher supersaturation state was achieved by the IND ASD with EUDRAGIT EPO as polymeric counterpart. EUDRAGIT EPO is a cationic polymer highly soluble below pH 5.0, therefore dissolving quickly in PBS at pH 2.0. Hence, a sudden rise in concentration is observed which leads to a maximum

concentration around 285 µg/mL. However, as a result of the inherent tendency of supersaturated systems to evolve to a more stable state through crystallization phenomena, a sudden decay in concentration followed, causing a drop of around 60% in concentration. Afterwards, a plateau concentration was achieved, corresponding to equilibrium crystalline solubility. The high concentration value, around 100 µg/mL, determined at this point is not a real value since it is affected by a large extinction effect, caused by the crystals in solution, and the lack of linearity demonstrated above 120 µg/mL Another hypothesis could be that a different polymorph with higher solubility was obtained after complete crystallization. However, that is not the case since the amorphous form is the most soluble solid form and its kinetic solubility is around 28 µg/mL

Upon dissolution in PBS at pH 2.0 of the IND ASD films comprising one of the nonionic polymers, namely the cellulosic polymers (HPMC E3 and HPMC E5) and the polyvinyl lactam polymers (KOLLIDON 30, PVP K29/32, COPOVIDONE K28), prolonged release profiles were produced with maximum concentrations being attained at the end of the dissolution run. The upward evolution of concentrations exceeding the apparent amorphous solubility of IND, shows that these polymers were effective to delay or prevent crystallization.

The dissolution profile displayed by IND/HPMC E3 ASD film followed a prolonged release trend, which was slowed down after 7h of dissolution, whereas the release profile of HPMC E5 showed a continuously increasing trend matching and surpassing the concentrations attained by IND/HPMC E3 ASD prototype. The difference between these polymers lies mainly on viscosity, which is higher in HPMC E5. The reduced molecular mobility caused by the high viscosity of the polymer is beneficial for the physical stability of the ASD formulation, thereby fostering ASD performance, being a plausible explanation for the attainment of higher degrees of supersaturation.[142, 143]

The IND ASD films comprising the polyvinyl polymers PVP K29/32 and COPOVIDONE K28 as drug-carrier showed similar prolonged release profiles without depicting any decrease in concentration within the experimental time frame, despite yielding lower IND concentrations than the IND/HPMC E3, IND/HPMC E5 and IND/KOLLIDON 30 amorphous films.

On the other hand, the anionic polymers HPMCAS-HF and EUDRAGIT EPO L100-55 maintained a prolonged release profile with slow diffusion of the API content into solution.

3.4.2. Dissolution in PBS pH 6.8

The dissolution profiling at pH 6.8 was slightly more challenging. IND is a weakly acidic drug compound, which at pH ranges above its pKa (4.5) turns into a negatively charged form, displaying higher aqueous solubility. Additionally, when assuming an amorphous form, IND solubility is further increased, with both

thermodynamic and kinetic solubilities falling out of the upper quantification limits of the spectroscopic techniques applied to monitor ASD prototype performance through dissolution.

Following the same strategy used for the dissolution studies performed at pH 2.0, the same binary ASD prototypes, with 30%, 60% and 80% drug loads, produced by the solvent evaporation method and by the fusion method, were tested in PBS at pH 6.8 as a way of complementing the study of their performance and dissolution behaviour.

The ASD films prepared by the solvent evaporation method were targeting 120 µg/mL whereas the ASD films prepared by the fusion method were formulated to meet the same overall film mass around 1 mg, These conditions were set prior to film preparation in order to compare the results at pH 6.8 with those registered at pH 2.0.

3.4.2.1. Dissolution of amorphous IND films in PBS pH 6.8

The methods developed were applied to produce amorphous films of IND using the same target concentration and mass. The respective dissolution profiles present in APPENDIX section (Figure A9) depict a complete release upon dissolution in PBS at pH 6.8. The amorphous films produced by solvent evaporation quickly reached the target concentration of 120 µg/mL and, as expected, the amorphous films of IND produced by fusion surpassed the maximum limits of quantification of the UV-Vis spectroscopic technique applied.

3.4.2.2. Dissolution of IND/ HPMCAS-HF ASDs in PBS pH 6.8

The ASD formulations of IND/HPMCAS-HF combined at 30%, 50%, 60% and 80% drug loads were investigated for their dissolution behavior in PBS medium at pH 6.8, monitored at IND maximum wavelength of absorbance (λ_{max}= 320nm), at 37ºC. The respective dissolution profiles are depicted in Figure 25.

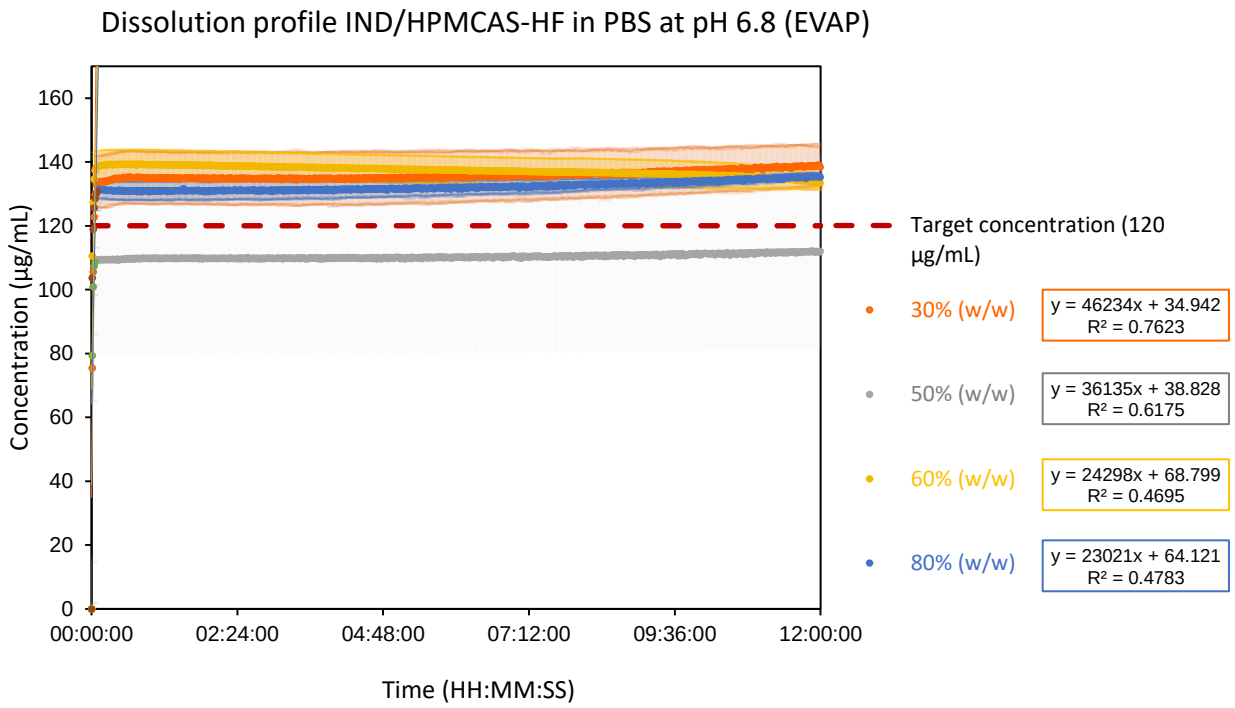

Figure 25. *Dissolution profiles of IND/ HPMCAS-HF ASD films produced by solvent evaporation with 30% drug load (orange), 50% drug load (grey), 60% drug load (yellow) and 80% drug load (blue), in PBS at pH 6.8, during a 12h period, at 37ºC, under constant orbital shaking. Target concentration 120 µg/mL (Red dashed line). Values represent mean IND concentration (n = 2) and Y-error bars indicate the standard deviation.*

The investigated IND/HPMCAS-HF amorphous films exhibited very similar release profiles and dissolution behaviour. These IND/HPMCAS-HF ASD prototypes managed to achieve maximum concentration almost instantly, as a result of the contribution of both IND and HPMCAS-HF high solubility at pH 6.8 to ASD performance.

Maximum concentration was attained between 130 and 140 µg/mL, very close to the target concentration of 120 µg/mL, and remained constant until the end of the dissolution run, since target concentration is lower than crystalline solubility at this pH. The only exception was the IND/HPMCAS-HF ASD film with 50% drug load, which despite depicting a similar profile trend, attained lower concentrations at around 110 µg/mL (yet still very close to the target concentration of 120 µg/mL considering the uncertainty associated to the respective measurements). Pipetting and sample deposition errors could explain this lower concentration.

The experimental screening protocol for dissolution in PBS at pH 6.8 was also followed to evaluate IND/HPMCAS-HF ASD films ranging from 30% to 80% drug loads, prepared by the fusion method, and the respective dissolution profiles are depicted in Figure 26.

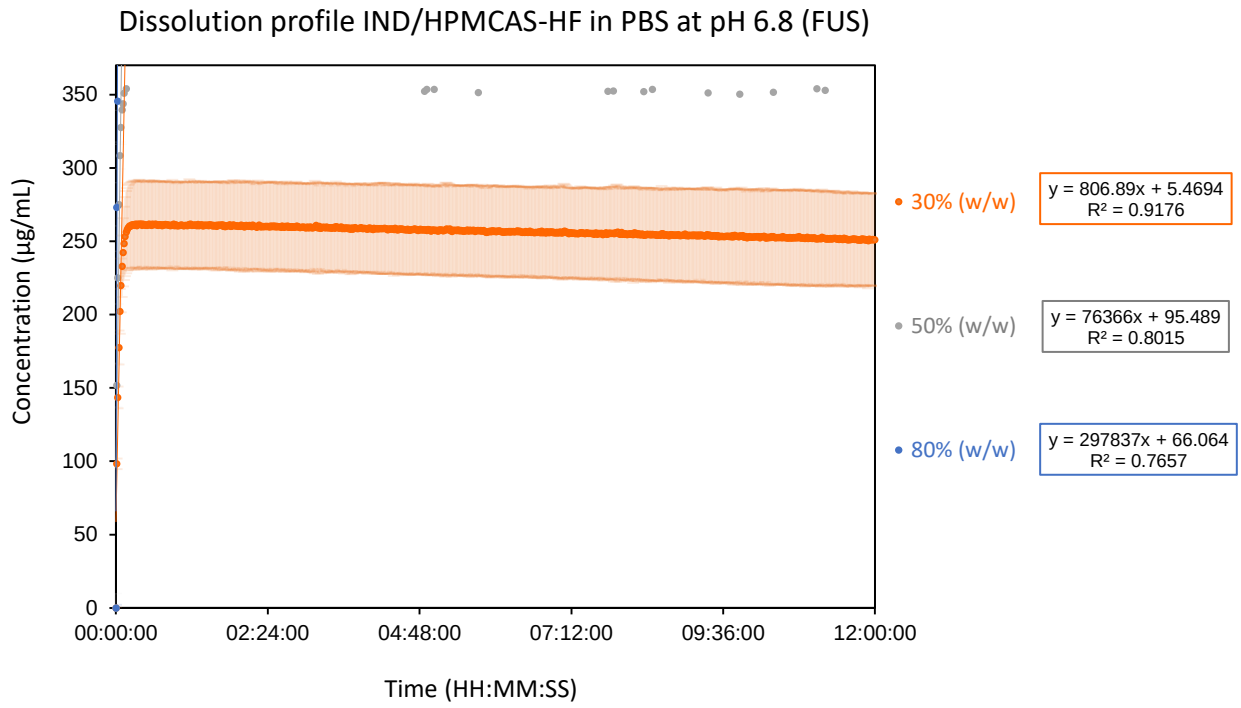

Figure 26. *Dissolution profiles of IND/ HPMCAS-HF ASD films produced by fusion with 30% drug load (orange), 50% drug load (grey) and 80% drug load (blue), in PBS at pH 6.8, during a 12h period, at 37ºC, under constant orbital shaking. Values represent mean IND concentration (n = 2) and Y-error bars indicate the standard deviation.*

Similarly to the equivalent ASD films prepared by solvent evaporation, the IND/HPMCAS-HF ASD films prepared by fusion generated high concentrations early in the dissolution experiment when tested in PBS at pH 6.8.

Moreover, the amorphous films produced by the fusion method have the potential to generate different maximum concentrations, depending on the drug load, with some of them falling way out of the upper quantification limit of the UV-Vis technique under use to assess ASD prototype dissolution behaviour. For this reason, no measurements were obtained for IND/HPMCAS-HF ASD film with 80% drug load and the IND/HPMCAS-HF ASD film with 50% drug load only registered a few measurements that were not enough to build a dissolution profile from which conclusions can be drawn.

The IND/HPMCAS-HF ASD with 30% drug load managed to quickly achieve maximum concentration, at around 260 µg/mL, and depicted a plateau concentration-time profile throughout the entire dissolution run. That concentration corresponds to 130 % release considering the mass of 1 mg deposited and the volume

of dissolution medium of 1.5 mL. The difference between the attained concentration and the maximum concentration that this type of formulation was designed to produce (200 µg/mL) may be due to variability in weighing of the mass of blend deposited in each deposition platform or due to dissolution medium evaporation.

3.4.2.3. Dissolution of IND/ EUDRAGIT EPO ASDs in PBS pH 6.8

The binary ASD films of IND and EUDRAGIT EPO combined at 30%, 50%, 60% and 80% drug loads were investigated for their dissolution behavior in PBS medium at pH 6.8 monitored at IND maximum wavelength of absorbance (ʎmax= 320nm), at 37ºC. The respective dissolution profiles are depicted in Figure 27.

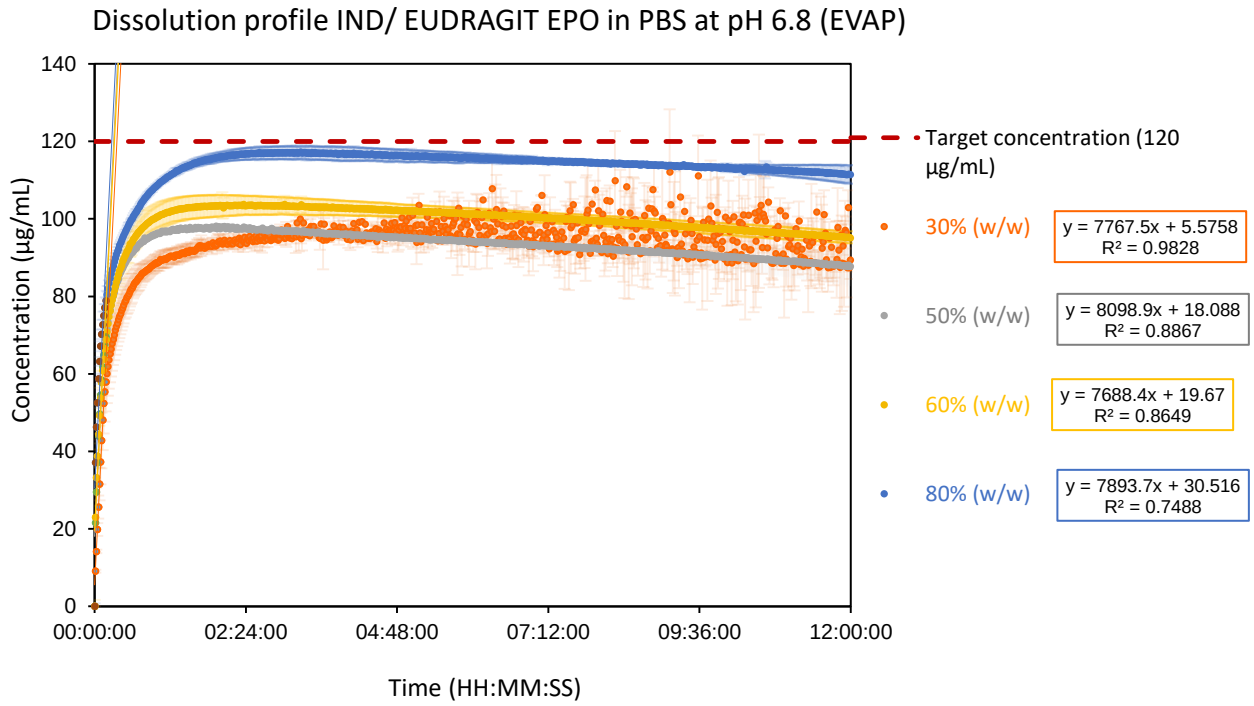

Figure 27. *Dissolution profiles of IND/ EUDRAGIT EPO ASD films produced by solvent evaporation with 30% drug load (orange), 50% drug load (grey), 60% drug load (yellow) and 80% drug load (blue), in PBS at pH 6.8, during a 12h period, at 37ºC, under constant orbital shaking. Target concentration 120 µg/mL (Red dashed line). Values represent mean IND concentration (n = 2) and Y-error bars indicate the standard deviation.*

The dissolution of IND/EUDRAGIT EPO ASD films manufactured by the solvent evaporation method in PBS at pH 6.8, rendered very similar dissolution profiles with very low variability associated to the concentration measurements, as can be seen by the small standard deviation magnitude.

The dissolution rates obtained did not show dependency from the drug load of the ASD formulation, since all amorphous films managed to release IND into the solution phase at a similar pace, taking approximately 1h to achieve maximum concentration plateaus. By comparison with the HPMCAS ASD films, dissolution of the Eudragit EPO films was slower but still managed to yield concentrations close to target concentration. These results reflect the fact that IND is highly soluble at pH 6.8, while Eudragit EPO is not (poorly soluble above pH 5). Furthermore, it is well known that Eudragit EPO swells above pH 5, thus limiting the diffusion of drug across the polymeric matrix and into solution. These two properties of Eudragit EPO explain the slower dissolution rate compared to HPMCAS ASDs.

All IND/EUDRAGIT EPO ASD films managed to generate maximum concentrations very close to the target concentration (120 µg/mL). In this case, target concentration is much lower than the equilibrium crystalline solubility, which means that no supersaturated solutions were generated. Nevertheless, a small difference was observed, in terms of maximum concentration, between the highest drug load, 80%, and all other, 116 µg/mL and around 100 µg/mL, respectively. This difference may be explained by the fact that, for the low drug load ASDs, that contain high amount of poorly soluble polymer (at pH 6.8), the drug dissolves at a much faster rate compared to the polymer and an outer shell of polymer is formed around the particles, thus entrapping the remaining API inside the particle. That is why the difference between maximum and target concentration is higher for the low drug load ASDs. In the case of high drug loads, no outer shell of polymer is formed because the amount of polymer is much lower and IND dissolution is not limited significantly by the polymer solubility issued. Therefore, maximum concentration was close to target concentration.

The IND/EUDRAGIT EPO ASD film with 30% drug load depicted very disperse readings after reaching maximum concentration. This “noisier” dataset may be explained by the presence of undissolved particles containing an outer shell of polymer (as discussed earlier), which affects the absorbance readings due to light scattering effects.

The experimental screening protocol for dissolution in PBS at pH 6.8 was extended to IND/EUDRAGIT EPO ASD formulations ranging from 30% to 80% drug loads, prepared by the fusion method, and the respective dissolution profiles are depicted in Figure 28.

The dissolution rates obtained show dependency on the drug load of the ASD formulation, since the amorphous films with higher drug loads managed to release IND into the solution phase at a faster pace. This dependency can be explained by the fact that EUDRAGIT EPO is poorly soluble at pH 6.8 and the IND release kinetics will be slower for those formulations that contain more polymer, since the polymer acts as a barrier to dissolution

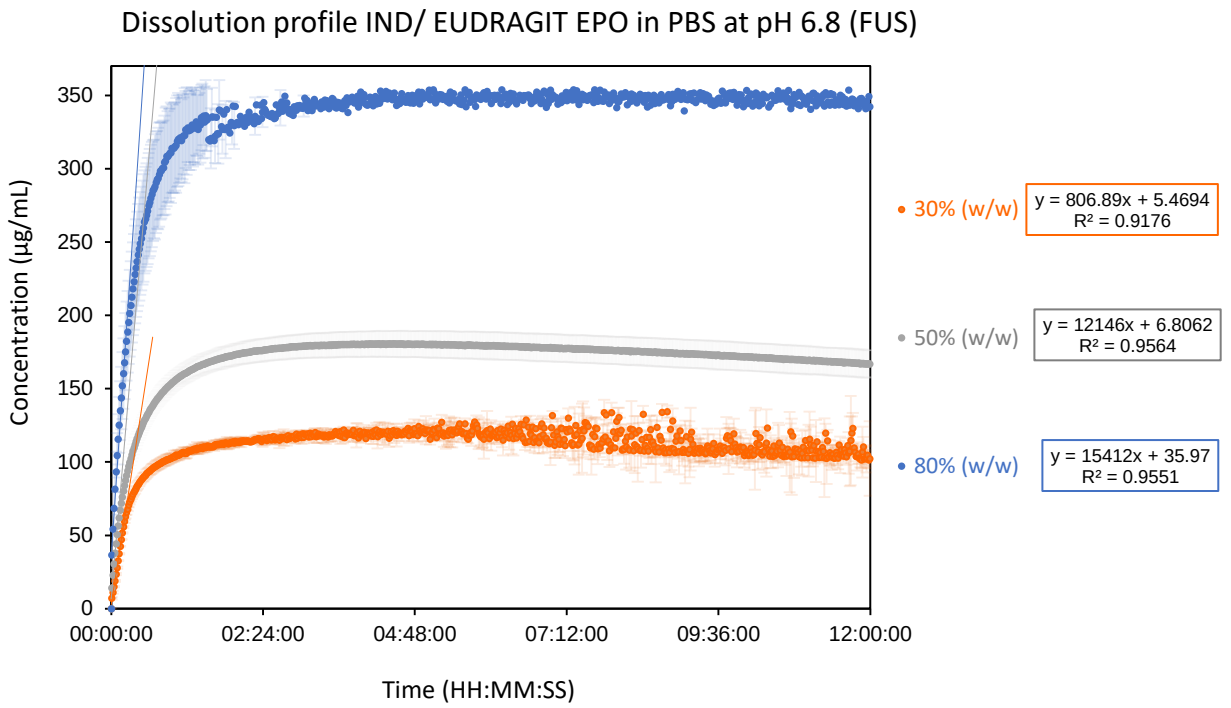

Figure 28. *Dissolution profiles of IND/ EUDRAGIT EPO ASD films produced by fusion with 30% drug load (orange), 50% drug load (grey) and 80% drug load (blue), in PBS at pH 6.8, during a 12h period, at 37ºC, under constant orbital shaking. Values represent mean IND concentration (n = 2) and Y-error bars indicate the standard deviation.*

In terms of extent of drug release, all IND/EUDRAGIT EPO ASD films generated maximum concentrations inferior to the maximum concentrations they were potentially formulated to attain. IND/EUDRAGIT EPO ASD film with 80% drug load attained a maximum concentration peak close to 350 µg/mL (inferior to the possible maximum around 533 µg/mL). On the other hand, the IND/EUDRAGIT EPO ASD film with 50% and 30% drug loads attained maximum concentrations of around 180 µg/mL and 120 µg/mL, instead of the maximum concentrations of 333 µg/mL and 200 µg/mL, respectively.

Regarding supersaturation maintenance, all the tested IND/EUDRAGIT EPO ASD films have managed to maintain the supersaturation levels attained or follow a very slow decay trend, with no significant crystallization being registered during the experimental time frame. The dissolution profiles of IND/EUDRAGIT EPO ASD films with 80% and 30% drug loads comprise some oscillation.

3.4.2.4. General Overview on IND/Polymer ASDs dissolution in PBS pH 6.8

In order to evaluate the impact of different polymers in the ASD performance, the binary ASD formulations produced by a solvent evaporation method, upon combination of one polymer candidate from a pool of 8 pharmaceutically interesting polymers with IND at 50% drug load, were investigated for their dissolution behavior in PBS medium at pH 6.8 monitored at IND maximum wavelength of absorbance (λ_{max}= 320nm), at 37ºC. The respective dissolution profiles are depicted in Figure 29.

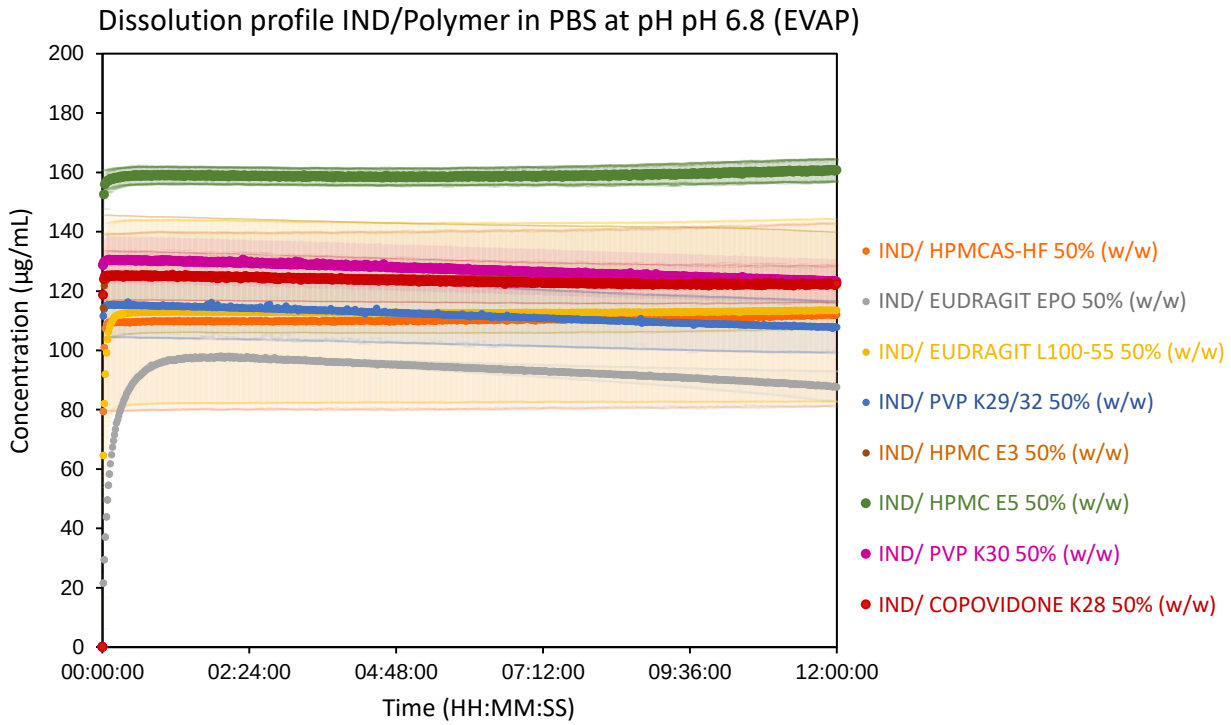

Figure 29. *Dissolution profiles of all different ASD films produced by solvent evaporation combining IND with one of the polymers under study at 50% drug load in PBS at pH 6.8, during a 12h period, at 37ºC, under constant orbital shaking. Values represent mean IND concentration (n = 2) and Y-error bars indicate the standard deviation.*

The investigated ASD prototypes exhibited very similar release profiles and dissolution behaviour upon dissolution in PBS at pH 6.8, managing to achieve maximum concentration rapidly. IND undergoes ionization when pH goes above 4.5, displaying a high solubility at pH 6.8, which is further enhanced when IND assumes an amorphous form. Therefore, the maximum concentration values obtained, close to target concentration of 120 µg/mL, indicate that ASD dissolution was mainly governed by IND solubility and dissolution rate, thereby the generation of high supersaturation degrees was expectable. However the supersaturation levels attained were distinct according to the polymeric counterpart comprised in the ASD film. The same protocol was followed to analyze the ASD produced by the fusion based method. However,

since the film mass deposited was high, the majority of the ASD films at 50% drug load exceeded the limits of quantification of the UV-Vis microplate reader precluding the evaluation of the respective dissolution profiles and comparison between performances.

3.5. Biorelevant dissolution studies

3.5.1. Biorelevant Dissolution of IND/ HPMCAS-HF ASDs

The IND/HPMCAS-HF solid dispersions combined at 30%, 50%, 60% and 80% drug loads were investigated for their dissolution behavior in biorelevant dissolution media FaSSGF at pH 1.6 followed by transition to FaSSIF at pH 6.5, monitored at IND maximum wavelength of absorbance (λ_{max}= 320nm) and at 37 ºC. Figure 30, depicts the respective concentration-time profiles.

At the beginning, all IND/HPMCAS-HF ASD prototypes prepared by solvent evaporation to achieve a target concentration of 120 µg/mL have generated supersaturated systems upon dissolution in fasted simulated gastric medium (FaSSGF) at pH 1.6, surpassing IND intrinsic solubility limit determined at pH 2.0, by following a gradual increase in the concentration-time profiles as depicted. The maximum supersaturation levels attained are inferior to the ones achieved by equivalent amorphous films of the same ASD prototype combinations in PBS at pH 2.0, as a result of a more acidic chemical environment unfavorable to both polymer and API.

The dissolution of IND/HPMCAS-HF solid dispersions in FaSSGF was hampered by HPMCAS-HF poor solubility in acidic environments, due to the occurrence of a previously mentioned polymer barrier effect, that consists in an API entrapment as a consequence of the accumulation of non-dissolved HPMCAS-HF at the superficial diffusion layer of the ASD film, hindering the contact between API and dissolution medium.

It is also important to bear in mind that these concentrations were measured in half the well volume (750 µL) and that factor might also explain the lower concentrations determined. The dynamics of agitation are much different in smaller dissolution medium volumes and that may explain the slower rate of dissolution compared to the assays in 1.5 mL PBS at pH 2. Furthermore, the composition of the medium is different in terms of buffer concentration and ionic strength and that may also explain the lower concentration achieved.

In the second phase of the biorelevant dissolution test, upon dissolution medium transition to fasted simulated intestinal medium (FaSSIF) at pH 6.5 and total volume of 1.5 mL, a sudden increment of IND concentration was observed as a result of the great enhancement of HPMCAS-HF and IND solubilities derived from ionization and conversion into negatively charged and hence more hydrophilic forms. The HPMCAS-HF ionization state is highly dependent of the protonation state of its succinate group (5.0), thus reflecting the pH-dependent solubility of this cellulosic polymer. As a result, HPMCAS-HF displays poor solubility below pH 4.0, where it is predominantly un-ionized, and a high solubility above pH 6.0, where succinate groups are completely ionized. Likewise, IND shares a similar solubility behaviour since it is a weakly acidic drug compound whose pKa (4.5) is very close to that of succinate group.

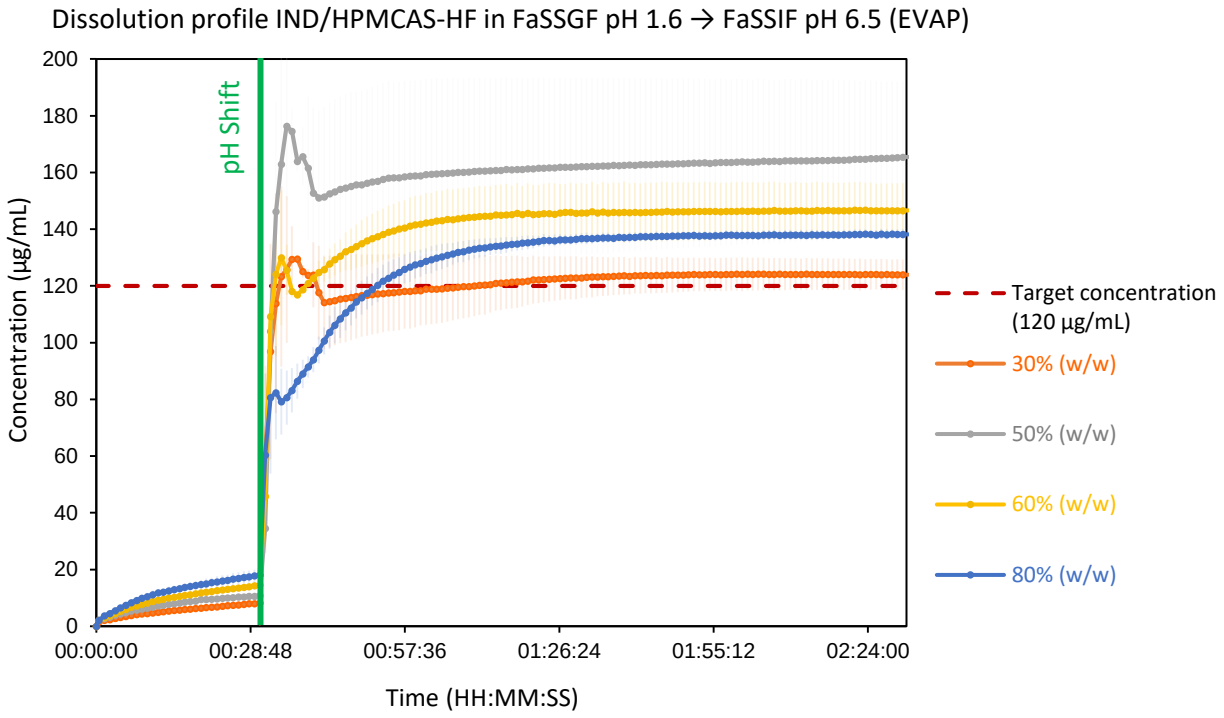

Figure 30. *Dissolution profiles of IND/ HPMCAS-HF ASD films produced by solvent evaporation with 30% drug load (orange), 50% drug load (grey), 60% drug load (yellow) and 80% drug load (blue), in FaSSGF at pH 1.6, during 30 min and upon transition to FaSSIF at pH 6.5 during 2h, at 37ºC, under constant orbital shaking. The vertical green line indicates pH shift time point. Target concentration 120 µg/mL (Red dashed line). Values represent mean IND concentration (n = 2) and Y-error bars indicate the standard deviation.*

In all cases, the ASDs completely dissolved after pH-shift since the target concentration (120 µg/mL) is much lower than IND solubility at pH 6.5. The differences in maximum concentration achieved for each IND ASD drug load can only be explained by differences in the film mass deposited in the deposition platform.

Nevertheless, some significant differences were detected in the initial rate of dissolution after pH-transition. The rate of concentration increase was greater for ASDs with lower drug load, reflecting the role of the

polymer as a facilitator of dissolution. Since HPMCAS is highly soluble at pH 6.5, the release of IND was favored for ASD with higher polymer content (lower drug loads).

Even though pH influence over solubility of both API and polymer has been more predominant, some components of the biorelevant dissolution media, such as bile salts and phospholipids (lecithin), present in solution at physiologically relevant concentrations, might have interfered with dissolution kinetics by enhancing the compounds solubilisation through micelle formation.

The experimental screening protocol for biorelevant dissolution testing in FaSSGF at pH 1.6 followed by transition to FaSSIF at pH 6.5 was also applied to evaluate IND/HPMCAS-HF ASD formulations ranging from 30% to 80% drug loads, prepared by the fusion method, and the respective dissolution profiles are depicted in Figure 31.

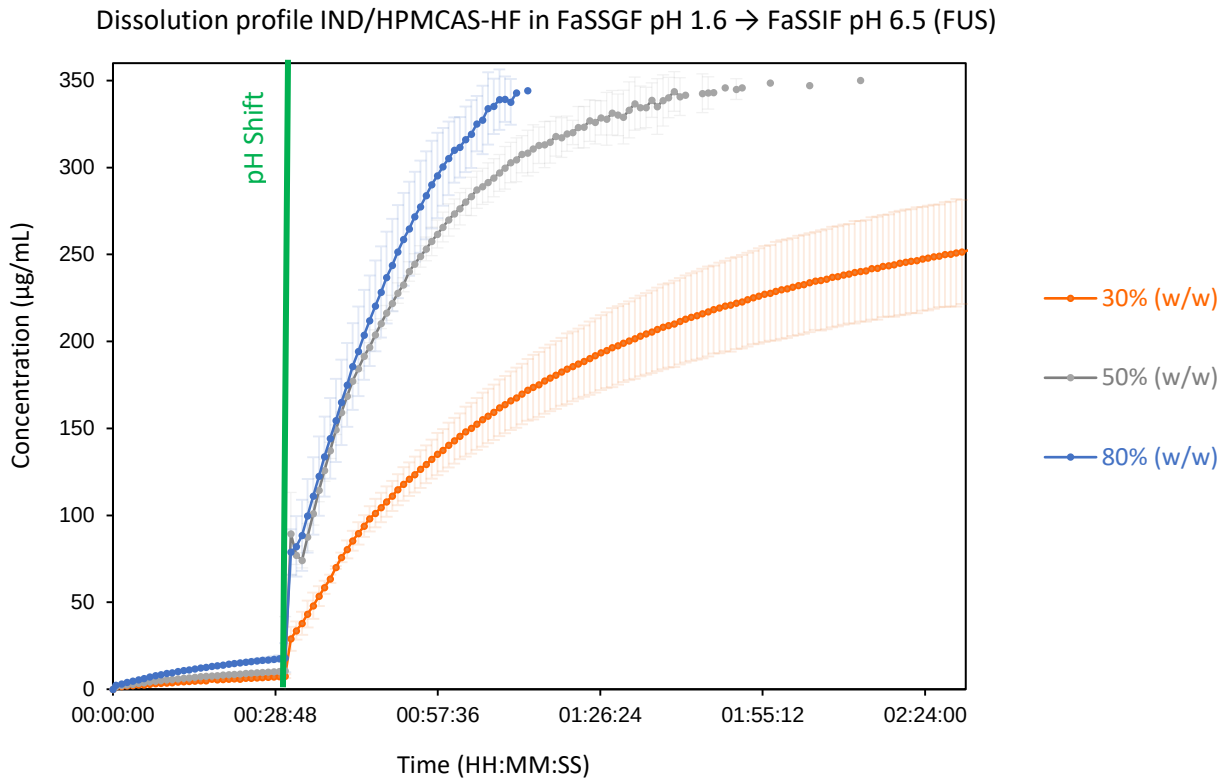

***Figure 31**. Dissolution profiles of IND/ HPMCAS-HF ASD films produced by fusion with 30% drug load (orange), 50% drug load (grey) and 80% drug load (blue), in FaSSGF at pH 1.6, during a 30 min and upon transition to FaSSIF at pH 6.5 during 2h, at 37ºC, under constant orbital shaking. The vertical green line indicates pH shift time point. Values represent mean IND concentration (n = 2) and Y-error bars indicate the standard deviation.*

Contrary to the ASD films produced by solvent evaporation, that have similar API contents despite having different drug loads, the amorphous films prepared by the fusion method have similar thickness and overall

mass, in an attempt to minimize the interference of surface area factors on diffusion and dissolution rate and extent. Nevertheless, they differ in both polymer and API contents, having the potential to generate different maximum concentrations.

Like previous presented profiles, the dissolution profiles portray a two-step curve with a sudden increase after transition from fasted simulated gastric medium (FaSSGF) at pH 1.6 to fasted simulated intestinal medium (FaSSIF) at pH 6.5. Moreover, upon dissolution in biorelevant media all ASD amorphous films under test originated supersaturated systems, at pH 1.6, surpassing IND intrinsic solubility limit.

Throughout the course of the dissolution run, it was verified that the higher the drug load of the IND/HPMCAS-HF amorphous film, the higher the concentrations attained either at acidic or alkaline biorelevant environments.

Initially, while dissolution testing was held in FaSSGF at pH 1.6, the concentration-time profiles produced by dissolution of the IND/HPMCAS-HF amorphous films depict a gradual increase resulting from the poorly soluble IND slow diffusion from the ASD matrix into the solution phase.

Similarly to previous results, the IND/HPMCAS-HF solid dispersions at 80% drug load and IND/HPMCAS-HF at 30% drug load achieved the top and bottom maximum concentrations of 18 µg/mL and 8 µg/mL, respectively, whereas the IND/HPMCAS-HF amorphous films with 50% drug load achieved an intermediate concentration of around 11 µg/mL. These results reflect the same behavior of the previously tested formulations portraying the effect of HPMCAS-HF and IND poor solubility and reinforce the same polymer barrier effect previously observed.

A slightly different dissolution behaviour was observed in the second phase of the biorelevant dissolution testing. Upon conversion of FaSSGF at pH 1.6 to FaSSIF at pH 6.5, a steep increase was observed, triggered by the sudden enhancement of both API and polymer solubilities upon pH-shift. However, the rate and extent of release was different for the three ASD drug loads.

The initial rate of release was faster for the 80% drug load and decreased for the ASDs with lower drug load. These results show that the content of IND dictates the rate of dissolution. Since the film mass is normalized (1 mg films) the high drug load films have higher IND content, which leads to higher dissolution rates. Polymer content is not so important for drug release, in this case, since the diffusion of drug is not affected by the polymer present due to its high solubility.

In terms of maximum concentration achieved, the extent of dissolution is only dictated by the amount of drug available to dissolve since the target concentrations are well below IND solubility at pH 6.5 Therefore, higher drug contents (higher drug loads) will result in higher maximum concentrations achieved.

It is also important to note that the formulation with 80% drug load managed to achieve concentrations higher than 350 µg/mL, approximately 1h and 15min under biorelevant dissolution testing, falling out of the equipment quantification limits afterwards. The same was observed for the 60% drug load, after 2h 15 min.

3.5.2. Biorelevant Dissolution of IND/ EUDRAGIT EPO ASDs

The IND/EUDRAGIT EPO ASD prototypes under test managed to generate supersaturated solutions way above the intrinsic solubility threshold, at pH 1.6, early in the dissolution process. The collected profiles show a two-step curve with a sudden increase in concentration after pH-shift, associated to the transition from FaSSGF to FaSSIF.

When exposed to FaSSGF at pH 1.6, the polymer comprised in these ASD films, EUDRAGIT EPO, becomes ionized, starting to display a higher hydrophilicity and hence a greater solubility. As a result, the ASD matrix starts to dismantle and the fast dissolving polymer promotes the release of API into the solution phase. However, it is important to mention that the model drug (IND) is not soluble at the pH ranges where EUDRAGIT EPO is more soluble and vice-versa.

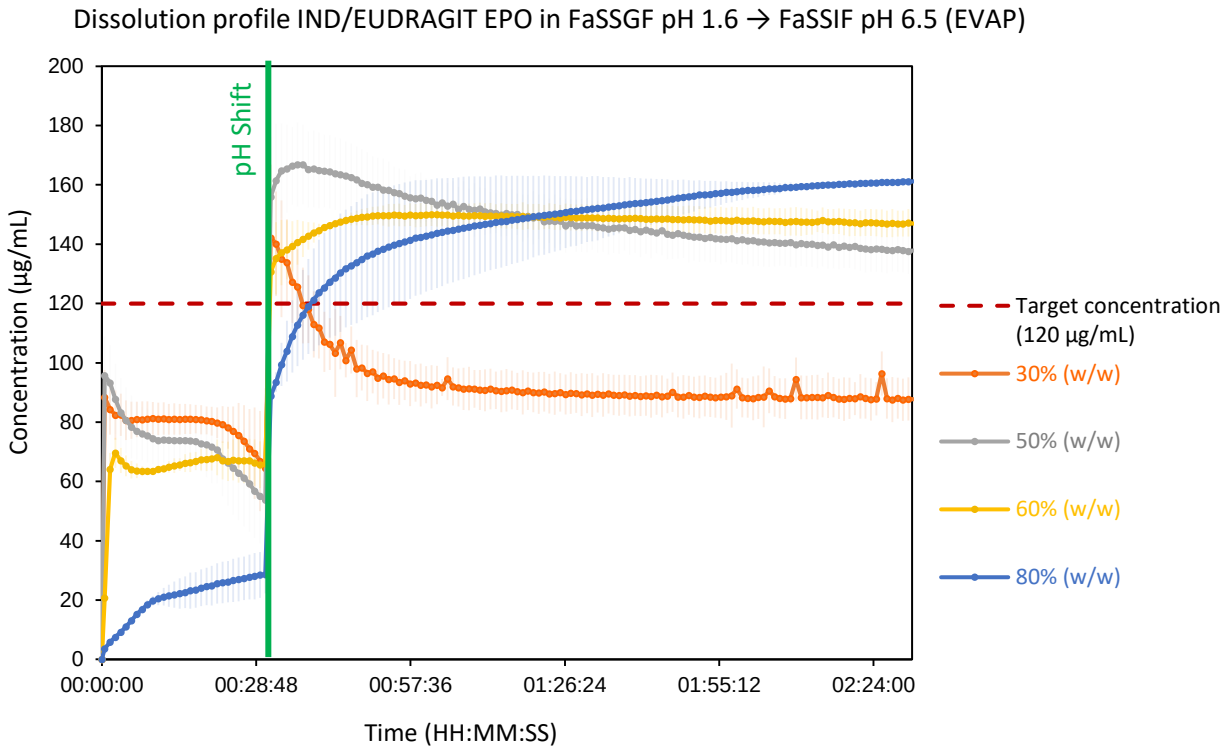

Figure 32. *Dissolution profiles of IND/ EUDRAGIT EPO ASD films produced by solvent evaporation with 30% drug load (orange), 50% drug load (grey), 60% drug load (yellow) and 80% drug load (blue), in FaSSGF at pH 1.6, during a 30 min and after transition to FaSSIF at pH 6.5 during 2h, at 37ºC, under constant orbital shaking. The vertical green line indicates pH shift time point. Target concentration 120 µg/mL (Red dashed line). Values represent mean IND concentration (n = 2) and Y-error bars indicate the standard deviation.*

Consequently, IND/EUDRAGIT EPO amorphous films with lower drug loads (higher polymer contents) display faster released rates, managing to attain higher supersaturation states in a shorter amount of time, since they are profiting from EUDRAGIT EPO physicochemical properties in a polymer-mediated release of

IND into the solution phase. That is the case of the IND/EUDRAGIT EPO amorphous films with 30% and 50% drug load which managed to reach the highest supersaturation levels in FaSSGF at pH 1.6, corresponding to 95 µg/mL and 88 µg/mL, respectively. Despite leading to higher supersaturation levels, the low drug loads, 30% and 50%, start to crystallize before the medium pH transition, as a result of the high driving force for crystallization that highly supersaturated systems exhibit. Crystallization is slightly faster for the 50% drug load ASD compared to the 30% drug load ASD because, in the latter, the amount of polymer dissolved is greater and so is the crystallization inhibition effect that results.

For the IND/EUDRAGIT EPO ASD formulations with higher drug loads, namely with 60% and 80% drug load, little to no crystallization was detected before pH transition. That can be explained by the lower extent of supersaturation achieved, as a result of slower dissolution kinetics and, therefore, the lower driving force for crystallization. As a consequence of having the lowest polymer content, the IND/EUDRAGIT EPO amorphous films with 80% drug load exhibited the slowest dissolution rate and did not manage to generate a level of supersaturation as high as other ASD prototypes combining IND with EUDRAGIT EPO, portraying a gradual concentration increase, which slowed down after 10 min into the dissolution run.

Following the transition from FaSSGF at pH 1.6 into FaSSIF at pH 6.5, a sudden increase in IND concentration was observed for all ASD prototypes under test, caused by a sudden enhancement of drug solubility due to IND ionization after pH-shift. On the contrary, the solubility of the polymeric counterpart, EUDRAGIT EPO, decreased after the pH-shift impacting the release of API from the ASD matrix. That is why the release of IND after pH-shift was much faster for the HPMCAS-HF ASDs compared to the EUDRAGIT EPO formulations.

After pH-shift two different situations were observed:

- For the high drug loads, 60% and 80%, IND concentration kept increasing until reaching a plateau. This gradual increase is explained by the release of undissolved IND that is favored at this pH where IND is highly soluble. A concentration steady-state was achieved, at the end of the dissolution experiment, which resulted from complete dissolution of IND in FaSSIF. It must be noted that, at pH 6.5, it was expected that all IND had dissolved since the target concentration is much lower than the equilibrium crystalline solubility, at pH 6.5.

- For the low drug loads, 50% and 30%, a decrease in IND concentration was observed which could erroneously lead to the conclusion that IND had crystallized from solution. That is not the case since the target concentration is much lower than the equilibrium crystalline solubility, at pH 6.5. One possible explanation for this decrease in IND concentration is the precipitation of the polymer at pH 6.5, where it is highly insoluble, and entrapment of some drug molecules in the EUDRAGIT EPO particles that crashed out of solution. This would explain why the decrease in IND is much more pronounced for the 30% drug load ASD that yielded much higher polymer concentrations at pH 1.6 but resulted in a significant crash of Eudragit

EPO particles after pH-transition. This crash led to the entrapment of a significant amount of IND molecules, hence the greater decrease in concentration.

The biorelevant dissolution testing protocol was also followed to evaluate dissolution of IND/EUDRAGIT EPO ASD films ranging from 30% to 80% drug loads, prepared by the fusion method. The respective dissolution profiles are depicted in Figure 33.

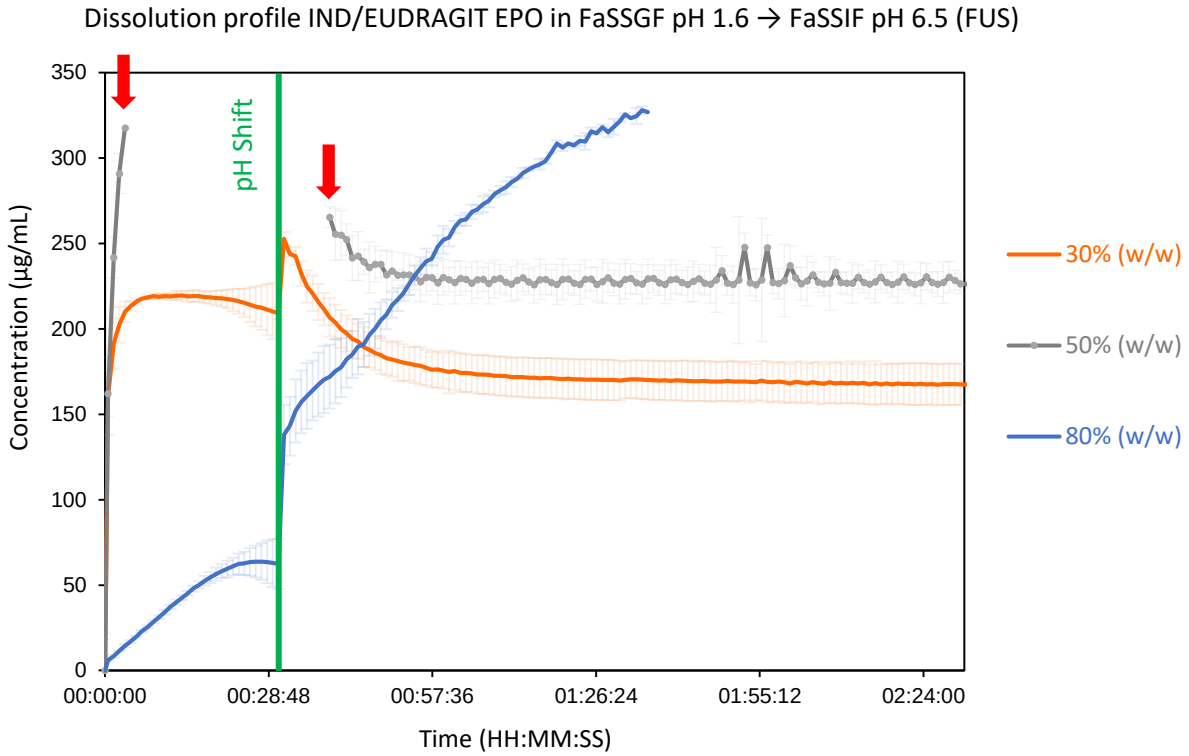

Figure 33. *Dissolution profiles of IND/ EUDRAGIT EPO ASD films produced by fusion with 30% drug load (orange), 50% drug load (grey) and 80% drug load (blue), in FaSSGF at pH 1.6, during a 30 min and after transition to FaSSIF at pH 6.5 during 2h, at 37ºC, under constant orbital shaking. The vertical green line indicates pH shift time point. Red arrows point out Values represent mean IND concentration (n = 2) and Y-error bars indicate the standard deviation.*

All the IND/EUDRAGIT EPO ASD films prepared by fusion have generated supersaturated systems when in solution, at pH 1.6, surpassing IND intrinsic solubility limit.

Unlike the previously tested films, the films prepared by fusion have different API quantities and, therefore, generate different maximum concentrations. The maximum concentrations that would be generated by the ASD films with 30%, 50% and 80% drug loads, if complete dissolution was attained, were approximately 200 µg/mL, 330 µg/mL and 530 µg/mL, respectively, for the final volume of 1.5 mL.

In the first part of the dissolution run in FaSSGF at pH 1.6, EUDRAGIT EPO is highly soluble providing a high driving force for dissolution, through the dismantling of the ASD matrix and exposure of IND to the dissolution medium. Therefore, for the low drug loads (high polymer contents), 30% and 50%, the extent of dissolution was much greater compared to the 80% drug load.

For the 30% drug load ASD dissolution was very fast and a plateau was attained around 200 µg/mL which corresponds to 50% drug release (1 mg of film containing 30% drug dissolved in 0.75 mL). Not all IND was dissolved because the rate of polymer dissolution from the surface of the film was so high that an outer shell of amorphous IND was formed on the surface, early in the dissolution run. This new drug-rich surface is very insoluble and prevents dissolution from occurring at this low pH.

With respect to the 50% drug load ASD, dissolution was also very fast and surpassed the upper limit of quantification of the equipment, hence no values were obtained after 3 minutes of dissolution. Higher concentrations were attained with this drug load, compared to the 30% drug load, because the amount of API available for dissolution in the 50% drug load film is much greater.

In the case of the 80% drug load, maximum concentration of 63 µg/mL was achieved after 25 min. This concentration is much lower than that attained by all other formulations because the amount of highly soluble polymer in the ASD is very low. Therefore, the dissolution rate of the 80% drug load ASD is limited by the kinetics of dissolution of the poorly soluble drug.

Upon transition from FaSSGF at pH 1.6 to FaSSIF at pH 6.5, the formulations with lower drug loads (30% and 50%) registered an instant peak concentration followed by a steep decrease in concentration until reaching a plateau. For the IND/ EUDRAGIT EPO ASD film with 50% drug load the plateau was attained at around 227 µg/mL whereas for the equivalent ASD film with 30% drug load was attained at around 168 µg/mL. The decay in concentration observed for these drug loads can be explained by the crash of Eudragit EPO particles, as a result of low polymer solubility at pH 6.5. This crash only occurred for the low drug load formulations since the amount of polymer dissolved before pH-shift was much greater. The precipitation of polymer particles led to the entrapment of some drug molecules in the Eudragit EPO particles that crashed out of solution, resulting in a decrease in free drug in solution.

Unlike the other amorphous films, the IND/ EUDRAGIT EPO ASD film with 80% drug load followed an increasing trend towards high drug concentrations, having surpassed the upper quantification limit of the equipment, after 1h 40min. That occurred because these amorphous films combining EUDRAGIT EPO with IND at 80% drug load are mostly comprised by API molecules highly soluble at pH 6.5, which are still available for dissolution due to the poor performance exhibited in FaSSGF at pH 1.6.

3.5.3. General Overview of IND/Polymer ASDs biorelevant dissolution

The ASD prototypes produced by the solvent evaporation method upon combination of one polymer candidate with IND at 50% drug load were investigated for their dissolution behavior in biorelevant dissolution media FaSSGF (pH 1.6) and FaSSIF (pH 6.5), monitored at IND maximum wavelength of absorbance (λ_{max}= 320nm), at 37ºC. Figure 34, shows the respective dissolution profiles.

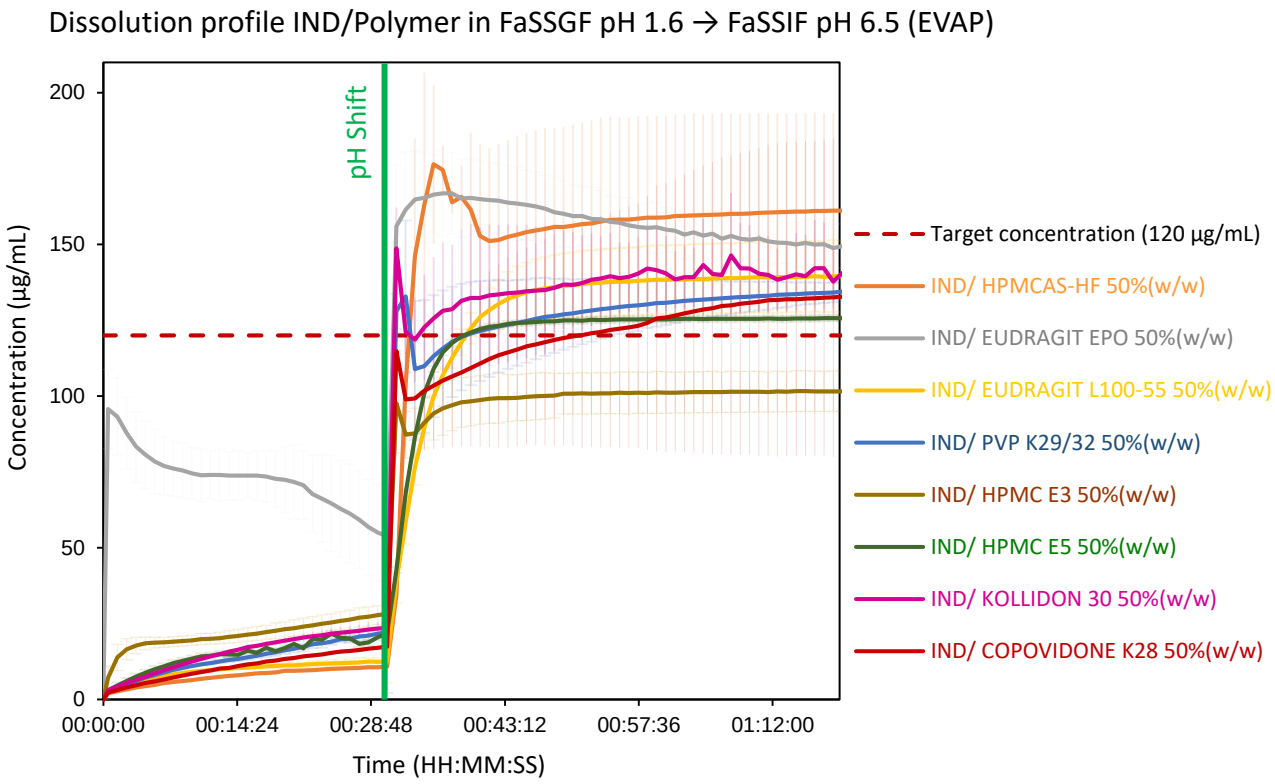

Figure 34. *Dissolution profiles of all different ASD films produced by solvent evaporation combining IND with one of the polymers under study at 50% drug load in FaSSGF at pH 1.6, during a 30 min and after transition to FaSSIF at pH 6.5 during 2h, at 37ºC, under constant orbital shaking. The vertical green line indicates pH shift time point. Target concentration of 120 µg/mL (Red dashed line). Values represent mean IND concentration (n = 2) and Y-error bars indicate the standard deviation.*

At the beginning, all ASD prototypes produced by solvent evaporation have managed to generate supersaturated systems when dissolved in biorelevant media, surpassing IND intrinsic solubility limit, at pH 1.6. The methacrylate polymer EUDRAGIT EPO exhibits high solubility below pH 5.0, resulting in a pronounced release of IND into solution since the ASD matrix tends to dismantle faster, enhancing drastically the contact between drug molecules and the solution phase. Therefore, upon dissolution of IND/EUDRAGIT EPO ASD film with 50% drug load in biorelevant medium FaSSGF at pH 1.6, a steep increase was observed generating a supersaturation state at around 95 µg/mL. From then on, the concentration of IND decreased, as a result of drug crystallizing from solution. Although EUDRAGIT EPO

is able to inhibit crystallization from solution, the supersaturation state achieved by the ASD was too high and the driving force for crystallization overcame the polymer crystallization inhibition effect. The dissolution profiles displayed by all other IND ASD films, in FaSSGF at pH1.6, was very similar and showed a small extent of drug release before pH-shift, compared to EUDRAGIT EPO ASDs. The same behavior was previously observed when ASDs prepared by solvent evaporation were dissolved in PBS at pH 2.0.

Upon transition from FaSSGF to FaSSIF at pH 6.5, amorphous IND becomes highly soluble due to ionization into a negatively charged form and considering that the target concentration (120 µg/mL) is much lower than IND solubility at pH 6.5, it is expected that all prototypes dissolve completely after pH-shift. Most polymers tested are also highly soluble at this pH, which resulted in a burst in dissolution for all prototypes, immediately after pH-shift.

The dissolution of ASDs comprising HPMC E5 and EUDRAGIT L100 – 55, right after pH shift, was much slower compared to the other prototypes, what may indicate that these polymers are not so effective at promoting drug release from the polymeric matrix.

On the other hand, dissolution of HPMCAS-HF ASD prototypes was so fast, after pH-shift, that complete dissolution was faster than the diffusion of drug molecules in the dissolution medium. That is why, after reaching peak concentration, at around 176 µg/mL, there is a small decay in concentration, corresponding to dilution of the drug molecules in the final 1.5 mL volume.

Finally, in the case of EUDRAGIT EPO, maximum concentration was achieved rapidly and was followed by a gradual decrease in concentration until the end of the experiment. This decay in concentration is not the result of crystallization since target concentrations are much lower than IND solubility at pH 6.5. This decay may be explained by the lower polymer solubility at this pH and the precipitation of polymer particles that imprison drug molecules in the matrix, therefore resulting in a decrease in free drug in solution.

The experimental screening protocol for biorelevant dissolution testing in FaSSGF at pH 1.6 and in FaSSIF at pH 6.5 was also followed to evaluate ASD formulations prepared by the fusion method, combining IND with a polymer candidate at 50% drug load. The respective dissolution profiles are depicted in Figure 35.

Upon dissolution in FaSSGF at pH 1.6, all ASD prototypes have managed to generate supersaturated systems when in solution, surpassing IND intrinsic solubility limit.

The IND/EUDRAGIT EPO ASD film with 50% drug load managed to attain an instant release of drug, having superseded the maximum limit of quantification right after 3 min of dissolution. The red arrows depicted in Figure 35 limit the area of IND/ EUDRAGIT EPO dissolution profile where the collected measures fell above the maximum limits of quantification. Apart from EUDRAGIT EPO, which is a cationic methacrylate polymer, highly soluble in aqueous media below pH 5.0, the remaining ASD prototypes evaluated under the scope of this screening study performed poorly and yielded supersaturated solutions below the apparent amorphous solubility threshold when dissolved in FaSSGF at pH 1.6.

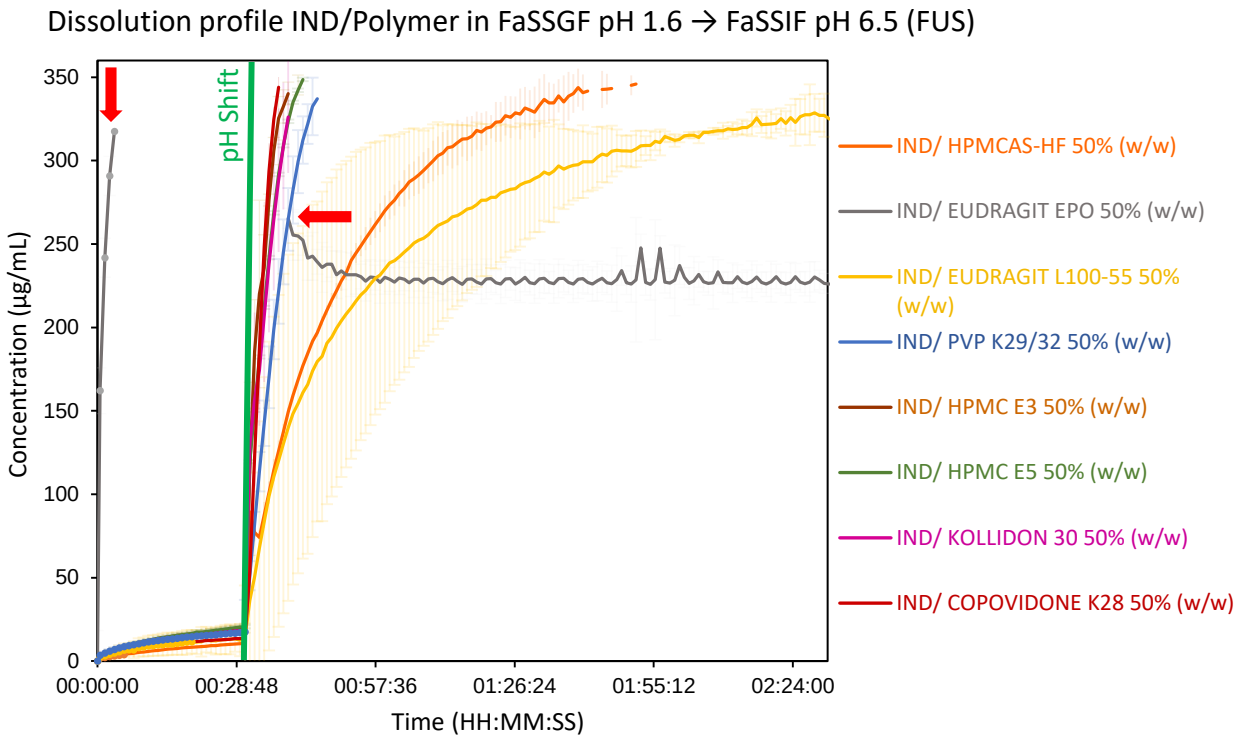

Figure 35. *Dissolution profiles of all different ASD films produced by fusion combining IND with one of the polymers under study at 50% drug load in FaSSGF at pH 1.6, during a 30 min and after transition to FaSSIF at pH 6.5 during 2h, at 37ºC, under constant orbital shaking. The vertical green line indicates pH shift time point. Values represent mean IND concentration (n = 2) and Y-error bars indicate the standard deviation.*

After the transition from FaSSGF at pH 1.6 to FaSSIF at pH 6.5, IND was released quickly and attained high concentrations in solution, yet following distinct trends depending on the polymer type. The binary ASD combining EUDRAGIT EPO with IND at 50% drug load, showed a decrease in concentration until reaching a plateau around 230 ± 10 µg/mL. This decay in concentration may be explained by the lower polymer solubility at this pH and the precipitation of polymer particles that imprison drug molecules in the matrix, therefore resulting in a decrease in free drug in solution. The “noisy” data collected also supports the formation of particles in solution that impact the light scattering properties of the dissolution medium.

The polyvinyl polymers and the cellulosic polymers registered a steep increase in concentration that went above the quantification limit of the equipment, after 40 ± 5 min. Considering the polymers tested, the ranking of dissolution rates of the respective IND ASDs was the following, from fastest to slowest: COPOVIDONE K28 > HPMC E3 > HPMC E5 ⇔ KOLLIDON K30 > PVP K29/32.

The IND ASD prototypes comprising the anionic polymers EUDRAGIT L100-55 and HPMCAS-HF, which are highly soluble at alkaline pH values, depicted prolonged release profiles in FaSSIF at pH 6.5, generating high supersaturation degrees at a slower rate.

3.6. Monitoring phase separation phenomena during ASD dissolution with Dynamic Light Scattering (DLS)

3.6.1. DLS analysis on IND/HPMCAS-HF ASD prototypes

To further investigate phase separation phenomena occurring in solution, such as crystallization or LLPS, during dissolution of IND/HPMCAS-HF ASD formulations with 50% drug load in PBS at pH 2.0, samples were collected at the maximum concentration peak and at the end of the dissolution. The time points that were sampled correspond to 5h and 12h, respectively, and were analyzed with Dynamic Light Scattering (DLS). The graphs depicting DLS size distribution of both samples is depicted in Figure 36.

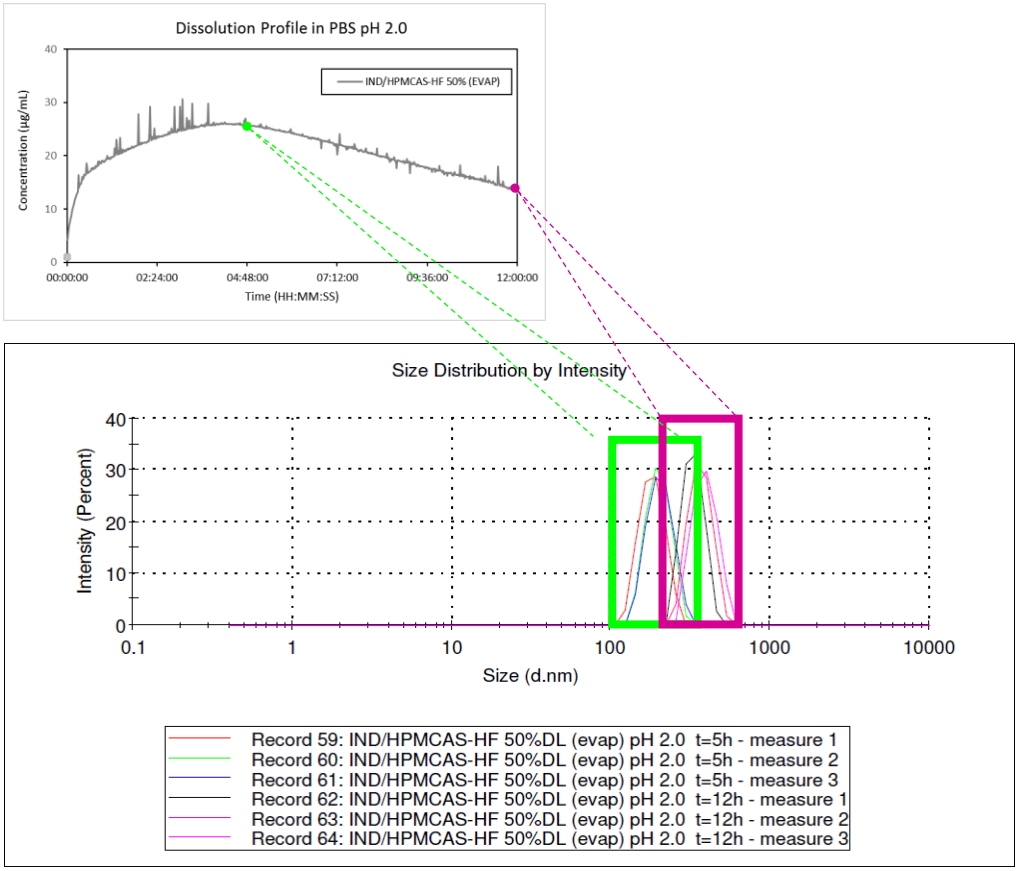

Figure 36. *Particle size distribution monitored by DLS at two time points - t= 5h (green rectangle) and t= 12h (purple rectangle) – in the course of the 12-hour dissolution run in PBS pH 2.0, at 37ºC, of IND/HPMCAS-HF ASD films produced by the solvent evaporation method.*

During dissolution in PBS at pH 2.0, the poor aqueous solubility of both HPMCAS-HF and IND below pH 5.0 hindered the release process of IND from the ASD film matrix into solution and, as a consequence, the level of supersaturation attained was not significant. The particle size assessment was in agreement with the dissolution profile obtained. At the 5h time point, drug concentration reached its maximum, above the apparent amorphous solubility of IND (around 28 µg/mL), at pH 2. Since concentrations reached and

surpassed amorphous solubility, liquid-liquid phase separation occurred and drug-rich colloidal species had formed. The generation of these colloids is supported by the size measurements obtained for the particles present in solution at that time.

At the maximum concentration peak, the sample collected comprised a particle population with sizes within the range of 100 – 300 nm, which according to several articles on DLS analysis of ASD formulations, corresponds to drug-rich colloids.[42,147–154] At the end of the dissolution run, the particle population was sized within the range of 200-650 nm. Such increase in the size of the particles present in solution is indicative of crystallization occurring in solution, with the formation of crystal drug aggregates of intermediate size, as confirmed by the gradual decrease in concentrations measured until the end of the experiment. [42,147–154]

It must be mentioned that despite a large amount of film remaining undissolved, the DLS measurements did not pick up any additional particles. That is because the undissolved sample remained in the film and pieces of the film did not go into solution.

The same protocol was followed to analyze IND/HPMCAS-HF ASD films with 50% drug load prepared by the fusion-base method, and the respective size distribution graph is depicted in Figure 37.

Similar dissolution behavior was observed for the supersaturated solutions generated upon dissolution of the IND/HPMCAS-HF ASD formulation with 50% drug load prepared by the fusion method in PBS at pH 2.0. The particle size analysis by DLS revealed to be in agreement with the dissolution profile obtained. At the maximum concentration peak, the sampled taken at the 5h time point was sized within the range of 100 – 300 nm, confirming the formation of colloidal species in solution within a size range of drug-rich colloids reported in previous articles. However, smaller particle sizes were detected at the end of dissolution, compared to those determined with the solvent evaporation films, with sizes between 150 – 350 nm, falling within the range of drug-rich colloids.[42,147–154]A plausible justification for such occurrence might be the collection of the sample so early in the crystallization process, as depicted by the dissolution profile that shows a decrease in concentration only after 7 hours into the dissolution process. Such particle population may comprise a majority of nanosized crystal aggregates starting to take form in solution or a mixture of the previous with small colloidal droplets. [42,147–154]

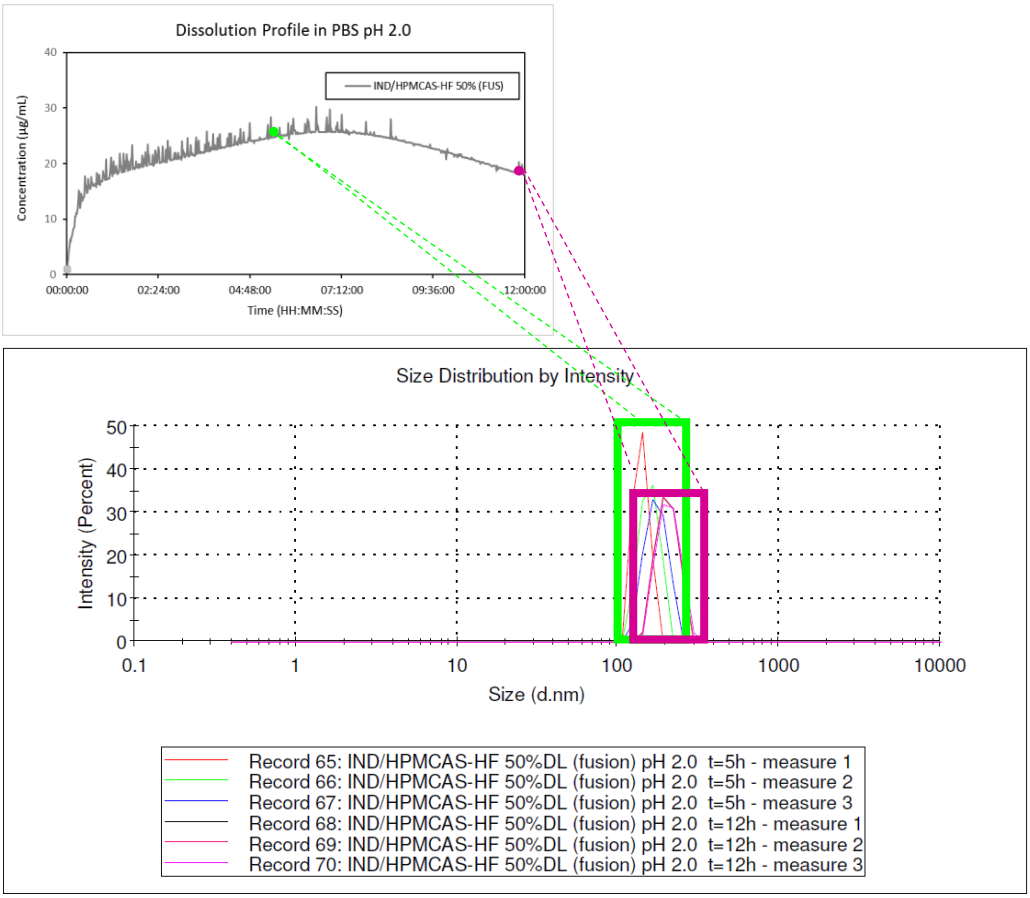

Figure 37. *Particle size distribution monitored by DLS at two time points - t= 5h (green rectangle) and t= 12h (purple rectangle) – in the course of the 12-hour dissolution run in PBS pH 2.0, at 37ºC, of IND/HPMCAS-HF ASD films produced by the fusion method.*

3.6.2. DLS analysis on IND/EUDRAGIT EPO ASD prototypes

To better characterize the supersaturated systems generated by IND/EUDRAGIT EPO ASD prototypes, the occurrence of phase separation phenomena, crystallization or LLPS, during dissolution of IND/EUDRAGIT EPO ASD films with 50% drug load in PBS at pH 2.0 was monitored by Dynamic Light Scattering (DLS). Samples were collected at 20 min and 12h time points, corresponding to the maximum concentration peak and the end of the dissolution run, respectively. The graphic depicting DLS size distributions is depicted in Figure 38.

The ASD formulations combining IND with EUDRAGIT EPO as polymeric counterpart delivered the best performance in terms of supersaturation rate and extent. In fact, from the pool of polymers under study, EUDRAGIT EPO generated the highest degrees of supersaturation when dissolved in PBS at pH 2.0. Unlike IND, which is poorly soluble below pH 4.5, EUDRAGIT EPO displayed high aqueous solubility in acidic pH and proved to be effective in the mediation of IND release from ASD film matrix into the solution phase:

Nevertheless, this polymer was not as effective as a stabilizer and precipitation inhibitor. As a result, the dissolution profiles of IND/EUDRAGIT EPO ASD formulations depicted a high concentration peak followed by a steep decay towards equilibrium solubility limit.

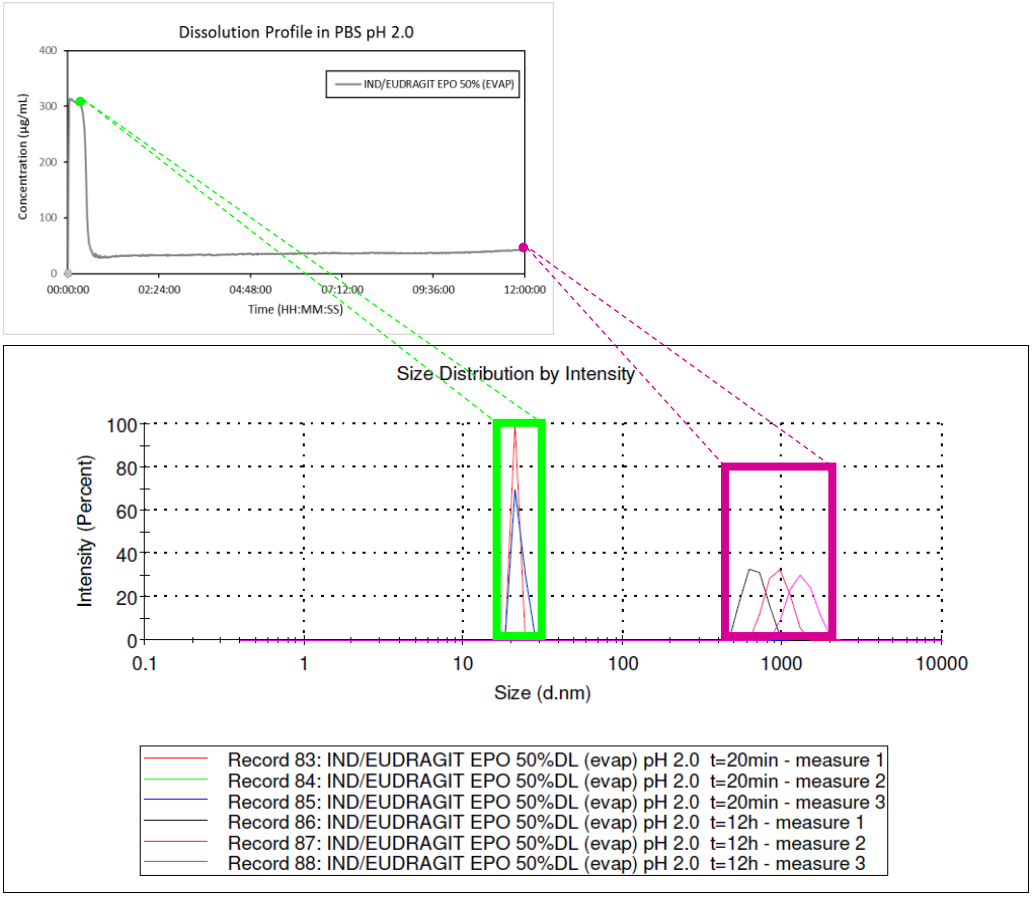

Figure 38. *Particle size distribution monitored by DLS at two time points - t= 20min (green rectangle) and t= 12h (purple rectangle) – in the course of the 12-hour dissolution run in PBS pH 2.0, at 37ºC, of IND/EUDRAGIT EPO ASD films produced by the solvent evaporation method.*

For the IND/EUDRAGIT EPO ASD films produced by solvent evaporation, at the maximum concentration peak, the collected sample comprised a particle population sized within the range of 20 – 30 nm, which denotes no occurrence of either crystallization or formation of colloidal species, which are typically found around 300 nm. [42,147–154] The expected outcome of the DLS analysis was the detection of colloidal species, since maximum concentration was much higher than the amorphous solubility of IND, at pH 2. The particles detected were significantly smaller (20-30 nm) and one possible explanation for that is that colloidal species had formed but did not have time to coalesce and generate the typical colloidal species reported in the literature (around 300 nm). After an intensive crystallization process, concentrations reached a plateau corresponding to equilibrium crystalline solubility. At the end of the dissolution run, a sample was collected and analyzed by DLS showing particles in the range of **450-2000 nm**, confirming the formation of large crystal drug aggregates in solution.

The same protocol was followed to analyze IND/ EUDRAGIT EPO ASD films with 50% drug load prepared by the fusion-base method, and the respective size distribution graph is depicted in Figure 39.

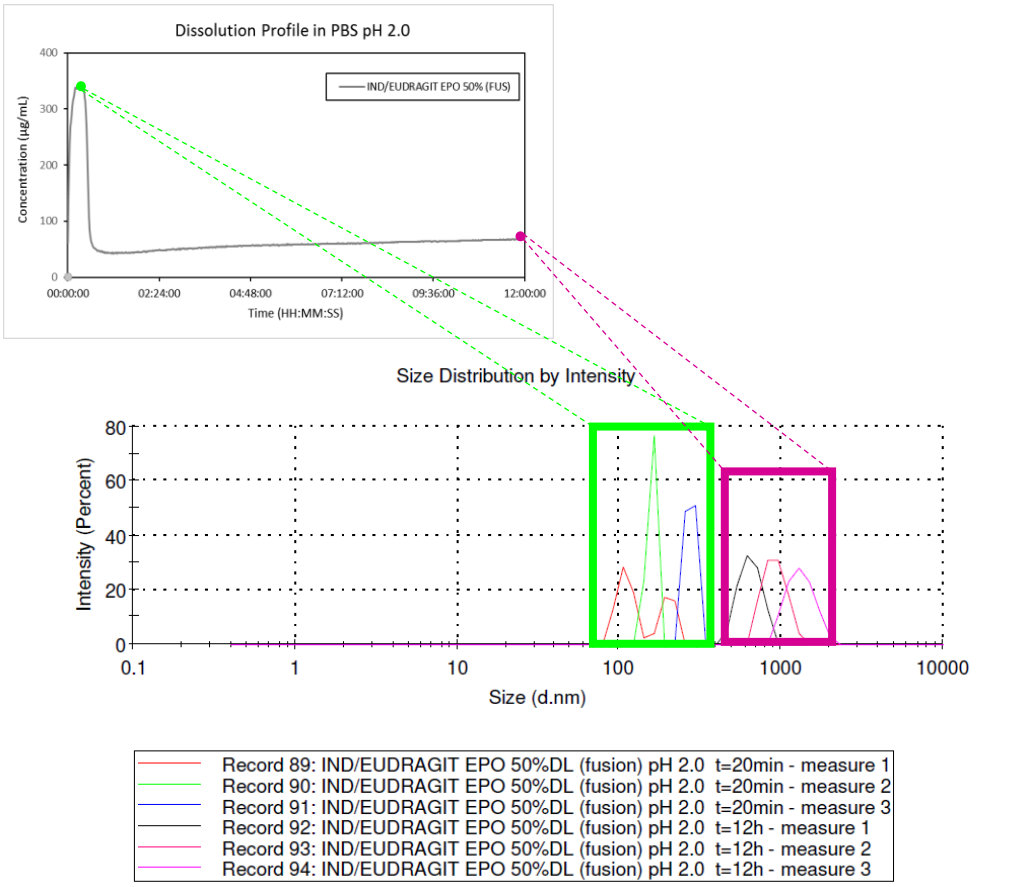

Figure 39. *Particle size distribution monitored by DLS at two time points - t= 20min (green rectangle) and t= 12h (purple rectangle) – in the course of the 12-hour dissolution run in PBS pH 2.0, at 37ºC, of IND/EUDRAGIT EPO ASD films produced by the fusion method..*

A similar dissolution profile was registered upon dissolution of the IND/EUDRAGIT EPO ASD formulation with 50% drug load prepared by the fusion method in PBS at pH 2.0. The particle size assessment performed on the samples collected revealed to be in agreement with the overall dissolution profile trend. Hence, at the 20 min time point, a maximum concentration peak was attained at a concentration approximately 12 times higher than the apparent amorphous solubility of IND. Therefore, the expectation was that LLPS occurred and colloidal species were formed. This was supported by the DLS results on the particles present in solution at that time.

At the maximum concentration peak, the sample collected comprised a particle population with sizes within the range of 70 – 350 nm, which confirms the presence of drug-rich colloids in PBS at pH 2.0.[42,147–154] At the end of the dissolution run, the particle population collected was sized within the range of 450-2500 nm. Such increase in the size of the particles present in solution is indicative of formation of large crystal

aggregates.[42,147–154] The ASD formulations combining IND with EUDRAGIT EPO as polymeric counterpart delivered the best performance in terms of supersaturation rate and extent. In fact, from the pool of polymers under study, EUDRAGIT EPO generated the highest degrees of supersaturation when dissolved in PBS at pH 2.0. Unlike IND, which is poorly soluble below pH 4.5, EUDRAGIT EPO displayed high aqueous solubility in acidic pH and proved to be effective in the mediation of IND release from ASD film matrix into the solution phase: Nevertheless, this polymer was not as effective as a stabilizer and precipitation inhibitor.

As a result, the dissolution profiles of IND/EUDRAGIT EPO ASD formulations depicted a high concentration peak followed by a steep decay towards equilibrium solubility limit. At the maximum concentration peak, the collected sample comprised a particle population sized within the range of 20 – 30 nm, which denotes no occurrence of either crystallization or formation of colloidal species, which are typically found around 300 nm.[42,147–154] The expected outcome of the DLS analysis was the detection of colloidal species, since maximum concentration was much higher than the amorphous solubility of IND, at pH 2. The particles detected were significantly smaller (20-30 nm) and one possible explanation for that is that colloidal species had formed but did not have time to coalesce and generate the typical colloidal species reported in the literature (around 300 nm).[42,147–154] After an intensive crystallization process, concentrations reached a plateau corresponding to equilibrium crystalline solubility. At the end of the dissolution run, a sample was collected and analyzed by DLS showing particles in the range of 450-2000 nm, confirming the formation of large crystal drug aggregates in solution. [42,147–154]

3.7. Assessment of Miscibility and Film Uniformity using Confocal Raman Microscopy

3.7.1. Microscopy imaging on the evaluation of ASD film integrity and uniformity

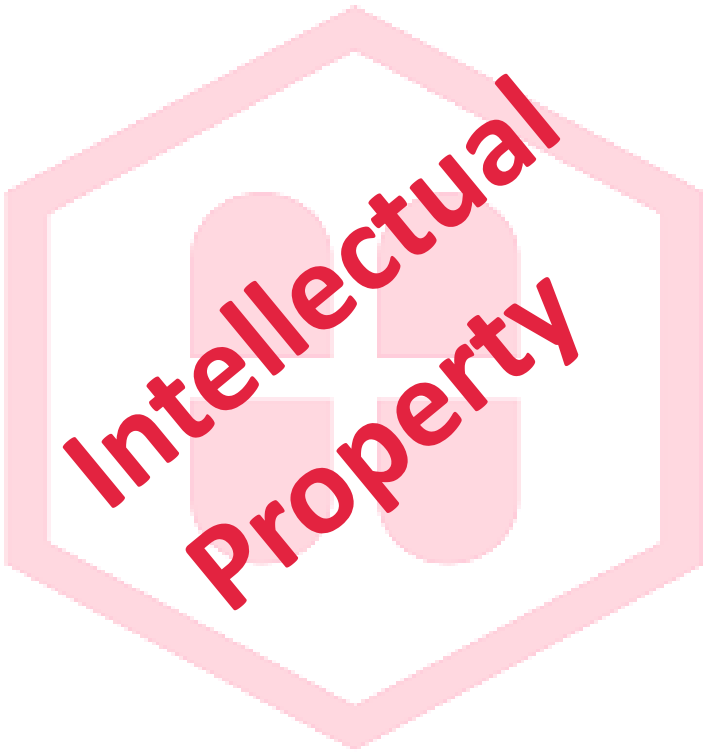

Figure 40. *Confocal Microscope Images of IND/ HPMCAS-HF ASD films: (A) General overlook. (B) Close image on a central area. (C) Zoom in on a specific area of the film in which was performed a large area scan.*

These images portray an ASD film prepared upon fusion of IND/HPMCAS-HF 50% (w/w) blend mixture deposited on the surface of a deposition platform. In terms of quality control, these images provide a detailed observation on the amorphous films prepared and enable evaluation of distribution evenness and uniformity of the ASD layer formed. At a macroscopic level it is possible to spot discontinuities in the film, which are usually difficult to detect at naked eye.

In image A (Figure 40) a general look over the deposition platform shows an apparently uniformly distributed film layer, in spite of the detected film coverage irregularities and rust marks near the upper right corner of the picture. Zooming in the center area (image B, Figure 40) unveils some unfilled areas following a concentric distribution pattern, which might have been formed as a result of the compression step performed during preparation process. Further zooming, in image C (Figure 40), shows thick ASD film veins and, on

the bottom, a brighter blot exposing deposition platform surface. No crystal shaped material was observed with Confocal Raman Microscopy Imaging.

3.7.2. Confocal Raman Microscopy analysis on IND/HPMCAS-HF and IND/EUDRAGIT EPO ASD prototypes

To evaluate the distribution of individual components on the ASD films produced using both methods developed under the scope of this project, large area scans were performed on ASD films combining IND with HPMCAS-HF and EUDRAGIT EPO at 50% drug load. The goal was to assess API and Polymer miscibility and changes in phase behavior that took place during manufacturing process and storage, before any further dissolution testing was performed.

In confocal Raman microscopy analysis, each large area scan image culminated in the creation of multi-spectral data sets comprising hundreds to thousands of spectra. Each image pixel is associated to a Raman spectrum carrying significant amounts of information on the composition of the ASD film material at the position where the spectrum was recorded. The entire multi-spectral data set was subjected to pre-processing filters and algorithms, such as background subtraction, Cosmic Ray Removal and Savitzky Golay Smoothing, so that relevant information could be extracted.

Upon pre-treatment, large area scans were used to perform a non-invasive determination of components spatial distribution, miscibility and phase behaviour exhibited by ASD films. To do so, a combination of single spectra of individual ASD components with the multi-spectral data set was carried out, resulting in the creation of colour-coded images, also known as Colour Bitmaps.

These images are distribution maps, colour-coded according to the respective components detected in the Raman spectrum of each scanned point within the image. In this work the colour code was defined as follows: IND (red), HPMCAS-HF (blue), EUDRAGIT EPO (yellow), so that the combination of drug with each of these polymers would originate the appearance of a different colour in the Colour Bitmap image. Hence, IND/HPMCAS-HF ASD film assumed the colour purple), whereas IND/EUDRAGIT EPO ASD films exhibited orange as colour. Further confirmation of components presence was accomplished through the analysis of an average spectral scan originating from a certain point within the multi-colored bitmap.

3.7.2.1. Confocal Raman Microscopy analysis on IND/HPMCAS-HF ASD films

Figure 41 presents the results of Confocal Raman Microscopy analysis of IND/ HPMCAS-HF ASD films with 50% drug load produced by the solvent evaporation method.

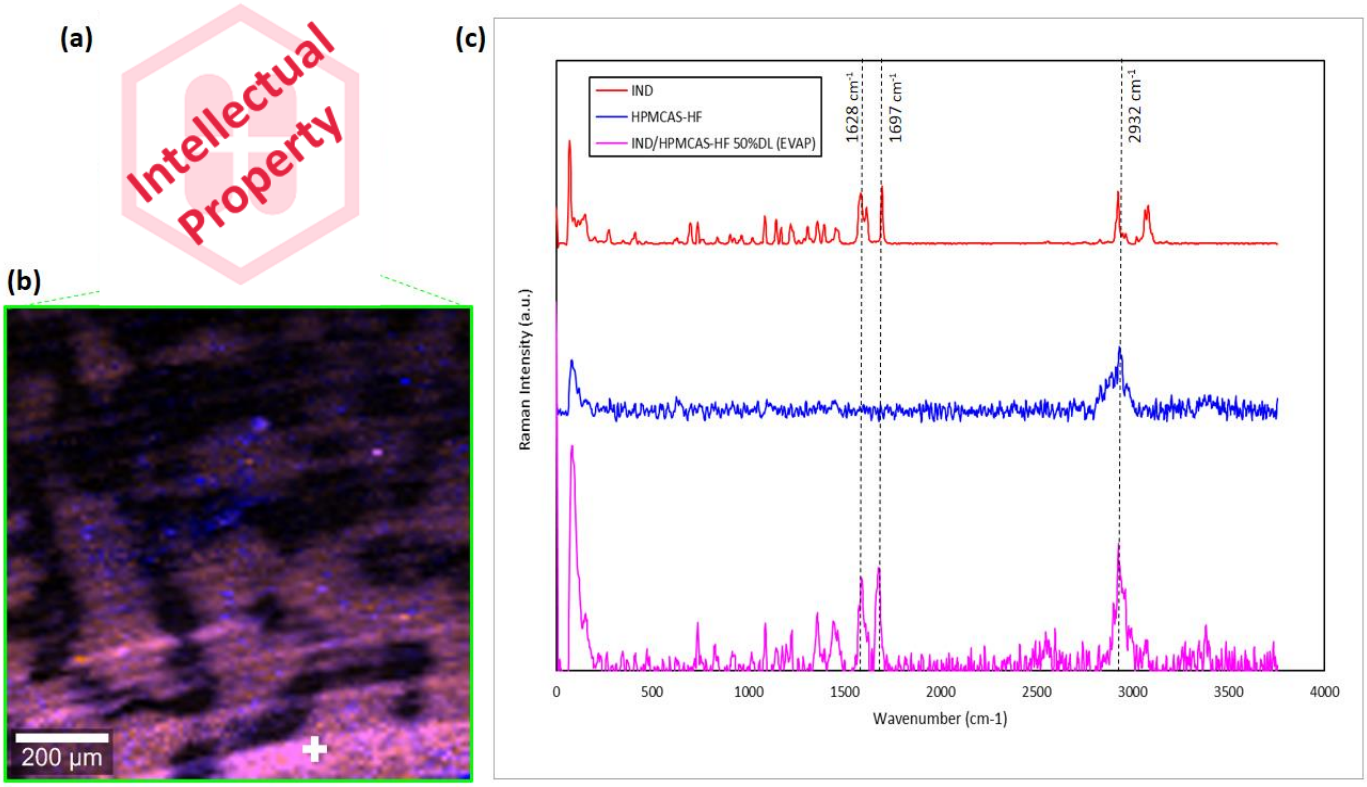

Figure 41. *Confocal Raman Microscopy Analysis on an IND/ HPMCAS-HF ASD film with 50% drug load produced by solvent evaporation: (a) Confocal Microscope Image providing a general overlook on the ASD film deposited on the surface of a deposition platform (b) Colour Bitmap correspondent to the film area selected by a green rectangle in image (a). (c) Raman Spectra combining the individual spectrum of IND (red) and HPMCAS-HF (blue) with the average spectral scan correspondent to the ASD film region marked in image (b) with a white cross (light purple). The dashed vertical lines indicate the peaks monitored at characteristic Raman shifts of each component of the ASD film.*

The large area scan taken from this sample, was converted in a Colour Bitmap depicted in image (b), Figure 41. The area chosen to be analyzed was carefully selected in order to guarantee the representativeness of the results. The dark background areas convey the existence of areas of the deposition platform surface without ASD film, proving some lack of uniformity at a microscale level. It is possible to spot some blue dots indicative of zones with HPMCAS-HF isolated. On the other hand, phase separation phenomena was not detected in great extent, since a large area of the image is colored in light purple, the conjoint color of both components (IND-red and HPMCAS-HF- blue), illustrative of a good miscibility between drug and polymer.

The average spectral scan corresponding to the image pixel marked with a white cross is depicted in image (c), Figure 41, along with the single spectra of both IND and HPMCAS-HF. Despite having been subjected to pre-processing algorithms, noise peaks can still be found within the Raman spectra, yet no significant interference hindering characteristic Raman shifts identification have been registered. Through a spectral correspondence it is possible to identify characteristic Raman shifts of IND and HPMCAS-HF in the Raman spectrum of the IND/HPMCAS-HF ASD film, with the matching peaks being signaled by vertical dashed lines. Such identification confirms the presence of both components in the ASD film matrix.

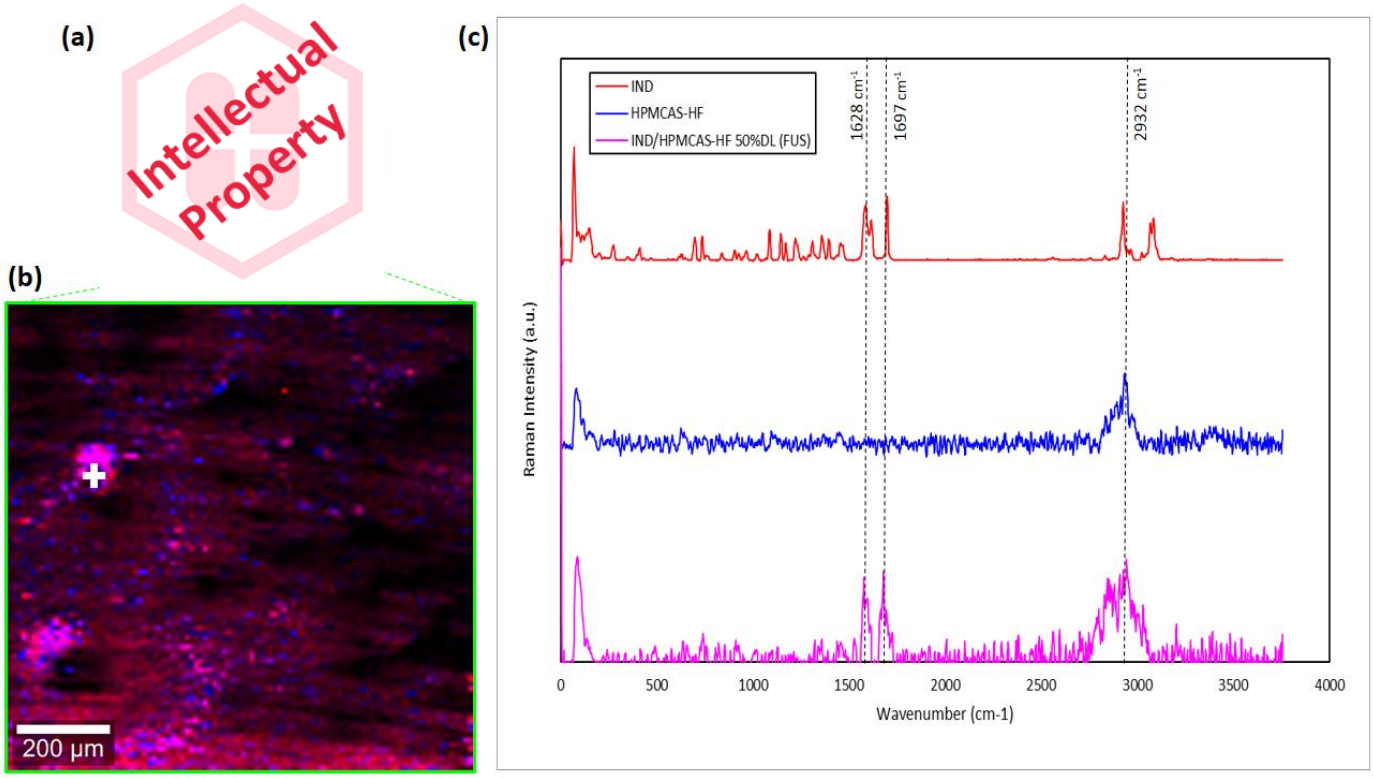

Figure 42. *Confocal Raman Microscopy Analysis on an IND/ HPMCAS-HF ASD film with 50% drug load produced by fusion method: (a) Confocal Microscope Image providing a general overlook on the ASD film deposited on the surface of a deposition platform. (b) Colour Bitmap correspondent to the film area selected by a green rectangle in image (a). (c) Raman Spectra combining the individual spectrum of IND (red) and HPMCAS-HF (blue) with the average spectral scan correspondent to the ASD film region marked in image (b) with a white cross (light purple). The dashed vertical lines indicate the peaks registered at characteristic Raman shifts of each component of the ASD film.*

The Raman signal exhibited at 1697 cm^{-1} corresponds to the amide C=O stretch of Y form of IND, whereas the peak at 1628 cm^{-1} is attributed to IND's carboxylic C=O stretch.[155–157] The HPMCAS-HF multiple-peak signal with higher intensity at 2932 cm^{-1} is assigned to asymmetrical and symmetrical stretch of CH_2 group.[158–160]Such analysis supports the rationale for reasonable molecular miscibility between drug and polymer with no significant phase separation occurrence during manufacturing and/or storage conditions

prior to screening testing. The relative intensity of the API and Polymer bands (1697 cm^{-1} and 2932 cm^{-1}, respectively) was taken into a good indicator for equalitarian presence of both in the ASD binary matrix of the film at the point from which the Raman Spectra is linked to.[158–160]

The same characterization protocol was followed to perform a Confocal Raman Microscopy analysis on IND/ HPMCAS-HF ASD films with 50% drug load produced by the fusion method (Figure 42), and similar conclusions were drawn. Despite the Raman shift correspondence, the Color Bitmap analysis denotes a higher amount of blue and also red dots indicating zones with isolated HPMCAS-HF and IND, respectively.

3.7.2.2. Confocal Raman Microscopy analysis on IND/EUDRAGIT EPO ASD films

Figure 43 shows the results of Confocal Raman Microscopy analysis of IND/ EUDRAGIT EPO ASD films with 50% drug load produced by the solvent evaporation method.

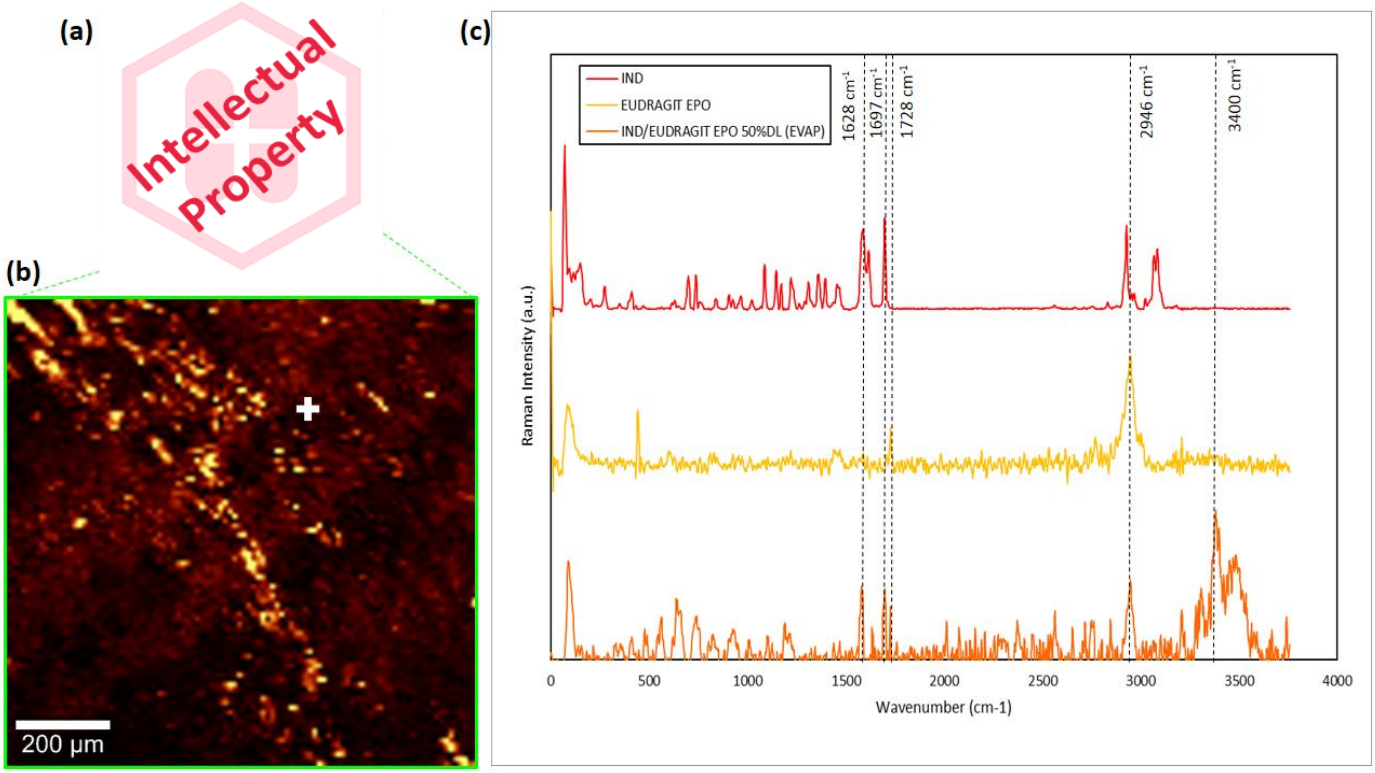

Figure 43. *Confocal Raman Microscopy Analysis on an IND/ EUDRAGIT EPO ASD film with 50% drug load produced by solvent evaporation: (a) Confocal Microscope Image providing a general overlook on the ASD film deposited on the surface of a deposition platform. (b) Colour Bitmap correspondent to the film area selected by a green rectangle in image (a). (c) Raman Spectra combining the individual spectrum of IND (red) and EUDRAGIT EPO (yellow) with the average spectral scan correspondent to the ASD film region marked in image (b) with a white cross (orange). The dashed vertical lines identify the peaks registered at characteristic Raman shifts of each component of the ASD film.*

The Large area scan collected from this sample, was converted in a Colour Bitmap depicted in image (b), Figure 43. The area chosen to be analyzed was carefully selected in order to ensure the representativeness of the present results. It is possible to observe some accumulation spots of EUDRAGIT EPO colored in yellow and others of IND colored in red, flanked by large orange areas of IND/EUDRAGIT EPO ASD film, denoting some phase separation. The darker regions of the Colour Bitmap represent areas with less material. Nonetheless, comparing to the prior analysis on IND/HPMCAS-HF ASD films components distribution, no large areas lacking material were identified, being synonym of a material more uniformly distributed over the deposition platform. Additionally, since large zones of the Colour Bitmap were orange colored (the color resultant of combination of API and Polymer), an agreeable distribution of ASD film components is depicted.

The average spectral scan correspondent to the image pixel marked with a white cross is depicted in image (c), Figure 43, along both IND and EUDRAGIT EPO single spectrum. Despite having been subjected to pre-treatment algorithms, Raman spectra exhibit noise peaks compromising the quality of the signal, albeit no significant interference hindering characteristic Raman shifts identification was registered.

A spectral signal evaluation was performed, with the matching Raman shifts being by identified by vertical dashed lines. The identification of IND and EUDRAGIT EPO characteristic Raman shifts in the Raman spectrum of the IND/EUDRAGIT EPO ASD film, confirmed the presence of these components in the film matrix. The Raman signal exhibited at 1697 cm^{-1} corresponds to the amide C=O stretch of Y form of IND, whereas the peak at 1628 cm^{-1} is attributed to IND's carboxylic C=O stretch. [155–157] EUDRAGIT EPO exhibits two characteristic Raman shifts; one at 1728 cm^{-1}, which is assigned to carbonyl C=O stretch vibrations and another at approximately 2800 cm^{-1} associated to stretching vibration of CH_3 and CH_2 groups. The band shift from 2800 cm^{-1} to 2946 cm^{-1} registered by the peak corresponding to the stretching vibration of CH_3 and CH_2 groups along with the wide Raman band at 3400 cm^{-1} may have resulted from intermolecular interactions established between drug and polymer during ASD formation.[134,137,161–166]

Moreover, the relative intensity of the API and Polymer bands (1697 cm^{-1} and 2946 cm^{-1}, respectively) was taken into consideration as a good indicator for equalitarian presence of both API and Polymer in the ASD binary matrix of the film at the point from which the Raman Spectra was recorded.

The same characterization protocol was applied to analyze IND/ EUDRAGIT EPO films with 50% drug load produced by the fusion method and the respective output results are presented in Figure 44. Similar conclusions derived from such evaluation since despite the Raman shifts correspondence, it is possible to

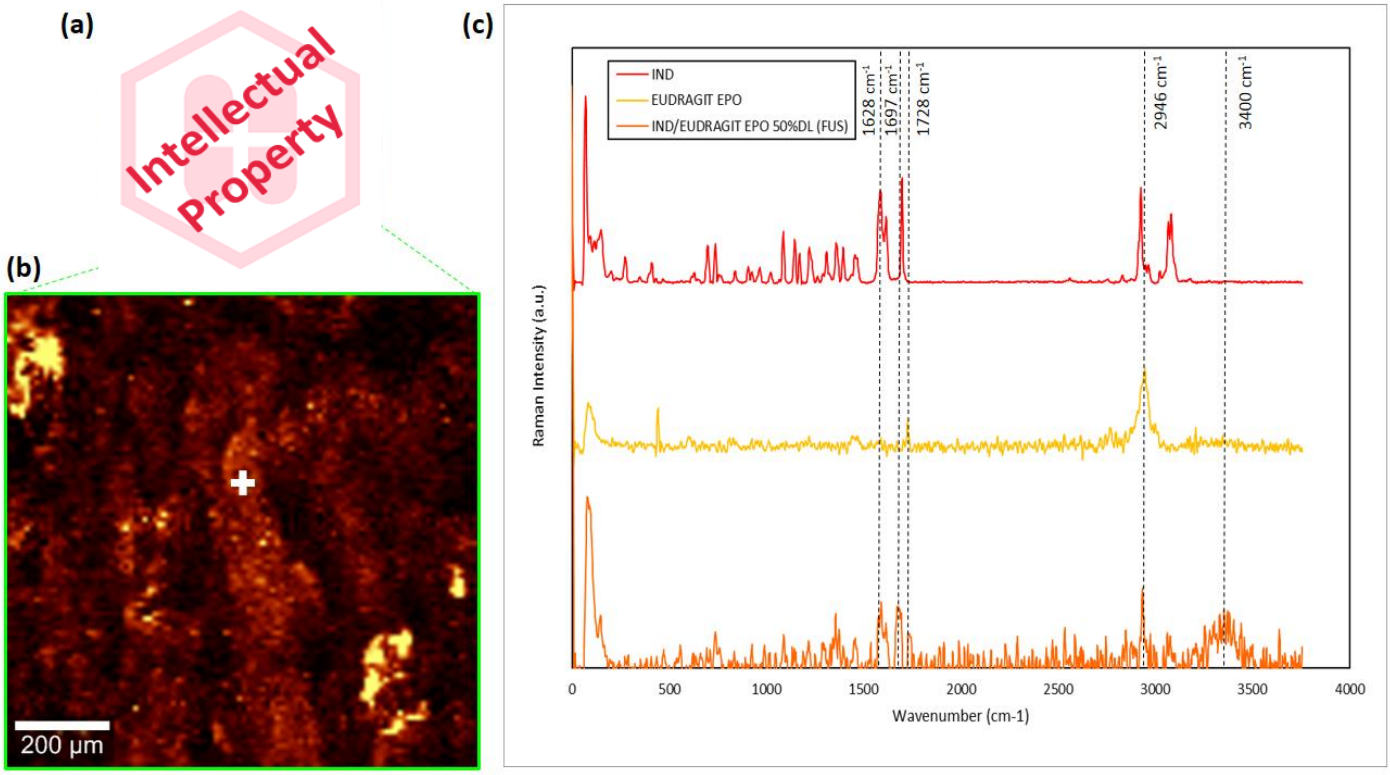

Figure 44. *Confocal Raman Microscopy Analysis on an IND/ EUDRAGIT EPO ASD film with 50% drug load produced by the fusion method: (a) Confocal Microscope Image providing a general overlook on the ASD film deposited on the surface of a deposition platform. (b) Colour Bitmap correspondent to the film area selected by a green rectangle in image (a). (c) Raman Spectra combining the individual spectrum of IND (red) and EUDRAGIT EPO (yellow) with the average spectral scan correspondent to the ASD film region marked in image (b) with a white cross (orange). The dashed vertical lines identify the peaks registered at characteristic Raman shifts of each component of the ASD film.*

4. Conclusions and Future Prospective

An innovative miniaturized dissolution screening methodology used to study the dissolution behavior of ASD prototypes and all the associated phenomena through UV-Vis spectroscopy has been successfully developed. The new dissolution approach produced reliable results and proved to be effective in the characterization of the dissolution behaviour of a broad design space of drug-polymer combinations during early stages of pharmaceutical drug product development.

This miniaturized dissolution screening approach proved simple, rapid and reproducible, while using readily available equipment and requiring minimal API quantities. A major advantage of the newly developed miniaturized screening methodology was the novelty regarding dissolution testing during early pre-formulation development, accomplished by allying an ASD deposition platform to a quartz microplate for UV-Vis spectroscopic determinations, enabling a non-invasive, real-time monitoring of ASD prototypes dissolution behaviour culminating in complete dissolution profiles comprising measurements registered every minute over a 12-hour run, or a different time span according to experimental specifications in force. Since it provides information on dissolution behaviour of ASD prototypes through the construction of dissolution profiles covering the entire dissolution run time span, this miniaturized methodology allows to fulfill a large gap found in the current screening methodologies, at Hovione, since traditional screening protocols only contemplate ASD physical stability aspects and polymer effect to inhibit crystallization of drug from supersaturated solutions.

In comparison to other miniaturized approaches previously reported in the literature, the dissolution screening methodology here proposed encompasses more advantages in terms of implementation, feasibility and workflow. For example, the ability to evaluate dissolution kinetics of a set of 24 different formulations, simultaneously. Moreover, unlike other screening methodologies published in the literature reporting the use of microplates, in this miniaturized screening methodology the microplate is only involved in the characterization step, not as a support for sample preparation. Hence, the number of prototypes that can be produced is independent from the microplate total capacity (number of wells) and the number of microplates at dispose, but instead depends on the number of deposition platforms available and on the amount of API and polymers available. Furthermore, another great benefit conveyed is the use of the same deposition and dissolution platform, throughout the entire screening program, from production to characterization.

In terms of ASD films preparation, both solvent evaporation and fusion methods proved effective, having resulted in amorphous films capable of generating dissolution profiles that matched the theoretical expected outcome. The possibility to submit the resultant amorphous films for evaluation by distinct characterization assays (e.g. UV-Vis spectroscopy, DLS, CRM) conveys versatility to the methodology, which is not common to traditional screening protocols that use several ASD production methods, specifically developed to meet the requirements of a certain characterization assay.

Hence, these miniaturized dissolution methodologies can be applied to screening of potential candidates for both SD and HME industrial scale production, and provide support to decision making for the best ASD prototypes both in terms of ASD dissolution performance and physical stability.

But it is important to ponder over the practical challenges concerning the film preparation methods developed, since it is a critical step involving very small amounts of ASD deposited.

Due to the surface tension properties of liquids, the solvent evaporation method enabled the preparation of ASD films with lower mass and thickness, adapting better to micro-scale dissolution monitoring. On the other hand, the fusion method, due to the rheological properties of the drug-polymer blends, did not allow the preparation of films with total mass inferior to 1 mg since inferior quantities would further compromise film uniformity and deposition onto the deposition platform. Therefore, for ASD films produced by the solvent evaporation method, target concentrations were fixed prior to evaluation of film dissolution, whereas for ASD films prepared by the fusion method, the overall film mass was fixed for all formulations.

For the purpose of this thesis, IND was selected as model drug and a pool of 8 pharmaceutically relevant polymers from 3 different classes was selected: methacrylate polymers (EUDRAGIT EPO, EUDRAGIT L100-55), polyvinyl lactam polymers (PVP K29/32, KOLLIDON K30, COPOVIDONE K28) and cellulosic derivate polymers (HPMCAS-HF, HPMC E3, HPMC E5). The shake-flask method was used to determine crystalline solubility by UV-Vis Spectroscopy. The UV extinction method applied to determination of LLPS onset transition concentration was successfully applied to estimate the apparent amorphous solubility of IND.

The dissolution profiles obtained by UV-Vis spectroscopy, via microplate reader, matched the theoretical expectations. By using PBS at two different pH values, one above and other below the pKa of IND (PBS at pH 2.0 and pH 6.8), it was possible to study the dissolution behaviour of ASD prototypes as a function of pH and evaluate the impact of the ionization state and solubility of the drug on the dissolution profiles obtained. Also, the effect of medium pH over polymers was investigated, with cationic polymers (EUDRAGIT EPO) yielding a great performance at pH 2.0 and cationic polymers depicting better performance at more alkaline pH values.

The biorelevant testing in FaSSGF at pH 1.6 and FaSSIF at pH 6.5, resulted in two-step curve dissolution profiles with ASD prototypes depicting a strong dissolution rate upon transition to pH 6.5, which reflects the higher solubility of IND, at this pH.

DLS analysis enabled monitoring the particles formed in solution upon attainment of supersaturation levels above apparent amorphous solubility limit. The particle size distribution graphs supported the formation of a new drug-rich colloidal phase during dissolution, revealing the presence of colloidal species at maximum concentration peak and larger particles at the end of the dissolution run indicating the formation of drug crystal aggregates.

The Confocal Raman Microscopy analysis on IND/ HPMCAS-HF and IND/ EUDRAGIT EPO ASD films prepared by the solvent evaporation and fusion methods depicted a reasonable overall uniformity of deposition, despite the micro-scale discontinuities detected. The large area scans were compared to single spectra of IND, HPMCAS-HF and EUDRAGIT EPO to produce Colour Bitmaps illustrative of the components' distribution within the film. The Raman Imaging results enabled a qualitative evaluation on drug-polymer miscibility and phase separation behaviour. These results were further confirmed upon evaluation of the characteristic Raman shifts of IND and the respective polymer in the average spectra taken from a pixel point of the area scanned. The area selected was considered as representative of the entire film surface.

Future Work

For application to high-throughput screening (HTS), sample preparation requires optimization, to better cope with time demands.

Table 5. *Summary of times expended upon production of ASD films on deposition platforms through the methods developed under the scope of this project.*

	Solvent evaporation	**Fusion**
Preparation time		
Set of 24 ASD prototypes	2h 30min	3h 30min
per unit (deposition platform)	5 min	7.5 min
Analysis time		
Dissolution run	12h	12h
Main challenges		
	Film uniformity	Film uniformity Accuracy of deposition

Table 5 summarizes the times involved in the miniaturized screening methodology developed. While the analysis time defined for the dissolution run only depending on the type of study intended to be performed, the time required for film preparation can be further optimized. According to the estimations performed, one deposition platform prepared with the solvent evaporation method takes around 5 minutes to be produced, whereas by the fusion method each deposition platform takes approximately 7.5 minutes of preparation.

Other parameters to be improved are film uniformity and accuracy of deposition as confirmed by the inconsistencies and areas with no deposited material spotted in larges area scans obtained as outcome of a Confocal Raman Imaging analysis on deposition platforms containing IND/HPMCAS-HF and IND/EUDRAGIT EPO ASD films produced by both methods.

In the future, it would be interesting to extend the study to other ASD film preparation methods or automated systems that assure uniformity of deposition and reproducibility while allowing faster production times.

The goal is to implement and validate High-throughput screening programs using this miniaturized screening methodologies for advanced characterization and formulation screening during early product development. Hence, it could be of interest to extend the study to the other real-case-studies so that new distinct results could be generated at the light of this screening methodology and be compared with results deriving from other methodologies in vogue.

It would be of interest to ally this methodology to mathematical in silico models to predict ASD performance and stability and to strengthen the robustness of this newly developed screening methodology. The study could also be extended to ternary ASD prototypes, encompassing different poorly-soluble drugs, polymer types or other formulation excipients, such as surfactants.

The long term vision for this project is the mass implementation of this miniaturized screening methodology in R&D of amorphous solid dispersions to enhance bioavailability of new drug candidates that otherwise would exhibit solubility-limited dissolution or undergo extensive precipitation upon dissolution, and ultimately to contribute to market approval of ASD-based drug products.

References

1. Austin D, Hayford T, Kile J, et al. *Research and Development in the Pharmaceutical Industry - Congressional Budget Office Report*.; 2021. www.cbo.gov/ publication/57025 (accessed in June 2021)

2. Dubin CH. Improving bioavailability & solubility: Each molecule is unique. Drug Development and Delivery. Published 2021. Accessed July 22, 2021. https://drug-dev.com/special-feature-improving-bioavailability-solubility-each-molecule-is-unique/ (accessed in June 2021)

3. Almeida e Sousa L, Reutzel-Edens SM, Stephenson GA, Taylor LS. Assessment of the Amorphous "Solubility" of a Group of Diverse Drugs Using New Experimental and Theoretical Approaches. *Mol Pharm*. 2015;12(2):484-495. doi:10.1021/mp500571m

4. Lu M, Xing H, Jiang J, et al. Liquisolid technique and its applications in pharmaceutics. *Asian J Pharm Sci*. 2017;12(2):115-123. doi:10.1016/j.ajps.2016.09.007

5. Shah N, Sandhu H, Choi DS, Chokshi H, Malick AW, eds. *Amorphous Solid Dispersions: Theory and Practice*. Vol 3. Springer NewYork Heidelberg Dordrecht London; 2014. doi:10.1007/978-1-4939-1598-9

6. Del Rio A. Exploring enantioselective molecular recognition mechanisms with chemoinformatic techniques. *J Sep Sci*. 2009;32(10):1566-1584. doi:10.1002/jssc.200800693

7. Khadka P, Ro J, Kim HH, et al. Pharmaceutical particle technologies: An approach to improve drug solubility, dissolution and bioavailability. *Asian J Pharm Sci*. 2014;9(6):304-316. doi:10.1016/j.ajps.2014.05.005

8. Boyd BJ, Bergström CAS, Vinarov Z, et al. Successful oral delivery of poorly water-soluble drugs both depends on the intraluminal behavior of drugs and of appropriate advanced drug delivery systems. *Eur J Pharm Sci*. 2019;137(May):104967. doi:10.1016/j.ejps.2019.104967

9. Ilevbare G, Marsac P, Mitra A. Performance and Characterization of Amorphous Solid Dispersions: An Overview. In: *Discovering and Developing Molecules with Optimal Drug-Like Properties*. ; 2015:287-343. doi:10.1007/978-1-4939-1399-2_10

10. Fahr A, Liu X. Drug delivery strategies for poorly water-soluble drugs. Douroumis D, Fahr A, eds. *Expert Opin Drug Deliv*. 2007;4(4):403-416. doi:10.1517/17425247.4.4.403

11. Mehtani D, Seth A, Sharma P, et al. Dissolution Profile Consideration in Pharmaceutical Product Development. In: *Dosage Form Design Considerations*. Elsevier; 2018:287-336. doi:10.1016/B978-0-12-814423-7.00009-5

12. Christopher Vimalson D, Parimalakrishnan S, Jeganathan NS, Anbazhagan S. Techniques to enhance solubility of hydrophobic drugs: An overview. *Asian J Pharm*. 2016;10(2):S67-S75.

13. Amidon GL, Lennernäs H, Shah VP, Crison JR. A Theoretical Basis for a Biopharmaceutic Drug Classification: The Correlation of in Vitro Drug Product Dissolution and in Vivo Bioavailability. *Pharm Res An Off J Am Assoc Pharm Sci*. 1995;12(3):413-420. doi:10.1023/a:101621280428

14. Kesharwani A, Kesharwani A, Maqbool A, Pathak S. Solubilization enhancement techniques : An overview. *Pharm Chem J*. 2017;4(6):121-130.

15. Savjani KT, Gajjar AK, Savjani JK. Drug Solubility: Importance and Enhancement Techniques. *ISRN Pharm*. 2012;2012:1-10. doi:10.5402/2012/195727

16. Shahrin N. Solubility and Dissolution of Drug Product: A Review. *Int J Pharm Life Sci*. 2013;2(1):33-41. doi:10.3329/ijpls.v2i1.15133

17. Aulton ME. Dissolution and solubility. In: *Pharmaceutics, The Science of Dosage Form Design*. 2nd edit. ; 2001:15-32. doi:10.1016/b0-08-045044-x/00134-6

18. Shargel L, Yu ABC, eds. *Applied Biopharmaceutics & Pharmacokinetics*. 7th edit. The McGraw-Hill Companies, Inc.; 2016.

19. Vertzoni M, Augustijns P, Grimm M, et al. Impact of regional differences along the gastrointestinal tract of healthy adults on oral drug absorption: An UNGAP review. *Eur J Pharm Sci*. 2019;134(February):153-175. doi:10.1016/j.ejps.2019.04.013

20. Gibaldi M, Boyes RN, Feldman S. Influence of First-Pass Effect on Availability of Drugs on Oral Administration. *J Pharm Sci*. 1971;60(9):1338-1340. doi:10.1002/jps.2600600909

21. Vasconcelos T, Sarmento B, Costa P. Solid dispersions as strategy to improve oral bioavailability of poor water soluble drugs. *Drug Discov Today*. 2007;12(23-24):1068-1075. doi:10.1016/j.drudis.2007.09.005

22. Markl D, Zeitler JA. A Review of Disintegration Mechanisms and Measurement Techniques. *Pharm Res*. 2017;34(5):890-917. doi:10.1007/s11095-017-2129-z

23. Newman A, ed. *Pharmaceutical Amorphous Solid Dispersions*. 1st edit. John Wiley & Sons, Inc.; 2015.

24. Tambosi G, Coelho PF, Luciano S, et al. Challenges to improve the biopharmaceutical properties of poorly water-soluble drugs and the application of the solid dispersion technology. *Rev Matéria (Rio Janeiro)*. 2018;23(4). doi:10.1590/s1517-707620180004.0558

25. Yihong Qiu, Yisheng Chen, Geoff G. Z. Zhang LY and RVM, ed. *Developing Solid Oral Dosage Forms - Pharmaceutical Theory & Practice*. 2nd edit. Elsevier Inc.; 2017.

26. Williams HD, Trevaskis NL, Charman SA, et al. Strategies to Address Low Drug Solubility in Discovery and Development. Christopoulos A, ed. *Pharmacol Rev*. 2013;65(1):315-499. doi:10.1124/pr.112.005660

27. Sahoo CK, Reddy GS, Reddy BV, Vojjala A. BIOAVAILABILITY ENHANCEMENT FOR POORLY SOLUBLE DRUGS: A REVIEW. *Innoriginal Int J Sci*. 2018;5(4):1-6. https://api.semanticscholar.org/CorpusID:98094471

28. Jain S, Patel N, Lin S. Solubility and dissolution enhancement strategies: current understanding and recent trends. *Drug Dev Ind Pharm*. 2015;41(6):875-887. doi:10.3109/03639045.2014.971027

29. Pudipeddi M, Serajuddin ATM. Trends in Solubility of Polymorphs. *J Pharm Sci*. 2005;94(5):929-939. doi:10.1002/jps.20302

30. Nicoud L, Licordari F, Myerson AS. Estimation of the Solubility of Metastable Polymorphs: A Critical Review. *Cryst Growth Des*. 2018;18(11):7228-7237. doi:10.1021/acs.cgd.8b01200

31. Chadha R, Saini A, Arora P, Bhandari S. Pharmaceutical cocrystals: A novel approach for oral bioavailability enhancement of drugs. *Crit Rev Ther Drug Carrier Syst*. 2012;29(3):183-218. doi:10.1615/CritRevTherDrugCarrierSyst.v29.i3.10

32. Miroshnyk I, Mirza S, Sandler N. Pharmaceutical co-crystals–an opportunity for drug product enhancement. *Expert Opin Drug Deliv*. 2009;6(4):333-341. doi:10.1517/17425240902828304

33. Skrdla PJ, Floyd PD, Dell'orco PC. Practical Estimation of Amorphous Solubility Enhancement Using Thermoanalytical Data: Determination of the Amorphous/Crystalline Solubility Ratio for Pure Indomethacin and Felodipine. *J Pharm Sci*. 2016;105(9):2625-2630. doi:10.1016/j.xphs.2016.03.036

34. Hilfiker R, Blatter F, Raumer M von. Relevance of Solid-state Properties for Pharmaceutical Products. In: *Polymorphism: In*

the Pharmaceutical Industry. Wiley-VCH Verlag GmbH & Co. KGaA; 2006:1-19. doi:10.1002/3527607889.ch1

35. Barker JA, Henderson D. What is "liquid"? Understanding the states of matter. *Rev Mod Phys*. 1976;48(4):587-671. https://journals.aps.org/rmp/pdf/10.1103/RevModPhys.48.587

36. Gupta PK. Non-crystalline solids: glasses and amorphous solids. *J Non Cryst Solids*. 1996;195(1-2):158-164. doi:10.1016/0022-3093(95)00502-1

37. Málek, Svoboda. Kinetic Processes in Amorphous Materials Revealed by Thermal Analysis: Application to Glassy Selenium. *Molecules*. 2019;24(15):2725. doi:10.3390/molecules24152725

38. Yoshioka S, Aso Y. Correlations between Molecular Mobility and Chemical Stability During Storage of Amorphous Pharmaceuticals. *J Pharm Sci*. 2007;96(5):960-981. doi:10.1002/jps.20926

39. Xavier F. Structure-Solubility-Stability Relationships : Solid State Forms of Active Ingredients. *Res Rev*. 2015;(July):1-32. doi:10.13140/RG.2.1.3839.2165

40. Pandian R, Kooi BJ, De Hosson JTM, Pauza A. Influence of electron beam exposure on crystallization of phase-change materials. *J Appl Phys*. 2007;101(5):053529. doi:10.1063/1.2710294

41. Teja SB, Patil SP, Shete G, Patel S, Bansal AK. Drug-excipient behavior in polymeric amorphous solid dispersions. *J Excipients Food Chem*. 2014;4(3):70-94.

42. Taylor LS, Zhang GGZ. Physical chemistry of supersaturated solutions and implications for oral absorption. *Adv Drug Deliv Rev*. 2016;101:122-142. doi:10.1016/j.addr.2016.03.006

43. Abiad MG, Carvajal MT, Campanella OH. A Review on Methods and Theories to Describe the Glass Transition Phenomenon: Applications in Food and Pharmaceutical Products. *Food Eng Rev*. 2009;1(2):105-132. doi:10.1007/s12393-009-9009-1

44. Zografi G, Newman A. Interrelationships Between Structure and the Properties of Amorphous Solids of Pharmaceutical Interest. *J Pharm Sci*. 2017;106(1):5-27. doi:10.1016/j.xphs.2016.05.001

45. Graeser KA, Patterson JE, Zeitler JA, Rades T. The Role of Configurational Entropy in Amorphous Systems. *Pharmaceutics*. 2010;2(2):224-244. doi:10.3390/pharmaceutics2020224

46. Baghel S, Cathcart H, O'Reilly NJ. Polymeric Amorphous Solid Dispersions: A Review of Amorphization, Crystallization, Stabilization, Solid-State Characterization, and Aqueous Solubilization of Biopharmaceutical Classification System Class II Drugs. *J Pharm Sci*. 2016;105(9):2527-2544. doi:10.1016/j.xphs.2015.10.008

47. Newman A, Hastedt JE, Yazdanian M. New directions in pharmaceutical amorphous materials and amorphous solid dispersions, a tribute to Professor George Zografi – Proceedings of the June 2016 Land O'Lakes Conference. *AAPS Open*. 2017;3(1):7. doi:10.1186/s41120-017-0017-6

48. Newman A. Rational Design for Amorphous Solid Dispersions. In: *Developing Solid Oral Dosage Forms*. Elsevier; 2017:497-518. doi:10.1016/B978-0-12-802447-8.00018-2

49. Vasconcelos T, Marques S, das Neves J, Sarmento B. Amorphous solid dispersions: Rational selection of a manufacturing process. *Adv Drug Deliv Rev*. 2016;100:85-101. doi:10.1016/j.addr.2016.01.012

50. Tran P, Pyo Y-C, Kim D-H, Lee S-E, Kim J-K, Park J-S. Overview of the Manufacturing Methods of Solid Dispersion Technology for Improving the Solubility of Poorly Water-Soluble Drugs and Application to Anticancer Drugs. *Pharmaceutics*. 2019;11(3):132. doi:10.3390/pharmaceutics11030132

51. Karimi-Jafari M, Padrela L, Walker GM, Croker DM. Creating Cocrystals: A Review of Pharmaceutical Cocrystal Preparation

Routes and Applications. *Cryst Growth Des*. 2018;18(10):6370-6387. doi:10.1021/acs.cgd.8b00933

52. Bavishi DD, Borkhataria CH. Spring and parachute: How cocrystals enhance solubility. *Prog Cryst Growth Charact Mater*. 2016;62(3):1-8. doi:10.1016/j.pcrysgrow.2016.07.001

53. Knapik-Kowalczuk J, Chmiel K, Pacułt J, Bialek K, Tajber L, Paluch M. Enhancement of the Physical Stability of Amorphous Sildenafil in a Binary Mixture, with either a Plasticizing or Antiplasticizing Compound. *Pharmaceutics*. 2020;12(5):460. doi:10.3390/pharmaceutics12050460

54. Mendonsa N, Almutairy B, Kallakunta VR, et al. Manufacturing strategies to develop amorphous solid dispersions: An overview. *J Drug Deliv Sci Technol*. 2020;55:101459. doi:10.1016/j.jddst.2019.101459

55. Sandhu H, Shah N, Chokshi H, Malick AW. Overview of Amorphous Solid Dispersion Technologies. In: N. Shah et al., ed. *Amorphous Solid Dispersions, Advances in Delivery Science and Technology*. Controlled Release Society; 2014:91-122. doi:10.1007/978-1-4939-1598-9_3

56. Guterres SS, Beck RCR, Pohlmann AR. Spray-drying technique to prepare innovative nanoparticulated formulations for drug administration: a brief overview. *Brazilian J Phys*. 2009;39(1a):205-209. doi:10.1590/S0103-97332009000200013

57. Santos D, Maurício AC, Sencadas V, Santos JD, Fernandes MH, Gomes PS. Spray Drying: An Overview. In: *Biomaterials - Physics and Chemistry - New Edition*. InTech; 2018:9-36. doi:10.5772/intechopen.72247

58. Chow AHL, Tong HHY, Chattopadhyay P, Shekunov BY. Particle Engineering for Pulmonary Drug Delivery. *Pharm Res*. 2007;24(3):411-437. doi:10.1007/s11095-006-9174-3

59. Anandharamakrishnan C, Ishwarya SP. Introduction to Spray drying. In: *Spray Drying Techniques for Food Ingredient Encapsulation*. 1st edit. John Wiley & Sons, Ltd.; 2015:1-36.

60. Ziaee A, Albadarin AB, Padrela L, Femmer T, O'Reilly E, Walker G. Spray drying of pharmaceuticals and biopharmaceuticals: Critical parameters and experimental process optimization approaches. *Eur J Pharm Sci*. 2019;127:300-318. doi:10.1016/j.ejps.2018.10.026

61. Barbosa G V, Science S, Dordrecht BM. Spray drying. In: *Dehydration of Foods*. Vol 1. Springer Science+Business Media Dordrecht; 1996:185-227.

62. Butreddy A, Bandari S, Repka MA. Quality-by-design in hot melt extrusion based amorphous solid dispersions: An industrial perspective on product development. *Eur J Pharm Sci*. 2021;158:105655. doi:10.1016/j.ejps.2020.105655

63. Kallakunta VR, Sarabu S, Bandari S, Tiwari R, Patil H, Repka MA. An update on the contribution of hot-melt extrusion technology to novel drug delivery in the twenty-first century: part I. *Expert Opin Drug Deliv*. 2019;16(5):539-550. doi:10.1080/17425247.2019.1609448

64. Moseson DE, Taylor LS. The application of temperature-composition phase diagrams for hot melt extrusion processing of amorphous solid dispersions to prevent residual crystallinity. *Int J Pharm*. 2018;553(1-2):454-466. doi:10.1016/j.ijpharm.2018.10.055

65. Agrawal AM, Dudhedia MS, Zimny E. Hot Melt Extrusion: Development of an Amorphous Solid Dispersion for an Insoluble Drug from Mini-scale to Clinical Scale. *AAPS PharmSciTech*. 2016;17(1):133-147. doi:10.1208/s12249-015-0425-7

66. Li Y, Pang H, Guo Z, et al. Interactions between drugs and polymers influencing hot melt extrusion. *J Pharm Pharmacol*. 2014;66(2):148-166. doi:10.1111/jphp.12183

67. Tan DK, Davis DA, Miller DA, Williams RO, Nokhodchi A. Innovations in Thermal Processing: Hot-Melt Extrusion and KinetiSol® Dispersing. *AAPS PharmSciTech*. 2020;21(8):312. doi:10.1208/s12249-020-01854-2

68. Vicente J, Pinto J, Menezes J, Gaspar F. Fundamental analysis of particle formation in spray drying. *Powder Technol*. 2013;247:1-7. doi:10.1016/j.powtec.2013.06.038

69. Hu Q, Wyttenbach N, Shiraki K, Choi DS. Miniaturized Screening Tools for Polymer and Process Evaluation. In: *Amorphous Solid Dispersions, Advances in Delivery Science and Technology*. Controlled Release Society; 2014:165-195. doi:10.1007/978-1-4939-1598-9_5

70. He Y, Ho C. Amorphous Solid Dispersions: Utilization and Challenges in Drug Discovery and Development. *J Pharm Sci*. 2015;104(10):3237-3258. doi:10.1002/jps.24541

71. Dai W-G, Pollock-Dove C, Dong LC, Li S. Advanced screening assays to rapidly identify solubility-enhancing formulations: High-throughput, miniaturization and automation. *Adv Drug Deliv Rev*. 2008;60(6):657-672. doi:10.1016/j.addr.2007.10.017

72. Dai WG, Dong LC, Li S, et al. Parallel screening approach to identify solubility-enhancing formulations for improved bioavailability of a poorly water-soluble compound using milligram quantities of material. *Int J Pharm*. 2007;336(1):1-11. doi:10.1016/j.ijpharm.2006.11.034

73. Lauer ME, Grassmann O, Siam M, et al. Atomic force microscopy-based screening of drug-excipient miscibility and stability of solid dispersions. *Pharm Res*. 2011;28(3):572-584. doi:10.1007/s11095-010-0306-4

74. Trasi NS, Bhujbal S V, Zemlyanov DY, Zhou Q (Tony), Taylor LS. Physical stability and release properties of lumefantrine amorphous solid dispersion granules prepared by a simple solvent evaporation approach. *Int J Pharm X*. 2020;2(July):100052. doi:10.1016/j.ijpx.2020.100052

75. Zhou L, Yang L, Tilton S, Wang J. Development of a high throughput equilibrium solubility assay using miniaturized shake-flask method in early drug discovery. *J Pharm Sci*. 2007;96(11):3052-3071. doi:10.1002/jps.20913

76. Simões MF, Pereira A, Cardoso S, et al. Five-Stage Approach for a Systematic Screening and Development of Etravirine Amorphous Solid Dispersions by Hot-Melt Extrusion. *Mol Pharm*. 2020;17(2):554-568. doi:10.1021/acs.molpharmaceut.9b00996

77. Mansky P, Dai W, Li S, et al. Screening Method to Identify Preclinical Liquid and Semi-Solid Formulations for low Solubility Compounds: Miniaturization and Automation of Solvent Casting and Dissolution Testing. *J Pharm Sci*. 2007;96(6):1548-1563. doi:10.1002/jps.20799

78. Shanbhag A, Rabel S, Nauka E, et al. Method for screening of solid dispersion formulations of low-solubility compounds-Miniaturization and automation of solvent casting and dissolution testing. *Int J Pharm*. 2008;351(1-2):209-218. doi:10.1016/j.ijpharm.2007.09.042

79. Weuts I, Van Dycke F, Voorspoels J, et al. Physicochemical properties of the amorphous drug, cast films, and spray dried powders to predict formulation probability of success for solid dispersions: Etravirine. *J Pharm Sci*. 2011;100(1):260-274. doi:10.1002/jps.22242

80. Wyttenbach N, Janas C, Siam M, et al. Miniaturized screening of polymers for amorphous drug stabilization (SPADS): Rapid assessment of solid dispersion systems. *Eur J Pharm Biopharm*. 2013;84(3):583-598. doi:10.1016/j.ejpb.2013.01.009

81. Barillaro V, Pescarmona PP, Van Speybroeck M, et al. High-Throughput Study of Phenytoin Solid Dispersions: Formulation Using an Automated Solvent Casting Method, Dissolution Testing, and Scaling-Up. *J Comb Chem*. 2008;10(5):637-643. doi:10.1021/cc8000585

82. Chiang PC, Ran Y, Chou KJ, et al. Evaluation of drug load and polymer by using a 96-well plate vacuum dry system for amorphous solid dispersion drug delivery. *AAPS PharmSciTech*. 2012;13(2):713-722. doi:10.1208/s12249-012-9795-2

83. Auch C, Harms M, Mäder K. Melt-based screening method with improved predictability regarding polymer selection for amorphous solid dispersions. *Eur J Pharm Sci*. 2018;124:339-348. doi:10.1016/j.ejps.2018.08.035

84. Davis MT, Egan DP, Kuhs M, et al. Amorphous solid dispersions of BCS class II drugs: A rational approach to solvent and polymer selection. *Chem Eng Res Des*. 2016;110:192-199. doi:10.1016/j.cherd.2016.04.008

85. Moore MD, Wildfong PLD. Informatics calibration of a molecular descriptors database to predict solid dispersion potential of small molecule organic solids. *Int J Pharm*. 2011;418(2):217-226. doi:10.1016/j.ijpharm.2011.06.003

86. Nepal PR, Han HK, Choi HK. Enhancement of solubility and dissolution of Coenzyme Q10 using solid dispersion formulation. *Int J Pharm*. 2010;383(1-2):147-153. doi:10.1016/j.ijpharm.2009.09.031

87. Betageri G V., Makarla KR. Enhancement of dissolution of glyburide by solid dispersion and lyophilization techniques. *Int J Pharm*. 1995;126(1-2):155-160. doi:10.1016/0378-5173(95)04114-1

88. Forster A, Hempenstall J, Tucker I, Rades T. The potential of small-scale fusion experiments and the Gordon-Taylor equation to predict the suitability of drug/polymer blends for melt extrusion. *Drug Dev Ind Pharm*. 2001;27(6):549-560. doi:10.1081/DDC-100105180

89. Guo Z, Boyce C, Rhodes T, et al. A novel method for preparing stabilized amorphous solid dispersion drug formulations using acoustic fusion. *Int J Pharm*. 2021;592:120026. doi:10.1016/j.ijpharm.2020.120026

90. Overhoff KA, Engstrom JD, Chen B, et al. Novel ultra-rapid freezing particle engineering process for enhancement of dissolution rates of poorly water-soluble drugs. *Eur J Pharm Biopharm*. 2007;65(1):57-67. doi:10.1016/j.ejpb.2006.07.012

91. Zhang M, Li H, Lang B, et al. Formulation and delivery of improved amorphous fenofibrate solid dispersions prepared by thin film freezing. *Eur J Pharm Biopharm*. 2012;82(3):534-544. doi:10.1016/j.ejpb.2012.06.016

92. Engers D, Teng J, Jimenez-Novoa J, et al. A solid-state approach to enable early development compounds: Selection and animal bioavailability studies of an itraconazole amorphous solid dispersion. *J Pharm Sci*. 2010;99(9):3901-3922. doi:10.1002/jps.22233

93. Jacobsen AC, Krupa A, Brandl M, Bauer-Brandl A. High-throughput dissolution/permeation screening —A 96-well two-compartment microplate approach. *Pharmaceutics*. 2019;11(5):227. doi:10.3390/pharmaceutics11050227

94. Moes JJ, Koolen SLW, Huitema ADR, Schellens JHM, Beijnen JH, Nuijen B. Pharmaceutical development and preliminary clinical testing of an oral solid dispersion formulation of docetaxel (ModraDoc001). *Int J Pharm*. 2011;420(2):244-250. doi:10.1016/j.ijpharm.2011.08.041

95. Guzmán HR, Tawa M, Zhang Z, et al. Combined use of crystalline salt forms and precipitation inhibitors to improve oral absorption of celecoxib from solid oral formulations. *J Pharm Sci*. 2007;96(10):2686-2702. doi:10.1002/jps.20906

96. Petruševska M, Urleb U, Peternel L. Evaluation of a high-throughput screening method for the detection of the excipient-mediated precipitation inhibition of poorly soluble drugs. *Assay Drug Dev Technol*. 2013;11(2):117-129. doi:10.1089/adt.2012.466

97. Bevernage J, Brouwers J, Clarysse S, et al. Drug Supersaturation in Simulated Human Intestinal Fluids Representing Different Nutritional States. *J Pharm Sci*. 2010;99(11):4525-4534. doi:10.1002/jps.22154

98. Brewster ME, Vandecruys R, Peeters J, Neeskens P, Verreck G, Loftsson T. Comparative interaction of 2-hydroxypropyl-β-cyclodextrin and sulfobutylether-β-cyclodextrin with itraconazole: Phase-solubility behavior and stabilization of supersaturated drug solutions. *Eur J Pharm Sci*. 2008;34(2-3):94-103. doi:10.1016/j.ejps.2008.02.007

99. Yeap YY, Lock J, Lerkvikarn S, Semin T, Nguyen N, Carrier RL. Intestinal mucus is capable of stabilizing supersaturation of

poorly water-soluble drugs. *J Control Release*. 2019;296:107-113. doi:10.1016/j.jconrel.2018.11.023

100. Janssens S, Nagels S, Armas HN de, D'Autry W, Van Schepdael A, Van den Mooter G. Formulation and characterization of ternary solid dispersions made up of Itraconazole and two excipients, TPGS 1000 and PVPVA 64, that were selected based on a supersaturation screening study. *Eur J Pharm Biopharm*. 2008;69(1):158-166. doi:10.1016/j.ejpb.2007.11.004

101. Vandecruys R, Peeters J, Verreck G, Brewster ME. Use of a screening method to determine excipients which optimize the extent and stability of supersaturated drug solutions and application of this system to solid formulation design. *Int J Pharm*. 2007;342(1-2):168-175. doi:10.1016/j.ijpharm.2007.05.006

102. Warren DB, Benameur H, Porter CJH, Pouton CW. Using polymeric precipitation inhibitors to improve the absorption of poorly water-soluble drugs: A mechanistic basis for utility. *J Drug Target*. 2010;18(10):704-731. doi:10.3109/1061186X.2010.525652

103. Yamashita T, Ozaki S, Kushida I. Solvent shift method for anti-precipitant screening of poorly soluble drugs using biorelevant medium and dimethyl sulfoxide. *Int J Pharm*. 2011;419(1-2):170-174. doi:10.1016/j.ijpharm.2011.07.045

104. Hu Q, Choi DS, Chokshi H, Shah N, Sandhu H. Highly efficient miniaturized coprecipitation screening (MiCoS) for amorphous solid dispersion formulation development. *Int J Pharm*. 2013;450(1-2):53-62. doi:10.1016/j.ijpharm.2013.04.040

105. Lee T, Lee J. Drug-carrier screening on a chip. *Pharm Technol North Am*. 2003;27(1):40-48.

106. Konno H, Taylor LS. Influence of Different Polymers on the Crystallization Tendency of Molecularly Dispersed Amorphous Felodipine. *J Pharm Sci*. 2006;95(12):2692-2705. doi:10.1002/jps.20697

107. Marsac PJ, Konno H, Taylor LS. A comparison of the physical stability of amorphous felodipine and nifedipine systems. *Pharm Res*. 2006;23(10):2306-2316. doi:10.1007/s11095-006-9047-9

108. Van Eerdenbrugh B, Taylor LS. Small scale screening to determine the ability of different polymers to inhibit drug crystallization upon rapid solvent evaporation. *Mol Pharm*. 2010;7(4):1328-1337. doi:10.1021/mp1001153

109. Poozesh S, Mahdi Jafari S. Are traditional small-scale screening methods reliable to predict pharmaceutical spray drying? *Pharm Dev Technol*. 2019;24(7):915-925. doi:10.1080/10837450.2019.1616208

110. Taresco V, Louzao I, Scurr D, et al. Rapid Nanogram Scale Screening Method of Microarrays to Evaluate Drug–Polymer Blends Using High-Throughput Printing Technology. *Mol Pharm*. 2017;14(6):2079-2087. doi:10.1021/acs.molpharmaceut.7b00182

111. Styliari ID, Conte C, Pearce AK, et al. High-Throughput Miniaturized Screening of Nanoparticle Formation via Inkjet Printing. *Macromol Mater Eng*. 2018;303(8):1800146. doi:10.1002/mame.201800146

112. Sanna M, Sicilia G, Alazzo A, et al. Water Solubility Enhancement of Pyrazolo[3,4- d]pyrimidine Derivatives via Miniaturized Polymer–Drug Microarrays. *ACS Med Chem Lett*. 2018;9(3):193-197. doi:10.1021/acsmedchemlett.7b00456

113. Lucas S. The Pharmacology of Indomethacin. *Headache J Head Face Pain*. 2016;56(2):436-446. doi:10.1111/head.12769

114. Desantis J, Mercorelli B, Celegato M, et al. Indomethacin-based PROTACs as pan-coronavirus antiviral agents. *Eur J Med Chem*. 2021;226(May 2020):113814. doi:10.1016/j.ejmech.2021.113814

115. Kiani P, Scholey A, Dahl TA, McMann L, Iversen JM, Verster JC. In vitro assessment of the antiviral activity of ketotifen, indomethacin and naproxen, alone and in combination, against SARS-CoV-2. *Viruses*. 2021;13(4):558. doi:10.3390/v13040558

116. N. C. Obitte. Some in vitro and pharmacodynamic evaluation of indomethacin solid lipid microparticles. *African J Pharm Pharmacol*. 2012;6(30):2309-2317. doi:10.5897/AJPP12.524

117. Murdande SB, Pikal MJ, Shanker RM, Bogner RH. Solubility advantage of amorphous pharmaceuticals: I. A thermodynamic analysis. *J Pharm Sci*. 2010;99(3):1254-1264. doi:10.1002/jps.21903

118. Taylor LS, Zografi G. Spectroscopic characterization of interactions between PVP and indomethacin in amorphous molecular dispersions. *Pharm Res*. 1997;14(12):1691-1698. doi:10.1023/A:1012167410376

119. Teleki A, Nylander O, Bergström CAS. Intrinsic Dissolution Rate Profiling of Poorly Water-Soluble Compounds in Biorelevant Dissolution Media. *Pharmaceutics*. 2020;12(6):493. doi:10.3390/pharmaceutics12060493

120. Neuhoff S, Ungell A-L, Zamora I, Artursson P. pH-Dependent passive and active transport of acidic drugs across Caco-2 cell monolayers. *Eur J Pharm Sci*. 2005;25(2-3):211-220. doi:10.1016/j.ejps.2005.02.009

121. Adegoke OA, Idowu OS, Olaniyi AA. Novel colorimetric assay of indomethacin using 4-carboxyl-2,6- dinitrobenzene diazonium ion. *Acta Pharm*. 2006;56(2):189-202.

122. Yoshioka M, Hancock BC, Zografi G. Crystallization of Indomethacin from the Amorphous State below and above Its Glass Transition Temperature. *J Pharm Sci*. 1994;83(12):1700-1705. doi:10.1002/jps.2600831211

123. Dupeyrón D, Kawakami, Ferreira, et al. Design of indomethacin-loaded nanoparticles: effect of polymer matrix and surfactant. *Int J Nanomedicine*. 2013;8(December):3467. doi:10.2147/IJN.S47621

124. Hellstén S, Qu H, Louhi-Kultanen M. Screening of Binary Solvent Mixtures and Solvate Formation of Indomethacin. *Chem Eng Technol*. 2011;34(10):1667-1674. doi:10.1002/ceat.201100072

125. Comer J, Judge S, Matthews D, et al. The intrinsic aqueous solubility of indomethacin. *ADMET DMPK*. 2014;2(1):18-32. doi:10.5599/admet.2.1.33

126. D.F. Swinehart. The Beer-Lambert Law. *J Appl Phys*. 1962;39(7):333-335. doi:10.1021/ed039p333

127. Mäntele W, Deniz E. UV–VIS absorption spectroscopy: Lambert-Beer reloaded. *Spectrochim Acta Part A Mol Biomol Spectrosc*. 2017;173:965-968. doi:10.1016/j.saa.2016.09.037

128. Almeida e Sousa L, Reutzel-Edens SM, Stephenson GA, Taylor LS. Supersaturation Potential of Salt, Co-Crystal, and Amorphous Forms of a Model Weak Base. *Cryst Growth Des*. 2016;16(2):737-748. doi:10.1021/acs.cgd.5b01341

129. Ilevbare GA, Taylor LS. Liquid–Liquid Phase Separation in Highly Supersaturated Aqueous Solutions of Poorly Water-Soluble Drugs: Implications for Solubility Enhancing Formulations. *Cryst Growth Des*. 2013;13(4):1497-1509. doi:10.1021/cg301679h

130. Po HN, Senozan NM. The Henderson-Hasselbalch Equation: Its History and Limitations. *J Chem Educ*. 2001;78(11):1499. doi:10.1021/ed078p1499

131. De Filippis P, Boscolo M, Gibellini M, Rupena P, Rubessa F. The Release Rate of Indomethacin from Solid Dispersions with Eudragite. *Drug Dev Ind Pharm*. 1991;17(14):2017-2028. doi:10.3109/03639049109048065

132. Ghatak A, Mandal PC, Sarkar M. Indomethacin: A NSAID sensitive to micro heterogeneity in alcohol–water mixtures. *Chem Phys Lett*. 2008;460(4-6):521-524. doi:10.1016/j.cplett.2008.06.056

133. Bogner RH, Murdande SB, Pikal MJ, Shanker RM. Solubility advantage of amorphous pharmaceuticals: II. application of quantitative thermodynamic relationships for prediction of solubility enhancement in structurally diverse insoluble pharmaceuticals. *Pharm Res*. 2010;27(12):2704-2714. doi:10.1007/s11095-010-0269-5

134. Liu H, Zhang X, Suwardie H, Wang P, Gogos CG. Miscibility Studies of Indomethacin and Eudragit® E PO by Thermal, Rheological, and Spectroscopic Analysis. *J Pharm Sci*. 2012;101(6):2204-2212. doi:10.1002/jps.23075

135. Higashi K, Seo A, Egami K, et al. Mechanistic insight into the dramatic improvement of probucol dissolution in neutral solutions by solid dispersion in Eudragit E PO with saccharin. *J Pharm Pharmacol*. 2016;68(5):655-664. doi:10.1111/jphp.12469

136. Chokshi RJ, Sandhu HK, Iyer RM, Shah NH, Malick AW, Zia H. Characterization of Physico-Mechanical Properties of Indomethacin and Polymers to Assess their Suitability for Hot-Melt Extrusion Processs as a Means to Manufacture Solid Dispersion/Solution**Mailing address of the place where the work was carried out, Ho. *J Pharm Sci*. 2005;94(11):2463-2474. doi:10.1002/jps.20385

137. Xie T, Gao W, Taylor LS. Impact of Eudragit EPO and hydroxypropyl methylcellulose on drug release rate, supersaturation, precipitation outcome and redissolution rate of indomethacin amorphous solid dispersions. *Int J Pharm*. 2017;531(1):313-323. doi:10.1016/j.ijpharm.2017.08.099

138. Moustafine RI, Zaharov IM, Kemenova VA. Physicochemical characterization and drug release properties of Eudragit® E PO/Eudragit® L 100-55 interpolyelectrolyte complexes. *Eur J Pharm Biopharm*. 2006;63(1):26-36. doi:10.1016/j.ejpb.2005.10.005

139. MENJOGE A, KULKARNI M. Mechanistic investigations of phase behavior in Eudragit®E blends. *Int J Pharm*. 2007;343(1-2):106-121. doi:10.1016/j.ijpharm.2007.05.033

140. Liu H, Wang P, Zhang X, Shen F, Gogos CG. Effects of extrusion process parameters on the dissolution behavior of indomethacin in Eudragit® E PO solid dispersions. *Int J Pharm*. 2010;383(1-2):161-169. doi:10.1016/j.ijpharm.2009.09.003

141. Huang J, Wigent RJ, Schwartz JB. Drug–polymer interaction and its significance on the physical stability of nifedipine amorphous dispersion in microparticles of an ammonio methacrylate copolymer and ethylcellulose binary blend. *J Pharm Sci*. 2008;97(1):251-262. doi:10.1002/jps.21072

142. Nair AR, Lakshman YD, Anand VSK, Sree KSN, Bhat K, Dengale SJ. Overview of Extensively Employed Polymeric Carriers in Solid Dispersion Technology. *AAPS PharmSciTech*. 2020;21(8):309. doi:10.1208/s12249-020-01849-z

143. Harika K, Sunitha K, Kumar PP, Maheshwar K, Rao MY. Basic Concepts Of Cellulose Polymers- A Comprehensive Review. *Arch Pharm Pract*. 2012;3(3):202-216. http://ezproxy.library.usyd.edu.au/login?url=http://search.proquest.com/docview/1289021500?accountid=14757%5Cnhttp://dd8gh5yx7k.search.serialssolutions.com/?ctx_ver=Z39.88-2004&ctx_enc=info:ofi/enc:UTF-8&rfr_id=info:sid/ProQ:healthcompleteshell&rft_val_fm

144. Long CM, Tang K, Chokshi H, Fotaki N. Surface Dissolution UV Imaging for Investigation of Dissolution of Poorly Soluble Drugs and Their Amorphous Formulation. *AAPS PharmSciTech*. 2019;20(3):113. doi:10.1208/s12249-019-1317-z

145. Konno H, Handa T, Alonzo DE, Taylor LS. Effect of polymer type on the dissolution profile of amorphous solid dispersions containing felodipine. *Eur J Pharm Biopharm*. 2008;70(2):493-499. doi:10.1016/j.ejpb.2008.05.023

146. Browne E, Worku ZA, Healy AM. Physicochemical Properties of Poly-vinyl Polymers and Their Influence on Ketoprofen Amorphous Solid Dispersion Performance: A Polymer Selection Case Study. *Pharmaceutics*. 2020;12(5):433. doi:10.3390/pharmaceutics12050433

147. Lim J, Yeap SP, Che HX, Low SC. Characterization of magnetic nanoparticle by dynamic light scattering. *Nanoscale Res Lett*. 2013;8(1):381. doi:10.1186/1556-276X-8-381

148. Tres F, Hall SD, Mohutsky MA, Taylor LS. Monitoring the Phase Behavior of Supersaturated Solutions of Poorly Water-Soluble Drugs Using Fluorescence Techniques. *J Pharm Sci*. 2018;107(1):94-102. doi:10.1016/j.xphs.2017.10.002

149. Purohit HS, Taylor LS. Phase Behavior of Ritonavir Amorphous Solid Dispersions during Hydration and Dissolution. *Pharm Res*. 2017;34(12):2842-2861. doi:10.1007/s11095-017-2265-5

150. Raina SA, Alonzo DE, Zhang GGZ, Gao Y, Taylor LS. Using Environment-Sensitive Fluorescent Probes to Characterize Liquid-Liquid Phase Separation in Supersaturated Solutions of Poorly Water Soluble Compounds. *Pharm Res*. 2015;32(11):3660-3673. doi:10.1007/s11095-015-1725-z

151. Stetefeld J, McKenna SA, Patel TR. Dynamic light scattering: a practical guide and applications in biomedical sciences. *Biophys Rev*. 2016;8(4):409-427. doi:10.1007/s12551-016-0218-6

152. Stewart AM, Grass ME, Brodeur TJ, et al. Impact of Drug-Rich Colloids of Itraconazole and HPMCAS on Membrane Flux in Vitro and Oral Bioavailability in Rats. *Mol Pharm*. 2017;14(7):2437-2449. doi:10.1021/acs.molpharmaceut.7b00338

153. Falke S, Brognaro H, Martirosyan A, Dierks K, Betzel C. A multi-channel in situ light scattering instrument utilized for monitoring protein aggregation and liquid dense cluster formation. *Heliyon*. 2019;5(12):e03016. doi:10.1016/j.heliyon.2019.e03016

154. Bonnett PE, Carpenter KJ, Dawson S, Davey RJ. Solution crystallisation via a submerged liquid–liquid phase boundary: oiling out. *Chem Commun*. 2003;3(6):698-699. doi:10.1039/b212062c

155. Thorson MR, Goyal S, Gong Y, Zhang GGZ, Kenis PJA. Microfluidic approach to polymorph screening through antisolvent crystallization. *CrystEngComm*. 2012;14(7):2404. doi:10.1039/c2ce06167h

156. Rossi B, Verrocchio P, Viliani G, Scarduelli G, Guella G, Mancini I. Vibrational properties of inclusion complexes: The case of indomethacin-cyclodextrin. *J Chem Phys*. 2006;125(4):044511. doi:10.1063/1.2217952

157. Banerjee M, Brettmann B. Stabilization of Metastable Indomethacin α in Cellulose Nanocrystal Aerogel Scaffolds. *Pharmaceutics*. 2021;13(4):441. doi:10.3390/pharmaceutics13040441

158. Müller M, Platten F, Dulle M, et al. Precipitation from amorphous solid dispersions in biorelevant dissolution testing: The polymorphism of regorafenib. *Int J Pharm*. 2021;603(May):120716. doi:10.1016/j.ijpharm.2021.120716

159. Chauhan H, Hui-Gu C, Atef E. Correlating the Behavior of Polymers in Solution as Precipitation Inhibitor to its Amorphous Stabilization Ability in Solid Dispersions. *J Pharm Sci*. 2013;102(6):1924-1935. doi:10.1002/jps.23539

160. Paisana MC, Lino PR, Nunes PD, Pinto JF, Henriques J, Paiva AM. Laser diffraction as a powerful tool for amorphous solid dispersion screening and dissolution understanding. *Eur J Pharm Sci*. 2021;163(January):105853. doi:10.1016/j.ejps.2021.105853

161. García MC, Martinelli M, Ponce NE, et al. *Multi-Kinetic Release of Benznidazole-Loaded Multiparticulate Drug Delivery Systems Based on Polymethacrylate Interpolyelectrolyte Complexes*. Vol 120. Elsevier B.V; 2018. doi:10.1016/j.ejps.2018.04.034

162. Dürrigl M, Kwokal A, Hafner A, et al. Spray dried microparticles for controlled delivery of mupirocin calcium: Process–tailored modulation of drug release. *J Microencapsul*. 2011;28(2):108-121. doi:10.3109/02652048.2010.535620

163. Štukelj J, Svanbäck S, Kristl J, Strachan CJ, Yliruusi J. Image-Based Investigation: Biorelevant Solubility of α and γ Indomethacin. *Anal Chem*. 2019;91(6):3997-4003. doi:10.1021/acs.analchem.8b05290

164. Fanous M, Bitar M, Gold S, et al. Development of immediate release 3D-printed dosage forms for a poorly water-soluble drug by fused deposition modeling: Study of morphology, solid state and dissolution. *Int J Pharm*. 2021;599:120417. doi:10.1016/j.ijpharm.2021.120417

165. Kindermann C, Matthée K, Strohmeyer J, Sievert F, Breitkreutz J. Tailor-made release triggering from hot-melt extruded complexes of basic polyelectrolyte and poorly water-soluble drugs. *Eur J Pharm Biopharm*. 2011;79(2):372-381. doi:10.1016/j.ejpb.2011.05.001

166. Moustafine RI, Sitenkov AY, Bukhovets A V., et al. Indomethacin-containing interpolyelectrolyte complexes based on Eudragit ® E PO/S 100 copolymers as a novel drug delivery system. *Int J Pharm*. 2017;524(1-2):121-133. doi:10.1016/j.ijpharm.2017.03.053

167. Matsumoto T, Zografi G. Physical properties of solid molecular dispersions of Indomethacin with Poly(vinylpyrrolidone) and Poly(vinylpyrrolidone-co-vinyl-acetate) in relation to Indomethacin Crystallization. *Pharm Res*. 1999;16(11):1722-1728.

168. Engers D, Teng J, Jimenez-Novoa J, et al. A Solid-State Approach to Enable Early Development Compounds: Selection and Animsal Bioavailability Studies of an Itraconazole Amorphous Solid Dispersion. *J Pharm Sci*. 2010;99(9):3901-3922. doi:10.1002/jps.22233

169. Gupta SS, Meena A, Parikh T, Serajuddin ATM. Investigation of Thermal and Viscoelastic Properties of Polymers Relevant to Hot Melt Extrusion, I: Polyvinylpyrrolidone and related polymers. *J Drug Target*. 2014;5(1):32-45. http://link.springer.com/10.1208/s12249-015-0426-6

170. Gupta SS, Meena A, Serajuddin ATM. Investigation of thermal and viscoelastic properties of polymers relevant to hot melt extrusion - III: Polymethacrylates and polymethacrylic acid based polymers. *J Excipients Food Chem*. 2014;5(1):32-45.

171. Vaka SRK, Bommana MM, Desai D, Djordjevic J, Phuapradit W, Shah N. Excipients for Amorphous Solid Dispersions. In: *Amorphous Solid Dispersions, Advances in Delivery Science and Technology*. ; 2014:123-161. doi:10.1007/978-1-4939-1598-9_4

172. Theil F, Milsmann J, Anantharaman S, van Lishaut H. Manufacturing Amorphous Solid Dispersions with a Tailored Amount of Crystallized API for Biopharmaceutical Testing. *Mol Pharm*. 2018;15(5):1870-1877. doi:10.1021/acs.molpharmaceut.8b00043

173. Mudie DM, Buchanan S, Stewart AM, et al. A novel architecture for achieving high drug loading in amorphous spray dried dispersion tablets. *Int J Pharm X*. 2020;2(December 2019):100042. doi:10.1016/j.ijpx.2020.100042

174. Rahman M, Ozkan S, Lester J, Farzana I, Bi V, Durig T. *Plasticizer Compatibility and Thermal and Rheological Properties of Plasdone Povidone And Copovidone Polymers for Hot-Melt Extrusion Applications (PTR-092)*.; 2012.

175. Alshahrani SM, Lu W, Park J-B, et al. Stability-enhanced Hot-melt Extruded Amorphous Solid Dispersions via Combinations of Soluplus® and HPMCAS-HF. *AAPS PharmSciTech*. 2015;16(4):824-834. doi:10.1208/s12249-014-0269-6

176. Chavan RB, Thipparaboina R, Kumar D, Shastri NR. Evaluation of the inhibitory potential of HPMC, PVP and HPC polymers on nucleation and crystal growth. *RSC Adv*. 2016;6(81):77569-77576. doi:10.1039/C6RA19746A

177. Boschmann E. AquaSolve: Hydrpxypropylmethylcellulose acetate succinate - Physical and chemical properties. *J Chem Educ*. 1987;64(10):891.

178. Widjaja M, Gan J, Talpaneni J, Tjandrawinata R. Determination of Eudragit® L100 in an Enteric-Coated Tablet Formulation Using Size-Exclusion Chromatography with Charged-Aerosol Detection. *Sci Pharm*. 2018;86(3):38. doi:10.3390/scipharm86030038

179. Ellenberger DJ, Miller DA, Williams RO. Expanding the Application and Formulation Space of Amorphous Solid Dispersions with KinetiSol®: a Review. *AAPS PharmSciTech*. 2018;19(5):1933-1956. doi:10.1208/s12249-018-1007-2

APPENDIX

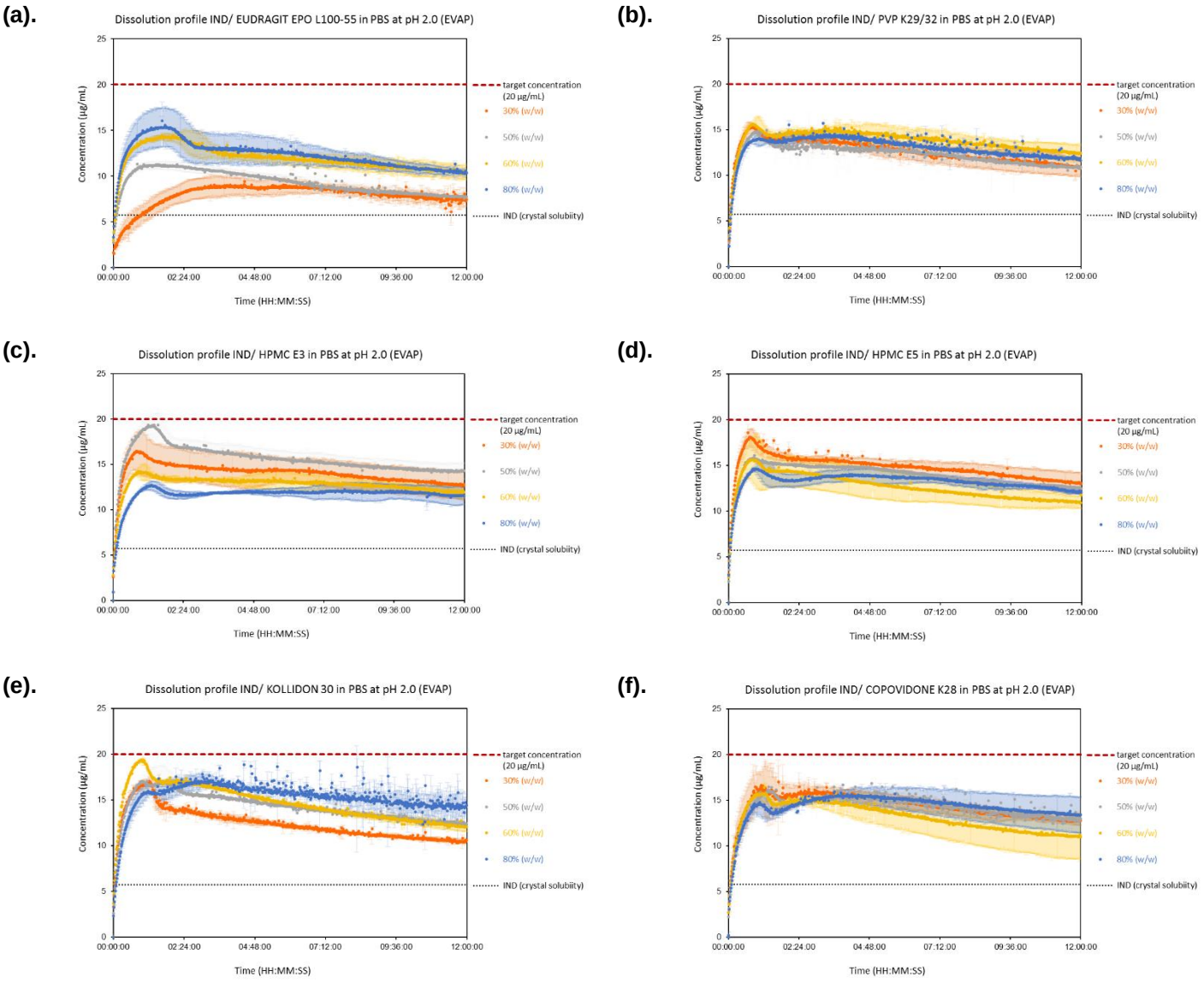

Figure A1. *Dissolution profiles of ASD films produced by solvent evaporation combining IND with (a) EUDRAGIT L100-55, (b) PVP K29/32, (c) HPMC E3, (d) HPMC E5, (e) KOLLIDON 30, (f) COPOVIDONE K28 at 30% drug load (orange), 50% drug load (grey), 60% drug load (yellow) and 80% drug load (blue), in PBS at pH 2.0, during a 12h period, at 37ºC, under constant orbital shaking. Target concentration of 20 µg/mL (Red dashed line). IND's crystal solubility (black dashed line). Values represent mean IND concentration (n = 2) and Y-error bars indicate the standard deviation.*

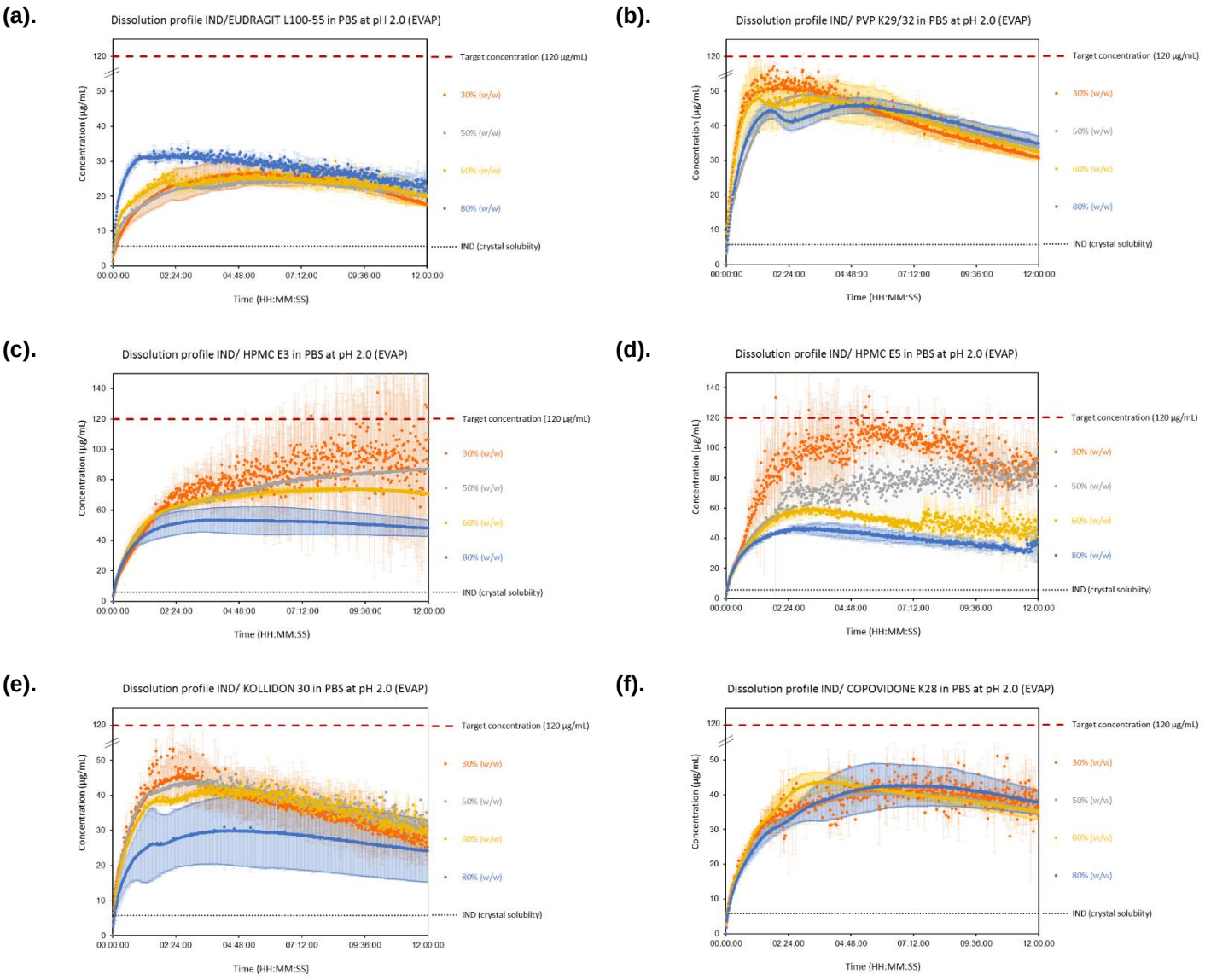

Figure A2. *Dissolution profiles of ASD films produced by solvent evaporation combining IND with (a) EUDRAGIT L100-55, (b) PVP K29/32, (c) HPMC E3, (d) HPMC E5, (e) KOLLIDON 30, (f) COPOVIDONE K28 at 30% drug load (orange), 50% drug load (grey), 60% drug load (yellow) and 80% drug load (blue), in PBS at pH 2.0, during a 12h period, at 37ºC, under constant orbital shaking. Target concentration of 120 µg/mL (Red dashed line). IND's crystal solubility (black dashed line). Values represent mean IND concentration (n = 2) and Y-error bars indicate the standard deviation.*

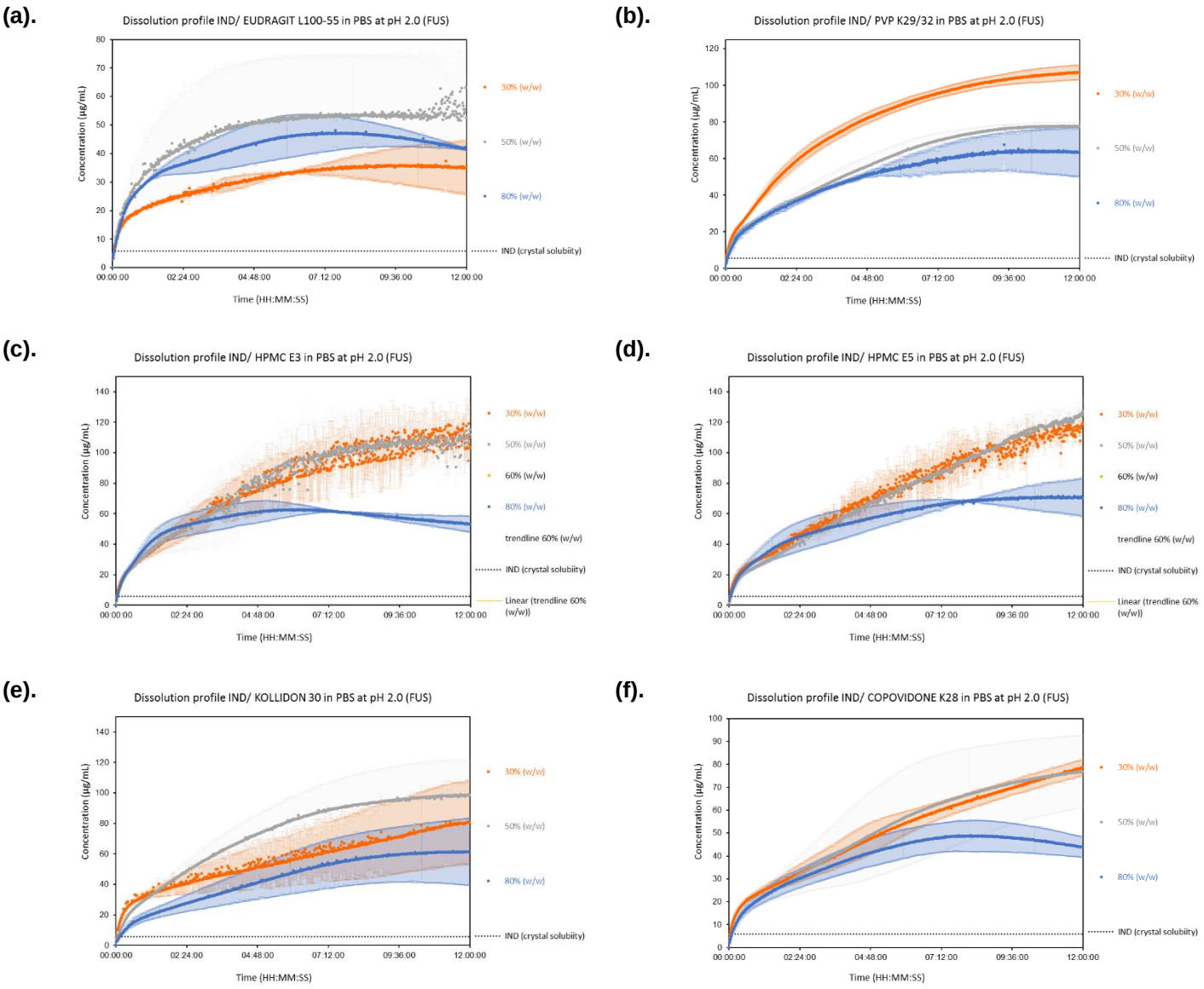

Figure A3. *Dissolution profiles of ASD films produced by the fusion method combining IND with (a) EUDRAGIT L100-55, (b) PVP K29/32, (c) HPMC E3, (d) HPMC E5, (e) KOLLIDON 30, (f) COPOVIDONE K28 at 30% drug load (orange), 50% drug load (grey), 60% drug load (yellow) and 80% drug load (blue), in PBS at pH 2.0, during a 12h period, at 37ºC, under constant orbital shaking. IND's crystal solubility (black dashed line). Values represent mean IND concentration (n = 2) and Y-error bars indicate the standard deviation.*

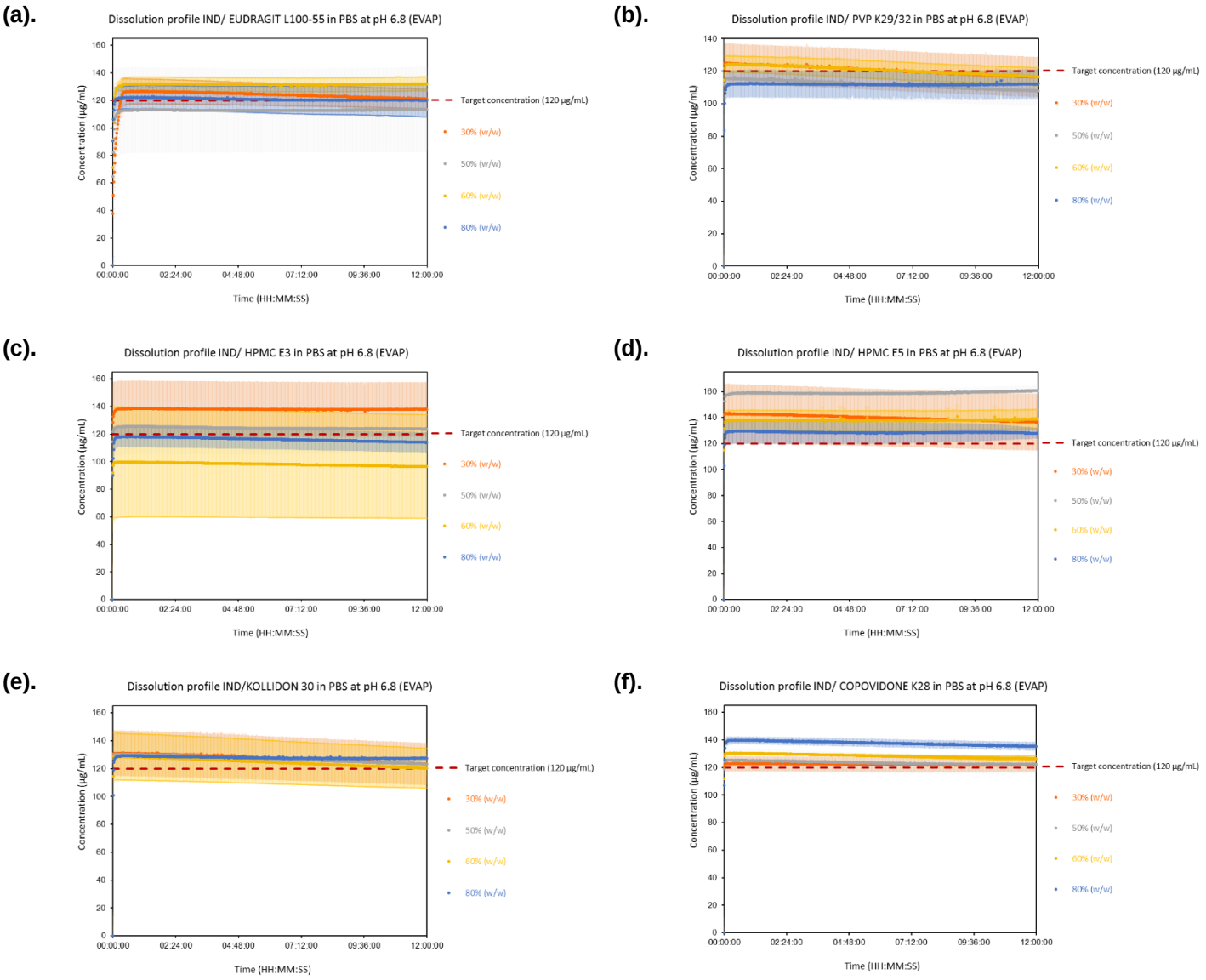

Figure A4. *Dissolution profiles of ASD films produced by solvent evaporation combining IND with (a) EUDRAGIT L100-55, (b) PVP K29/32, (c) HPMC E3, (d) HPMC E5, (e) KOLLIDON 30, (f) COPOVIDONE K28 at 30% drug load (orange), 50% drug load (grey), 60% drug load (yellow) and 80% drug load (blue), in PBS at pH 6.8, during a 12h period, at 37ºC, under constant orbital shaking. Target concentration of 120 µg/mL (Red dashed line). Values represent mean IND concentration (n = 2) and Y-error bars indicate the standard deviation.*

(a).

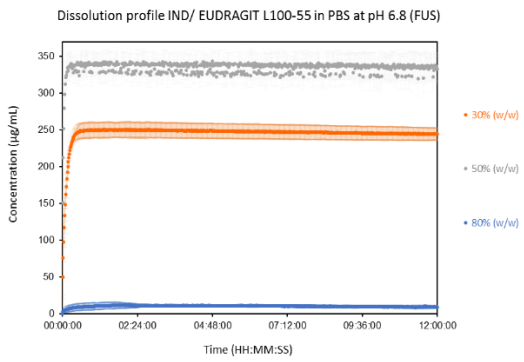

(b).

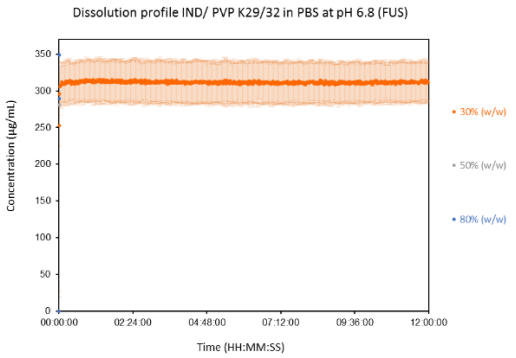

(c).

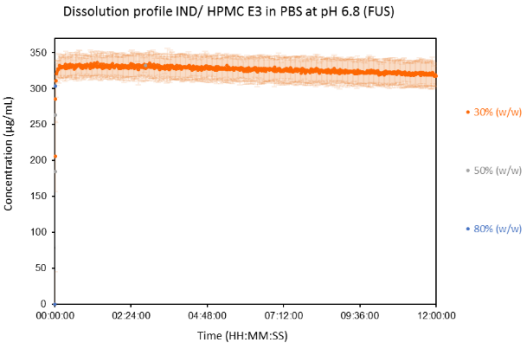

(d).

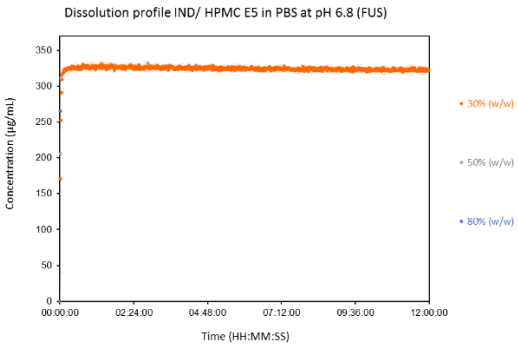

(e).

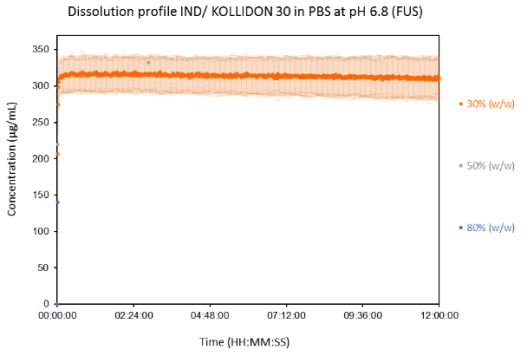

(f).

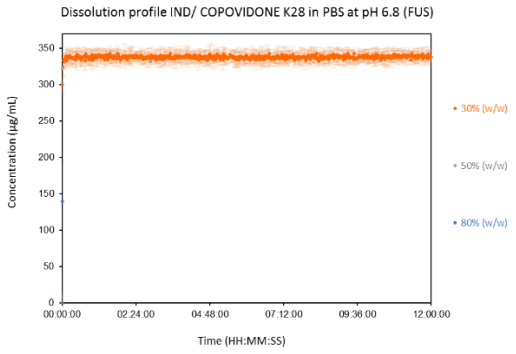

Figure A5. *Dissolution profiles of ASD films produced by the fusion method combining IND with (a) EUDRAGIT L100-55, (b) PVP K29/32, (c) HPMC E3, (d) HPMC E5, (e) KOLLIDON 30, (f) COPOVIDONE K28 at 30% drug load (orange), 50% drug load (grey), 60% drug load (yellow) and 80% drug load (blue), in PBS at pH 6.8, during a 12h period, at 37ºC, under constant orbital shaking Values represent mean IND concentration (n = 2) and Y-error bars indicate the standard deviation.*

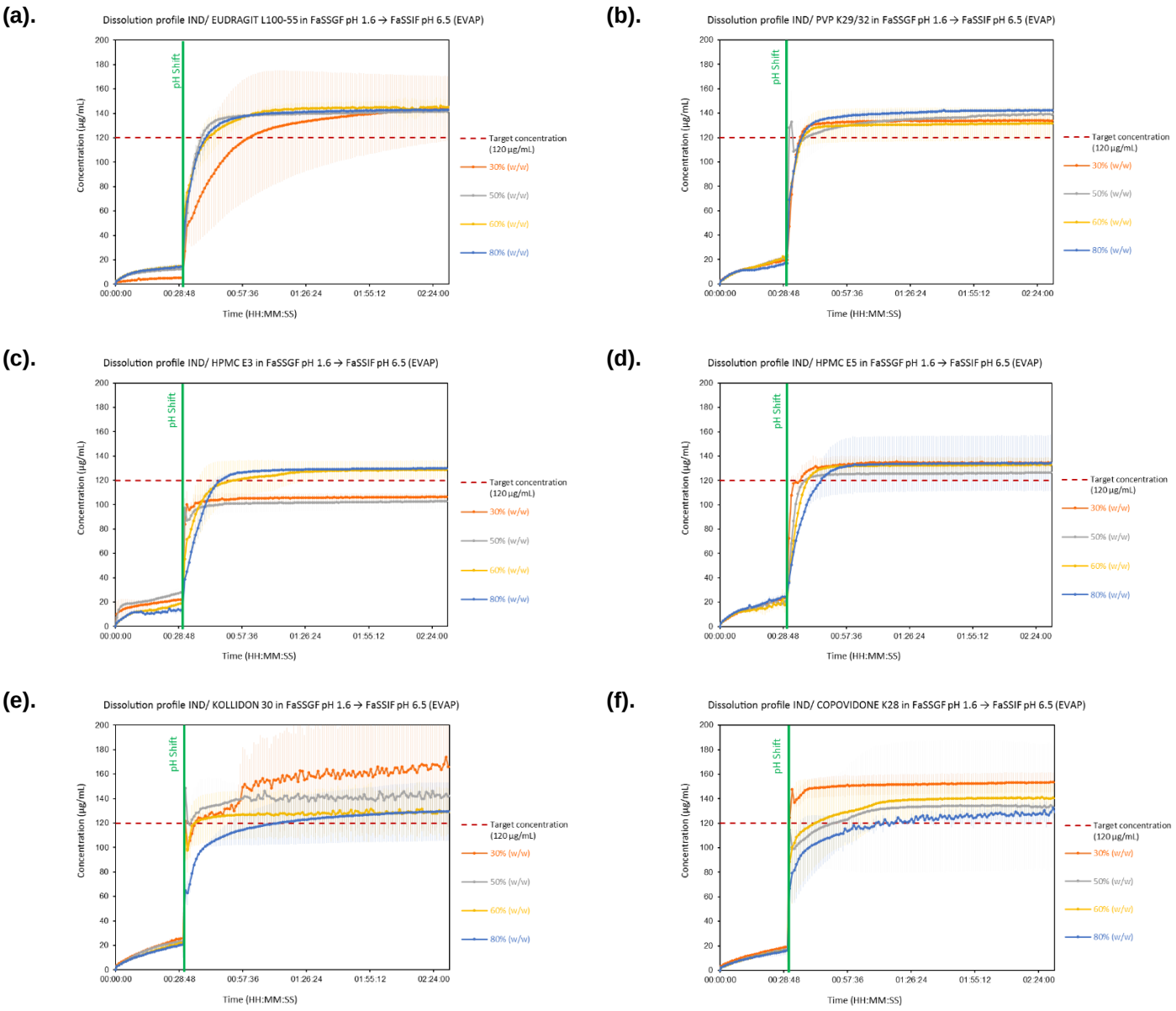

Figure A6. *Dissolution profiles of ASD films produced by solvent evaporation combining IND with (a) EUDRAGIT L100-55, (b) PVP K29/32, (c) HPMC E3, (d) HPMC E5, (e) KOLLIDON 30, (f) COPOVIDONE K28 at 30% drug load (orange), 50% drug load (grey), 60% drug load (yellow) and 80% drug load (blue), in FaSSIF at pH 1.6, during a 30 min, and upon conversion, in FaSSIF at pH 6.5, during 2h, at 37ºC, under constant orbital shaking. The vertical green line indicates pH shift time point. Target concentration of 120 µg/mL (Red dashed line). Values represent mean IND concentration (n = 2) and Y-error bars indicate the standard deviation.*

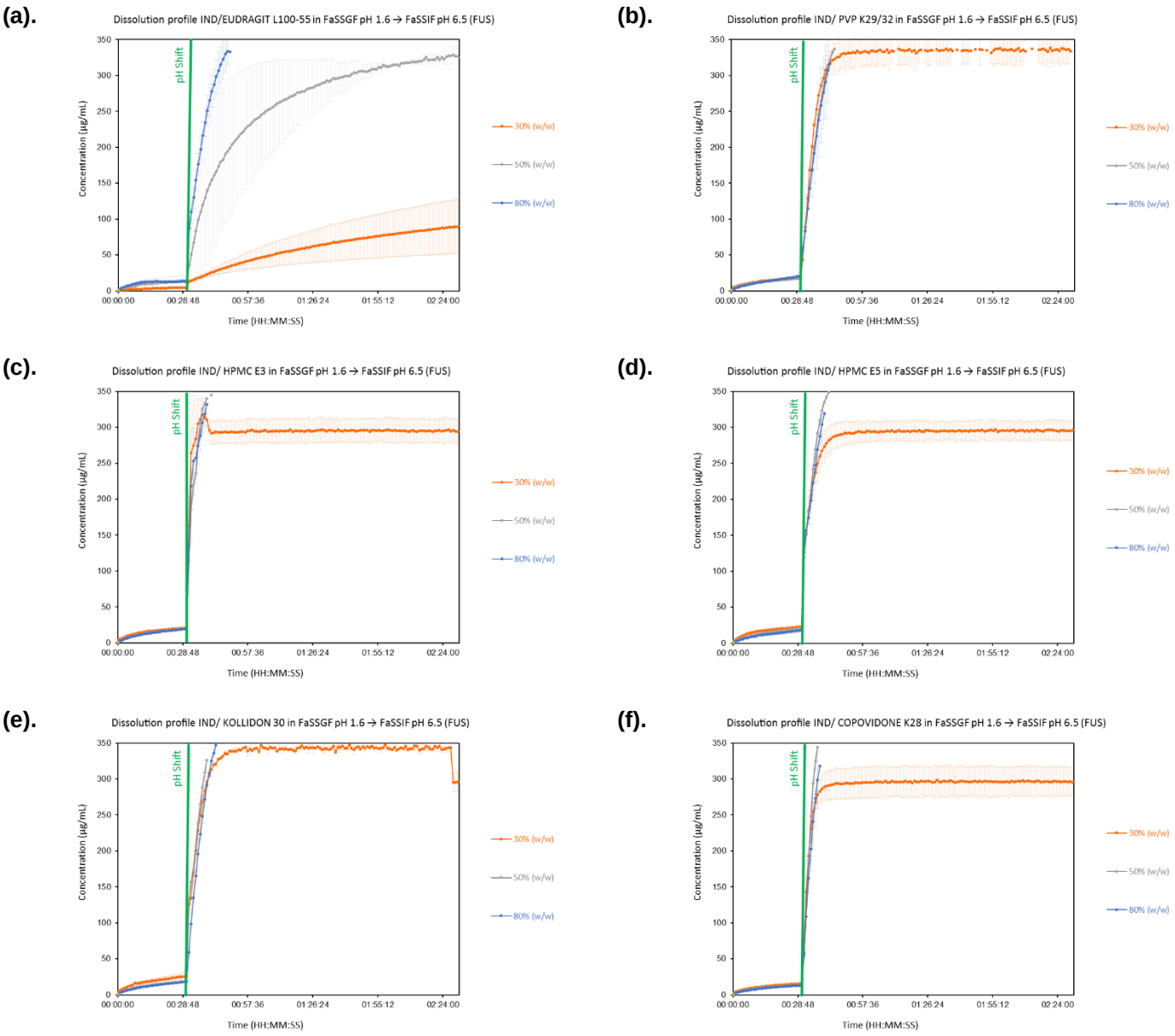

Figure A7. *Dissolution profiles of ASD films produced by the fusion method combining IND with (a) EUDRAGIT L100-55, (b) PVP K29/32, (c) HPMC E3, (d) HPMC E5, (e) KOLLIDON 30, (f) COPOVIDONE K28 at 30% drug load (orange), 50% drug load (grey), 60% drug load (yellow) and 80% drug load (blue), in FaSSIF at pH 1.6, during a 30 min, and upon conversion, in FaSSIF at pH 6.5, during 2h, at 37ºC, under constant orbital shaking. The vertical green line indicates pH shift time point. Values represent mean IND concentration (n = 2) and Y-error bars indicate the standard deviation.*

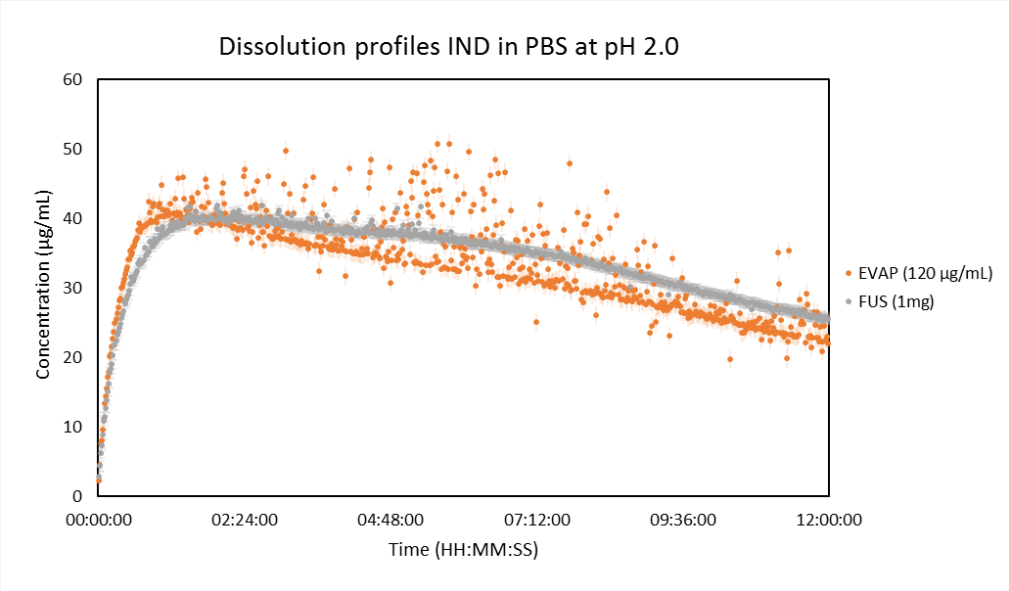

Figure A8. *Dissolution profiles of IND amorphous films produced by the fusion method (grey) and by solvent evaporation (orange), in PBS at pH 2.0, during a 12h period, at 37ºC, under constant orbital shaking. Values represent mean IND concentration (n = 2) and Y-error bars indicate the standard deviation.*

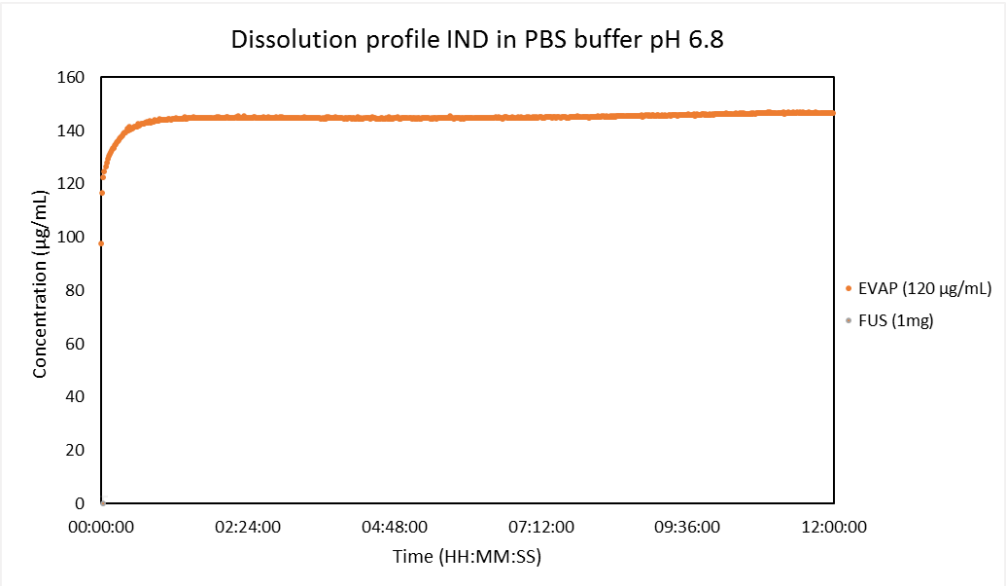

Figure A9. *Dissolution profiles of IND amorphous films produced by the fusion method and by solvent evaporation, in PBS at pH 6.8, during a 12h period, at 37ºC, under constant orbital shaking. Values represent mean IND concentration (n = 2) and Y-error bars indicate the standard deviation.*

Polymers	Supplier	M_w (g/mol)	Ionization	Hygroscopicity	T_g (°C)	T_{deg} (°C)	Solubility
HPMCAS-HF							
Hydroxypropylmethyl cellulose acetate succinate grade HF	Shin-Etsu AQOAT®	50000	Anionic	Low	122	258–276	Water soluble above pH 6.8
EUDRAGIT EPO							
Poly(butylmethacrylate-co-(2-dimethylaminoethyl)methacrylate-co-methyl methacrylate) 1:2:1	EVONIK	47000	Cationic	Low	57	250	Water soluble below pH 5.0
EUDRAGIT L100-55							
Poly(methacrylic acid-co-ethylacrylate) 1:1	EVONIK	320000	Anionic	Low	111	176	Water soluble above pH 5.5
METHOCEL E3 Premium LV EP							
Hydroxyl propyl methylcellulose (HPMC) E3	DOW Europe	20000	Nonionic	High	174	200	Water soluble
METHOCEL E5 Premium LV							
Hydroxyl propyl methylcellulose (HPMC) E5	DOW Europe	28700	Nonionic	High	154	200	Water soluble
PVP K29/32							
Polyvinylpyrrolidone K29/32	ASHLAND	58000	Nonionic	High	164	173	Water soluble
KOLLIDON 30							
Polyvinylpyrrolidone K30	BASF	44000 – 54000	Nonionic	High	160	171	Water soluble
COPOVIDONE K28							
Polyvinylpyrrolidone-(co)vinyl acetate 60:40	BASF	45000–70000	Nonionic	High	105	270	Water soluble

Table A1. *Physicochemical properties of the pool of polymers used in this project. The Information comprised in the table was provided by the suppliers or collected from the following referenced articles* [41,46,66,135,142,143,146,167–179]